The role of anisotropy and fiber dispersion in the mechanics and remodeling of biological tissues

Andrey Melnik
St Catherine's College
University of Oxford

A thesis submitted for the degree of
Doctor of Philosophy

Hilary 2015

The role of anisotropy and fiber dispersion in the mechanics and remodeling of biological tissues

Andrey Melnik

St Catherine's College

University of Oxford

A thesis submitted for the degree of

Doctor of Philosophy

Hilary 2015

Abstract

In many soft biological tissues mechanical strength and anisotropy are determined primarily by the presence of fibers, in particular collagen.

When an isotropic material is subject to a uniaxial tension, the principal strain transverse to the direction of applied load is always negative. However, in fiber reinforced materials the transverse principal strain can change its sign as the load increases, passing through the zero-points, known as *perversions*. We investigate how the number of perversions in a material reinforced by two symmetrically aligned families of distributed fibers depends both on the degree of fiber dispersion and the model used for fiber dispersion. Angular integration and three variants of the generalized structure tensor approach are considered and discussed. The study of perversions clearly demonstrates the qualitative difference between these approaches in the case of high dispersion of fibers. The results suggest that this difference is primarily due to the way compressive fibers are modeled.

Fiber alignment in biological tissues is created and maintained by the cells, which respond to mechanical stimuli arising from properties of the surrounding material. This coupling between mechanical anisotropy and tissue remodeling can be modeled in nonlinear elasticity by a fiber-reinforced hyperelastic material where remodeling is represented as the change in fiber orientation. We study analytically a simple model of fiber reorientation in a rectangular elastic tissue reinforced by two symmetrically arranged families of fibers subject to constant external loads. In this model, the fiber direction tends to align with the maximum principal stretch or strain. We characterize the global behaviour of the system for all material parameters and applied loads, and show that provided the fibers are tensile initially, the system converges to a stable equilibrium, which corresponds to either complete or intermediate fiber alignment.

Finally, we consider a model for the coupled growth and fiber reorientation in an elastic incompressible disk. The dynamics of our model is extremely sensitive to the initial condition and characterized by an infinite number of equilibrium states of fiber arrangement. We observed that the stress-induced fiber reorientation and growth laws used in our model produce specific fiber orientation pattern, which suggest a possible mechanism for self-organisation.

Acknowledgements

I am immensely grateful to Alain Goriely, whose kind supervision and support guided me through the years of study for the degree of Doctor of Philosophy. Thanks for our meetings, which encouraged me, inspired love for the topic and also allowed to learn a few things beyond mathematics.

I would like to thank Derek Moulton, Ellen Kuhl, Helen Byrne and Eamonn Gaffney for their feedback on my work at various stages. Also many thanks to everyone at the Mathematical Institute who shared with me their ideas, knowledge and enthusiasm through numerous discussions and arguments.

I would also like to thank Andrei Korobeinikov, Vladimir Sobolev, Valeriy Sokolovskiy, Victoriya Isakhanova and Sergey Melnik, whose influence and personal example amplified my interest in mathematical research and eventually contributed to the start of my studies at Oxford. Thanks to my new and old friends, and to my family for their support.

Statement of authorship

Chapter 2 consists mainly of the review of existing models. I introduce the iGST model for distributed fiber reinforcing, which is my original contribution.

Chapter 3 consists entirely of the original research done in collaboration with Hudson Borja Da Rocha. The most of the research is conducted and the most of the results are obtained by me. The contribution of Hudson Borja Da Rocha is the analysis of the GST model.

Chapters 4, 5 consist entirely of the original research conducted by me.

Alexei invited all his friends to a party. He has so many friends that when they stand in a circle, they cannot hear or see each other, or communicate otherwise. However, Alexei has a white ribbon, which he can pass to the next person on his right or on his left. The person who receives the ribbon can also pass it in either direction, and so on. Everyone is capable of remembering things and doing simple arithmetics. Is there a single algorithm that if followed by all Alexei's friends allows him to count their number?

- Author unknown. A mathematical problem for secondary school.

Contents

1 Introduction and Background **1**

1.1 Mechanics in biological tissues 1

1.2 Collagen fibers in soft biological tissues 3

1.3 The framework of non-linear elasticity 6

1.3.1 Kinematics 7

1.3.2 Conservation laws and stress tensors 12

1.3.3 Constitutive equation, restriction and assumptions 15

1.3.4 Objectivity 17

1.3.5 Isotropy and anisotropy 18

1.3.6 Multiplicative decomposition for finite growth 21

2 Models for fiber dispersion and fiber remodeling **24**

2.1 Introduction 24

2.2 Constitutive modeling of distributed fiber reinforcing 26

2.2.1 Angular integration (AI) approach for distributed fiber reinforcing 27

2.2.2 Exclusion of contracted fibers 30

2.2.3 Generalized structure tensor approach for distributed fiber reinforcing 31

2.2.4 GST for axisymmetric dispersion and accounting for contracted fibers (GSTx) 35

2.2.5 Alternative scheme for fiber exclusion in GST (iGST) 39
2.2.6 Generalized higher-order structure tensor models (GHOST) 40

3 Orthotropic fiber reinforced material in uniaxial tension 46

3.1 Introduction 46
3.2 Normal homogeneous deformations of orthotropic fiber-reinforced material 47
3.3 Sufficient symmetry conditions 48
3.3.1 Orthotropic material 51
3.3.2 An example of orthotropically symmetric fiber arrangement . . 52
3.4 Uniaxial tension of a material with two families of fibers 55
3.4.1 Fiber-reinforced material with two families of fibers 55
3.4.2 Comparison of the models in uniaxial tension 58
3.4.2.1 Transversely isotropic case 58
3.4.2.2 Perversion points of the transverse strain 61
3.5 Conclusion 65

4 Simple model for fiber reorientation 69

4.1 Introduction 69
4.2 Strain-induced fiber reorientation subject to constant stress 72
4.2.1 The case of strict fiber alignment 72
4.2.1.1 Analysis 75
4.2.1.2 Extreme equilibrium states 76
4.2.1.3 Intermediate equilibrium states 79
4.2.1.4 Unstrained fibers states 82
4.2.1.5 Singularities 84
4.2.1.6 Global behaviour 86
4.2.2 The case of fiber dispersion captured by the GST model. 90

4.2.2.1 Analysis . . . 92
4.2.2.2 Extreme equilibrium states . . . 92
4.2.2.3 Intermediate equilibrium state . . . 93
4.2.2.4 Unstrained fibers states . . . 94
4.2.2.5 Singularities . . . 95
4.2.2.6 Global behaviour . . . 96
4.2.3 The case of fiber dispersion captured by the AI model. . . . 98
4.3 Stress-induced reorientation subject to constant stresses . . . 99
4.4 Strain-induced reorientation subject to constant strains . . . 101
4.5 Stress-induced reorientation subject to constant strains . . . 103
4.5.1 Singularities . . . 105
4.5.2 Extreme equilibrium states . . . 105
4.5.3 Unstrained fibers states . . . 106
4.5.4 Intermediate eqiulibrium states . . . 106
4.6 Conclusions and discussion . . . 111

5 Coupled growth and remodeling in a fiber-reinforced elastic disk 115

5.1 Introduction and motivation . . . 115
5.2 The model . . . 120
5.2.1 Solution to the static part . . . 125
5.2.1.1 Special case of homogeneous growth . . . 127
5.2.2 Equilibrium solutions . . . 129
5.3 The dynamics of remodeling . . . 133
5.3.1 Dynamical growth in the absence of fiber reorientation . . . 136
5.3.2 Fiber reorientation in the absence of growth . . . 136
5.3.3 Combined dynamical growth and fiber reorientation . . . 138
5.4 Conclusion and discussion . . . 141

6 Conclusion **145**

A Computation of GHOSTs

(the transversely isotropic case) **148**

B Methods for determining the number of perversion points **153**

B.1 Perversion diagram for GST 153

B.2 Perversion diagram for GSTx 154

B.3 Perversion diagram for AI, iGST 155

B.4 Expressions for the AI model 157

B.5 Expressions for the iGST model 158

C An implication of rotational symmetry for diagonal tensors **163**

Chapter 1

Introduction and Background

1.1 Mechanics in biological tissues

The mechanics of biological tissues is studied by biomechanics [21]. Examples of biological tissues in animals include blood, bone, muscle, epithelium and nerves. Living tissues consist of cells surrounded by extracellular matrix and are characterised by complex organisation on many scales, which is necessary to enable and optimise tissue's physiological function. For instance, the branching structure of vasculature provides an efficient way of nutrient delivery by reducing the path while increasing the exchange area. Specific mechanical properties, such as flexibility of skin and strength and light weight of bones, are also provided by tissues' structure. The study of the mechanics of biological tissues aims to understand and predict their mechanical behaviour and also to explain related biological processes. Fung [21] states that *"The motivation for research in this area comes from the realization that biology can no more be understood without biomechanics than an airplane can without aerodynamics"*.

One of the most important connections between mechanics and biology is related to the process of development and maintenance of organs and tissues, known as *morphogenesis*. Understanding and controlling the morphogenesis is indispensable to the

treatment of many congenital and acquired diseases. Although the morphology of a species is primarily defined by the genome, the morphogenesis involves many biochemical, cellular and histological processes, which may be coordinated by mechanical signals. The mechanism by which cells sense and respond to mechanical stress is known as *mechanotransduction*. Mechanical forces serve as important regulators at the cellular and molecular levels, and they are equally potent as chemical signals [39]. This can be illustrated by the role mechanical stress plays in the development of bone tissue: long-term exposure to microgravity experienced by astronauts leads to bone resorption, whereas mechanical strain stimulates bone deposition and also directs bone versus cartilage formation. Soft tissues are influenced by mechanical stresses as well. For instance, endothelium cells respond to shear stress by altering their expression of proteins [39]. The mechanical cue for morphogenesis may originate, *e.g.* from the constant or cyclic loads the tissue experiences or from the stiffness of the extracellular matrix. The mechanical environment of the cells can change as a result of their activity. Hence there is a coupling between the activity of cells and their mechanical environment, which can be schematically represented as follows:

$$\text{Cells} \quad \begin{array}{c} \xrightarrow{\text{Cell response}} \\ \xleftarrow{\text{Mechanotransduction}} \end{array} \quad \text{Mechanical environment}$$

In the context of continuum solid mechanics and biomechanics, the evolution of tissues consists of three related but separate processes: the *morphogenesis*, which is understood as a macroscopic change of shape, the *growth*, which refers to the increase in mass and volume and the *remodeling*, which corresponds to the changes in mechanical properties, such as anisotropy or stiffness [2, 68].

1.2 Collagen fibers in soft biological tissues

Biological tissues can be classified as hard tissues (*e.g.* teeth or bones) or soft tissues (*e.g.* skin or arteries). Soft tissues are characterised by nonlinear anisotropic behaviour over finite strains [38]. In many soft biological tissues mechanical strength and anisotropy are determined primarily by the presence of fibers, in particular collagen [19, 75].

Collagen is a fibrous protein having a triple-helical structure normally of length 300nm and width 1.5nm, which is present in the extracellular matrix of most tissues in vertebrates and has outstanding mechanical properties. The collagen protein family consists of tens of different proteins, which differ in structure and properties. The most widely occurring collagen type is the fibril-forming collagen type I, which is the primary structural element in the mammalian connective tissue and the most abundant protein in mammals. Collagen constitutes the major part of tendons, ligaments and most of the organic part of bone and dentin, it is also the most important load-bearing component of soft tissues such as skin and arteries [19, 38].

In vivo all fibrillar collagens are synthesized in the form of precursors - procollagens, which later assemble into fibrils under the effect of specific proteinases, and can potentially form higher level structures such as fascicles and tendon fibres. Fibrils with somewhat different properties are formed *in vitro* in reconstituted collagen gels as a result of the self-assembly of cleaved and dissolved fibrillar collagen. In both cases, the mechanical properties of the collagen and the tissue are defined by the arrangement and alignment of the collagen fibrils, which are comprised by cross-linked collagen molecules [19]. Synthesized and reconstituted collagen can be remodelled by cells. The effects of the cell activity on the collagen include the realignment of collagen fibrils, collagen turnover, collagen cross-linking and fibril growth. We focus on the collagen realignment, as it is the primary factor defining the anisotropic mechanical properties.

Collagen fiber reorientation in collagen gels can be facilitated by various physical mechanisms. One mechanism involves gel compaction in one direction and fiber reorientation in a perpendicular direction. This process is driven by the cells and traction forces they exert onto the collagen fibers. These forces can be transmitted across the collagen network from one fibril to another through interconnections. Constraints preventing the gel from contraction in some directions induce the compaction of collagen network in the unrestricted (perpendicular) directions. As a result, the fibers are reoriented along the restricted direction. Therefore collagen reorientation can be controlled by adhesion at the boundary or other factors opposing the translation of fibers. [19, 63]. Another mechanism effectively resulting into collagen reorientation consists in the collagen turnover accompanied by the production of highly aligned collagen, which is synthesised by cells in accordance to their orientation [71].

It was observed that the mechanical environment can induce and direct collagen synthesis and realignment. For instance, the orientation of collagen fibers can be controlled by micropatterning of the substrate. It was demonstrated in [71] that cells align parallel to the direction of microgrooves in the surfaces of a silicone membrane and produce collagen fibres oriented in the same direction. Another example is mechanically induced collagen alignment described by Eastwood et al. in [15]. They studied a cell-populated collagen lattice, which was stretched by an external load applied in a particular direction. By comparing fibroblast morphology in different regions of the specimen and the changes that take place when the loading is removed, they conclude that the fibroblasts align themselves with the direction of the maximum principle strain.

Mechanically induced collagen realignment in particular and remodeling of tissues in general are of great importance for tissue engineering, as regenerating or creating tissues with sufficient mechanical integrity is one of the most difficult challenges in this area [5]. Mechanical stimuli can be used to produce artificial tissues with enhanced

mechanical properties. Often the best results are achieved when a tissue is subject to a cyclic loading that mimics physiological conditions. For example, Niklason et al. [54] developed a method to produce artificial bovine vessels cultured under pulsatile intraluminal pressure. These vessels, compared to vessels grown under nonpulsed conditions, possessed significantly higher rupture strength and their histological appearance was more similar to that of native vessels.

Collagen remodeling can be addressed using continuum mechanics. For example, Barocas and Tranquillo developed a biphasic model for cell-populated collagen gels, wherein one phase includes collagen fibril network with entrapped cells and the other phase represents biological solution. Their model takes into account inhomogeneous cell distribution, anisotropic fiber distribution, directed stress generation and strain-induced fiber alignment. The collagen orientation patterns predicted by this model for a cardiac valve are consistent with experiments [61, 56].

Driessen et al. [11] suggested a model for mechanically induced collagen remodeling in the aortic valve that includes passive anisotropic response. They assumed that the valve is a fiber-reinforced elastic material with two discrete fiber directions at each point, wherein the evolution of fiber content and orientation depends on the values of principal stretches and is defined by first-order differential equations. The fiber architecture resulting from the evolution strongly resembled the experimental data from native valves. This model was further developed to allow for continuously distributed collagen fibers [13]. A similar model was later proposed to investigate the helical arrangement of collagen in the arterial wall, where it is oriented more circumferentially in the inner layer than in the outer [14]. It was assumed in this model that the collagen fibers realign towards preferred directions, situated between the principal stretch directions.

Further studies of collagen fiber remodeling consider gradual realignment with the direction given as a function of stress in the arterial wall (*e.g.* [30, 48]), in the bifurc-

ation of the carotid artery (*e.g.* [29]). See also [41, 40, 42] for the study of collagen reorientation, where the elastic collagen response is modelled using the transversely isotropic chain model, and also [32] for the discussion of the strain-driven fiber reorientation. The importance of models for mechanically induced collagen reorientation is not motivated exclusively by their applications to the development of bioartificial tissues. Such models can also shed light on the evolution of the optimal structure in a native tissue, its adaptive capabilities and how its architecture enables physiological functions.

We study the anisotropic elastic behaviour of soft collagen-rich tissues using the framework of non-linear elasticity. Basic concepts and results of this framework are summarised in the following section. We also use the framework of incompatible growth to address residual stresses developed in many tissues *in vivo* and in gels, whose compaction often accompanies fiber reorientation *in vitro*. The overview and discussion of the modelling of biological growth and remodeling can be found *e.g.* in [2, 49].

1.3 The framework of non-linear elasticity

In this Chapter we present a summary of basic notions and results of continuum mechanics and non-linear elasticity. While following the conventional order of introducing ideas of this framework we aim to skip details that are redundant in the current context but keep a certain degree of self-sufficiency for the narration. We start by describing the kinematics of a continuum body, then we define the stress tensors and formulate relevant properties and their link to the conservation laws. Next we discuss the concept of constitutive equation, strain-energy function, objectivity and (an-)isotropy, and present some particular examples of fiber-reinforced materials. We finish the technical background by touching on the matter of incompatible growth and virtual

configurations. For a thorough presentation of the theory of non-linear elasticity the reader is referred to the literature [3, 33, 16, 55].

1.3.1 Kinematics

A 3-dimensional continuum object, henceforth *body*, is represented by a topological space, consisting of material points and their neighborhoods. The body can be homeomorphically mapped to a subset of the Euclidean space $\mathbb{R}^3$, which corresponds to the 3-dimensional physical space the body is observed in. The map is not unique and each such homeomorphism is identified with a *configuration* of the body. In order to describe relative changes the body undergoes in different configurations, one configuration is distinguished from the rest, denoted $\mathcal{B}_0$, and is called the *reference configuration*. Each material point in the reference configuration has a position $\mathbf{X} \in \mathcal{B}_0 \subseteq \mathbb{R}^3$, and we use symbol $\mathcal{B}_0$ ambiguously for both the reference configuration (*i.e.* the homeomorphism from the topological space) and its image in $\mathbb{R}^3$. The body may deform and at a given time t take a different configuration, called *current configuration* $\mathcal{B}_t$. Lower case $\mathbf{x}$ is used to denote a material point position in the current configuration, thus $\mathbf{x} \in \mathcal{B}_t$. Due to continuity and continuous invertibility of the homeomorphisms, there exists a *motion* $\boldsymbol{\chi} : \mathcal{B}_0 \times [t_0, t_{\text{end}}] \to \mathcal{B}_t$. Therefore, one can write

$$\mathbf{x} = \boldsymbol{\chi}(\mathbf{X}, t), \qquad \mathbf{X} = \boldsymbol{\chi}^{-1}(\mathbf{x}, t). \tag{1.1}$$

For a fixed time t, one can consider a *deformation, i.e.* the state of motion evaluated at the given instant of time, $\boldsymbol{\chi}_t(\mathbf{X}) \equiv \boldsymbol{\chi}(\mathbf{X}, t)$.

Some configurations in $\mathbb{R}^3$ may be *stress-free configurations*, meaning that no part of material exerts any force on any other part. It is natural and convenient to use such configurations as reference configurations.

Expressing motion or any other process or quantity as a function of the reference

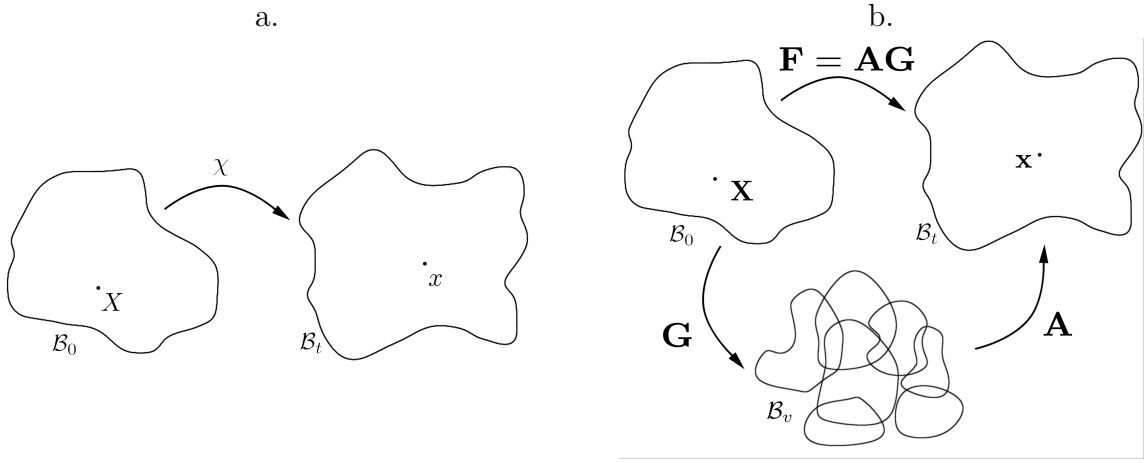

Figure 1.1: a. The reference configuration $\mathcal{B}_0$ and the current configuration $\mathcal{B}_t$ are related by motion χ. b. Multiplicative decomposition of the deformation gradient $\mathbf{F}$ into the growth tensor $\mathbf{G}$ and the elastic deformation gradient $\mathbf{A}$. $\mathcal{B}_v$ is the virtual stress-free configuration.

position $\mathbf{X}$ is called the *Lagrangian (material) form*, whereas describing them as a function of the current position $\mathbf{x}$ is called the *Eulerian (spatial) form*. Since $\boldsymbol{\chi}$ is continuously invertible, the choice of Lagrangian or Eulerian descriptions is a matter of convenience. For example, the velocity field of material points is given in the Lagrangian form by

$$\mathbf{v}_0(\mathbf{X}, t) = \frac{\partial}{\partial t}\boldsymbol{\chi}(\mathbf{X}, t), \tag{1.2}$$

and in the Eulerian form by

$$\mathbf{v}(\mathbf{x}, t) = \frac{\partial}{\partial t}\boldsymbol{\chi}(\boldsymbol{\chi}^{-1}(\mathbf{x}, t), t). \tag{1.3}$$

The acceleration experienced by particle is the material derivative of the velocity

$$D_t\mathbf{v}(\mathbf{x}, t) = \frac{d}{dt}\mathbf{v}_0(\mathbf{X}, t) = \frac{\partial}{\partial t}\mathbf{v}(\mathbf{x}, t) + \mathrm{grad}\mathbf{v} \cdot \mathbf{v}, \tag{1.4}$$

as can be seen from

$$\mathbf{v}(\boldsymbol{\chi}(\mathbf{X}, t), t) \equiv \frac{\partial}{\partial t}\boldsymbol{\chi}(\mathbf{X}, t). \tag{1.5}$$

We used the gradient operator above and will also require the divergence operator for further elaborations. The convention is that the operators Grad, Div (starting with a capital letter) denote the differentiation with respect to the material position $\mathbf{X}$, whereas operators grad, div denote the differentiation with respect to the spatial position $\mathbf{x}$. Let $\bullet$ denote a scalar, vector or tensor field defined on the body (and therefore in reference and current configurations), then

$$\mathrm{Grad}(\bullet) = \frac{\partial}{\partial \mathbf{X}}(\bullet), \quad \mathrm{grad}(\bullet) = \frac{\partial}{\partial \mathbf{x}}(\bullet), \tag{1.6}$$

$$\mathrm{Div}(\bullet) = \mathrm{tr}\frac{\partial}{\partial \mathbf{X}}(\bullet), \quad \mathrm{div}(\bullet) = \mathrm{tr}\frac{\partial}{\partial \mathbf{x}}(\bullet). \tag{1.7}$$

For example, let $\mathbf{A}(\mathbf{X}) = A_{ij}(\mathbf{X})\mathbf{E}_i \otimes \mathbf{e}_j$ be a two-point tensor defined in referential form and $\{\mathbf{E}_i\}$, $\{\mathbf{e}_i\}$ be the Cartesian bases in the reference and current configurations, $\mathbf{x} = x_i\mathbf{e}_i$, $\mathbf{X} = X_i\mathbf{E}_j$, then we have

$$\mathrm{grad}\mathbf{A} = \frac{\partial A_{ij}}{\partial x_k}\mathbf{E}_i \otimes \mathbf{e}_j \otimes \mathbf{e}_k, \quad \mathrm{div}\mathbf{A} = \frac{\partial A_{ij}}{\partial x_j}\mathbf{E}_i. \tag{1.8}$$

We use the summation convention, assuming that the sum is taken over a repeated index, unless specified otherwise. In practice we will be using only orthonormal bases and there is no need to distinguish between upper and lower indices, therefore the summation applies regardless of the indices' position. Note that although some authors [3] make a difference between the gradient and derivative operators (one is the transpose of another), we identify them:

$$\bullet(\mathbf{x} + \varepsilon\mathbf{u}) = \bullet(\mathbf{x}) + \mathrm{grad}\,\bullet\,(\mathbf{x}) \cdot \mathbf{u} + o(\varepsilon) = \bullet(\mathbf{x}) + \frac{\partial \bullet}{\partial \mathbf{x}}(\mathbf{x}) \cdot \mathbf{u} + o(\varepsilon). \tag{1.9}$$

When utilizing curvilinear coordinates, *e.g.* polar spherical or cylindrical, the geometrical quantities should be treated in the way that respects the dependence of local bases orthonormal $\{\mathbf{E}_i\}$, $\{\mathbf{e}_i\}$ on the position. For instance, the product rule should

be applied when taking derivatives.

As an example, one can derive the expression for the divergence of a second-order tensor field in cylindrical coordinates. First, from (1.9) it follows that

$$\mathrm{grad}(\bullet) = \frac{\partial(\bullet)}{\partial \xi_i} \otimes \mathbf{g}^i = \sum_i |\mathbf{g}^i| \frac{\partial(\bullet)}{\partial \xi_i} \otimes \mathbf{e}^i = \frac{\partial(\bullet)}{\partial r} \otimes \mathbf{e}_1 + \frac{1}{r}\frac{\partial(\bullet)}{\partial \theta} \otimes \mathbf{e}_2 + \frac{\partial(\bullet)}{\partial z} \otimes \mathbf{e}_3,$$

where $(\xi_1, \xi_2, \xi_3) = (r, \theta, z)$ are cylindrical coordinates, $\{\mathbf{g}^i\}$ is the natural local covariant basis, such that $\mathbf{g}^j \cdot \mathbf{g}_i = \delta_i^j$, $\mathbf{g}_i = \partial \mathbf{x}/\partial \xi_i = |\mathbf{g}^i|\mathbf{e}_i$. After substituting $A_{ij}\mathbf{e}_i \otimes \mathbf{e}_j$ in place of $\bullet$ and double-contracting the result with the identity tensor we obtain

$$\begin{aligned} \mathrm{div}\mathbf{A} = & \left(\tfrac{\partial A_{11}}{\partial r} + \tfrac{\partial A_{13}}{\partial z} + \tfrac{1}{r}\left(A_{11} - A_{22} + \tfrac{\partial A_{12}}{\partial \theta}\right)\right)\mathbf{e}_1 + \\ & \left(\tfrac{\partial A_{21}}{\partial r} + \tfrac{\partial A_{23}}{\partial z} + \tfrac{1}{r}\left(A_{12} + A_{21} + \tfrac{\partial A_{22}}{\partial \theta}\right)\right)\mathbf{e}_2 + \\ & \left(\tfrac{\partial A_{31}}{\partial r} + \tfrac{\partial A_{33}}{\partial z} + \tfrac{1}{r}\left(A_{31} + \tfrac{\partial A_{32}}{\partial \theta}\right)\right)\mathbf{e}_3. \end{aligned} \tag{1.10}$$

The derivative of a scalar function $W(\mathbf{A})$ with respect to a two-point tensor $\mathbf{A} = A_{ij}\mathbf{e}_i \otimes \mathbf{E}_j$ is defined by

$$\frac{\partial W}{\partial \mathbf{A}} = \frac{\partial W}{\partial \mathrm{A}_{ij}} \mathbf{e}_i \otimes \mathbf{E}_j. \tag{1.11}$$

It is assumed that $\mathcal{B}_0$ and $\mathcal{B}_t$ are measurable open sets in $\mathbb{R}^3$ and have non-zero volumes, and also that $\boldsymbol{\chi}$ is differentiable. The latter allows to consider a local measure of deformation, the *deformation gradient tensor*

$$\mathbf{F}(\mathbf{X}, t) = \mathrm{Grad}\boldsymbol{\chi}(\mathbf{X}, t) = \mathrm{F}_{ij}\mathbf{e}_i \otimes \mathbf{E}_j, \quad \mathrm{F}_{ij} = \frac{\partial x_i}{\partial X_j}. \tag{1.12}$$

The geometrical meaning of the deformation gradient is the relation between a material line element $\mathrm{d}\mathbf{X}$ in the reference configuration and its image in the current configuration $\mathrm{d}\mathbf{x} = \mathbf{F}\mathrm{d}\mathbf{X}$. If given a rectifiable curve in the reference configuration $\boldsymbol{\Phi}(s) : [0, 1] \to \mathcal{B}_0$, its length can be computed as $L_{[a,b]} = \int_a^b \sqrt{\mathrm{d}\mathbf{X}.\mathrm{d}\mathbf{X}}ds$. By analogy the length of the same curve in the current configuration is $l_{[a,b]} = \int_a^b \sqrt{\mathrm{d}\mathbf{x}.\mathrm{d}\mathbf{x}}ds$.

We assume the linear map $\mathbf{F}$ is invertible and preserves the orientation, *i.e.* $J = \det \mathbf{F} > 0$. Therefore, by the *polar decomposition theorem* [16, p.188], there exist unique $\mathbf{R}$, $\mathbf{U}$ and $\mathbf{V}$ such that

$$\mathbf{F} = \mathbf{RU} = \mathbf{VR}, \tag{1.13}$$

where $\mathbf{R} = \mathbf{R}^{-T}$ is called the *rotation tensor*, $\mathbf{U} = \mathbf{U}^T$ and $\mathbf{V} = \mathbf{V}^T$ are the *right* and *left stretch tensors*. The stretch tensors share the same distinct real positive eigenvalues λ_i, $i = 1, 2, 3$, although the sets of (unit) eigenvectors, called respectively *principal referential directions* and *principal spatial directions*, can be different.

The *right Cauchy-Green deformation tensor* and the *left Cauchy-Green deformation tensor* are defined respectively as

$$\mathbf{C} = \mathbf{F}^T\mathbf{F} = \mathbf{U}^2, \qquad \mathbf{B} = \mathbf{F}\mathbf{F}^T = \mathbf{V}^2. \tag{1.14}$$

The Cauchy-Green deformation tensors are symmetric, disregard the rotational component and allow for an expression of the stretch ratio λ of a material line elements as

$$\lambda^2 = \frac{|\mathrm{d}\mathbf{x}|^2}{|\mathrm{d}\mathbf{X}|^2} = \frac{\mathrm{d}\mathbf{X}.\mathbf{C}\mathrm{d}\mathbf{X}}{\mathrm{d}\mathbf{X}.\mathrm{d}\mathbf{X}} = \frac{\mathrm{d}\mathbf{x}.\mathrm{d}\mathbf{x}}{\mathrm{d}\mathbf{x}.\mathbf{B}^{-1}\mathrm{d}\mathbf{x}}. \tag{1.15}$$

It follows that $\mathbf{C}$ and $\mathbf{B}$ have the same eigenvalues, λ_i^2 and the same *deformation invariants*, defined as

$$I_1 = \mathrm{tr}\mathbf{C} = \mathrm{tr}\mathbf{B} = \lambda_1^2 + \lambda_2^2 + \lambda_3^2, \tag{1.16}$$

$$I_2 = \mathrm{tr}^2\mathbf{C} - \mathrm{tr}\mathbf{C}^2 = \mathrm{tr}^2\mathbf{B} - \mathrm{tr}\mathbf{B}^2 = \lambda_1^2\lambda_2^2 + \lambda_2^2\lambda_3^2 + \lambda_3^2\lambda_1^2, \tag{1.17}$$

$$I_3 = \det\mathbf{C} = \det\mathbf{B} = \lambda_1^2\lambda_2^2\lambda_3^2. \tag{1.18}$$

1.3.2 Conservation laws and stress tensors

In order to describe the mechanics of a body one has to endow the purely geometrical construction we described above with physical quantities such as mass, force or temperature. Once physical quantities are defined, one can impose mass and momentum conservation laws and the second law of thermodynamics as well.

Let $\rho_0(\mathbf{X}, t)$ and $\rho(\mathbf{x}, t)$ be the density of the body measured with respect to volume elements in the reference and current configuration. The conservation of mass reads

$$\int_{\Omega_0} \rho_0(\mathbf{X}, t) dX = \int_{\Omega_t} \rho(\mathbf{x}, t) dx, \tag{1.19}$$

where Ω_0 and $\Omega_t = \boldsymbol{\chi}(\Omega_0)$ are respectively a region in the reference configuration and its image in the current configuration, dX and dx are volume elements. Using integration by substitution and $dx = JdX$ in the right-hand side one can localize the conservation of mass to obtain

$$\rho_0(\mathbf{X}, t) = J(\mathbf{X}, t)\rho(\mathbf{x}, t). \tag{1.20}$$

Let a smooth oriented surface $\mathcal{S}$ split a region in the current configuration in two parts, which exert forces on each other. Let da denote the area of a small portion of the surface, let $\mathbf{n}$ be a normal to the surface, which is used to tell one part of the region from the other. The *Cauchy postulate* asserts that the contact force exerted by the material in the direction of $\mathbf{n}$ on the surface element da equals $\mathbf{t}da$, where $\mathbf{t} = \mathbf{t}(\mathbf{x}, t, \mathbf{n})$ is the *Cauchy traction vector*. In addition to the contact force, which is generated within the material in response to the deformation or motion, there can be a contribution from an external body force $\mathbf{f}(\mathbf{x}, t)dV$ acting upon a volume element

dV. The conservation of linear momentum reads

$$\int_{\partial\Omega_t} \mathbf{t}(\mathbf{x},t,\mathbf{n})da + \int_{\Omega_t} \mathbf{f}(\mathbf{x},t)dV = D_t \int_{\Omega_t} \rho(\mathbf{x},t)\mathbf{v}(\mathbf{x},t). \tag{1.21}$$

The standard argument that the surface area of the boundary and the volume scale as $|\partial\Omega_t| \sim \varepsilon^2$, $|\Omega_t| \sim \varepsilon^3$ as $\varepsilon = \mathrm{diam}(\Omega_t) \to 0$ and the assumption of continuity lead to the existence of *the Cauchy stress tensor* $\boldsymbol{\sigma}$, which relates the traction vector $\mathbf{t}$ to the normal $\mathbf{n}$

$$\mathbf{t}(\mathbf{x},t,\mathbf{n}) = \boldsymbol{\sigma}(\mathbf{x},t)\mathbf{n}. \tag{1.22}$$

Now we can localize (1.21) and write down the conservation of linear momentum in the form known as the *Cauchy momentum equation*

$$\mathrm{div}\boldsymbol{\sigma} + \mathbf{f} - \rho D_t\mathbf{v} \;=\; 0. \tag{1.23}$$

If the body is in mechanical equilibrium ($\mathbf{v} = \mathrm{const}$) and the body force is neglected, then the Cauchy momentum equation becomes

$$\mathrm{div}\boldsymbol{\sigma} \;=\; 0. \tag{1.24}$$

The *conservation of the angular momentum* for a non-polar material implies that the Cauchy stress is a symmetric tensor

$$\boldsymbol{\sigma}^T = \boldsymbol{\sigma}. \tag{1.25}$$

One can obtain alternative stress measures by mapping (pulling back) the Cauchy stress tensor to the reference configuration. The deformation gradient $\mathbf{F}$ defines a natural correspondence between the reference oriented surface element $d\mathbf{A} = \mathbf{N}dA$

and its current counterpart $d\mathbf{a} = \mathbf{n}da$, which is given by the *Nanson's formula*

$$\mathbf{n}da = J\mathbf{F}^{-T}\mathbf{N}dA. \tag{1.26}$$

This relation leads to the definition of the *first Piola-Kirchhoff stress tensor*

$$\mathbf{P} = J\boldsymbol{\sigma}\mathbf{F}^{-T}, \tag{1.27}$$

which expresses current forces with respect to the referential area, allowing an equivalent form of the Cauchy momentum equation

$$\mathrm{Div}\mathbf{P} + J\mathbf{f} - \rho_0 D_t\mathbf{v} \;\; = \;\; 0. \tag{1.28}$$

The first Piola-Kirchhoff stress tensor is not symmetric. The *second Piola-Kirchhoff stress tensor* however is, and is defined by

$$\mathbf{S} = \mathbf{F}^{-1}\mathbf{P} = J\mathbf{F}^{-1}\boldsymbol{\sigma}\mathbf{F}^{-T},$$

which relates the reference oriented surface element to the referential traction (*i.e.* the preimage of current traction in the reference configuration) $\mathbf{t}_0 = \mathbf{F}^{-1}\mathbf{t}$,

$$\mathbf{t}_0 = \mathbf{F}^{-1}\mathbf{t}da = \mathbf{F}^{-1}\mathbf{P}\mathbf{N}dA = \mathbf{S}\mathbf{N}dA.$$

A particular convenience of using symmetric tensors consists in having all eigenvalues real.

1.3.3 Constitutive equation, restriction and assumptions

The constitutive equation is the relation between the motion and the stress. If the Cauchy stress tensor at a given reference point $\mathbf{X}$ at time t is fully determined by the deformation gradient $\mathbf{F}$ at this point, that is

$$\boldsymbol{\sigma}(\mathbf{X}, t) = \mathfrak{g}(\mathbf{F}(\mathbf{X}, t), \mathbf{X}), \tag{1.29}$$

then the material is called *Cauchy-elastic*. A material is called *hyperelastic* or a *Green-elastic material* if there exists a *strain-energy (density) function* $W(\mathbf{F}, \mathbf{X})$, such that the first Piola-Kirchhoff stress is given by [3, p.477-478]

$$\mathbf{P}(\mathbf{X}, t) = \frac{\partial W}{\partial \mathbf{F}}(\mathbf{F}(\mathbf{X}, t), \mathbf{X}), \tag{1.30}$$

or, equivalently, the Cauchy stress is given by

$$\boldsymbol{\sigma}(\mathbf{X}, t) = J^{-1} \frac{\partial W}{\partial \mathbf{F}}(\mathbf{F}(\mathbf{X}, t), \mathbf{X}) \mathbf{F}(\mathbf{X}, t)^T. \tag{1.31}$$

Relation (1.30) can be derived from certain assumptions by applying so-called *Coleman-Noll procedure* to the *Clausius-Duhem inequality*, which is a local form of the *second law of thermodynamics* [33, p.208]. A part of this procedure is varying the deformation gradient and its time derivative over all allowable values. Consequently, in the presence of internal constraints different expressions for stress tensors, analogous to (1.30), (1.31) will be obtained. For a constraint

$$q(\mathbf{F}(\mathbf{X}), \mathbf{X}) = 0, \tag{1.32}$$

the strain-energy W in (1.30), (1.31) must be replaced by

$$W(\mathbf{F}, \mathbf{X}) - p(\mathbf{X}, t)q(\mathbf{F}, \mathbf{X}), \tag{1.33}$$

where p plays the role of a Lagrange multiplier. For an incompressible material the constraint is $q(\mathbf{F}(\mathbf{X}, t), \mathbf{X}) = \det \mathbf{F}(\mathbf{X}, t) - 1$, and one obtains

$$\begin{aligned} \mathbf{P}(\mathbf{X}, t) &= -p(\mathbf{X}, t)\mathbf{F}^{-T} + \frac{\partial W}{\partial \mathbf{F}}(\mathbf{F}(\mathbf{X}, t), \mathbf{X}), & (1.34) \\ \boldsymbol{\sigma}(\mathbf{X}, t) &= -p(\mathbf{X}, t)\mathbf{1} + \frac{\partial W}{\partial \mathbf{F}}(\mathbf{F}(\mathbf{X}, t), \mathbf{X})\mathbf{F}(\mathbf{X}, t)^T. & (1.35) \end{aligned}$$

The constitutive equation for a hyperelastic material is *local*, meaning that the value of stress at a given point is only affected by the motion in the neighbourhood of this point through the value of the deformation gradient. Also the stress does not depend on the deformation history, but only on the current value of deformation gradient. A material is called *homogeneous* if the strain-energy $\mathbf{W}$ and the response function $\mathfrak{g}$ depend on position only via the deformation gradient (for a related notion of uniformity see [55, p.175]).

There are additional conditions, which the strain-energy function must satisfy in order to comply with our experience of real elastic materials. For instance, every material can attain an unstrained state, corresponding to a *stress-free* configuration. If this configuration is taken as the reference configuration, then we have

$$\frac{\partial W}{\partial \mathbf{F}}(\mathbf{1}, \mathbf{X}) \equiv 0. \tag{1.36}$$

One can also assume that $\mathbf{F} = \mathbf{1}$ is the global minimizer of the strain energy. Note that only derivatives of $W(\mathbf{F})$ contribute to stress, hence without loss of generality one can demand $W(\mathbf{1}) = 0$.

Examples of additional restrictions on the strain energy function and stress-response

include the *tension-extension inequalities, Baker-Ericksen inequalities* and *polyconvexity*. Details about these constitutive inequalities can be found in [70, p. 153]. In Section 3 we use as an assumption a weakened version of the tension-extension inequlity, which ensures that a material extends in the axial direction when subject to uniaxial tensile loading.

1.3.4 Objectivity

The *objectivity requirement* (also known as *frame-indifference*) means that a feasible physical law or phenomenon is independent from the observer and hence the choice of the frame of reference. In particular, observed quantities measured in the current configuration must change in accordance with the change of the coordinate system used to measure them. That means that if the change of the coordinate system is defined by a rigid body motion $\hat{\boldsymbol{\chi}}(\mathbf{x}, t) = \mathbf{Q}(t)\mathbf{x} + \mathbf{c}(t)$ superimposed on the current configuration $\mathcal{B}_t$, then a value of a current tensor quantity $\mathbf{Z} = \mathrm{Z}_{i_1 \dots i_m} \mathbf{e}_{i_1} \otimes \cdots \otimes \mathbf{e}_{i_m}$ must change according to

$$\hat{\mathbf{Z}} = \mathrm{Z}_{i_1 \dots i_m} \mathbf{Q}(t)\mathbf{e}_{i_1} \otimes \cdots \otimes \mathbf{Q}(t)\mathbf{e}_{i_m}. \tag{1.37}$$

Such quantities are called *objective*. For Cauchy-elastic materials the objectivity of the Cauchy stress reads

$$\boldsymbol{\sigma}(\mathbf{Q}(t)\mathbf{F}) = \mathbf{Q}(t)\boldsymbol{\sigma}(\mathbf{F})\mathbf{Q}(t)^T. \tag{1.38}$$

This condition for hyperelastic materials means that the strain-energy function is invariant with respect to superimposed rotations,

$$W(\mathbf{QF}) = W(\mathbf{F}), \qquad \forall \mathbf{F}, \forall \mathbf{Q} \in O(3). \tag{1.39}$$

This is equivalent to the statement that W can be expressed as a function of the right Cauchy-Green deformation tensor, *i.e.*

$$W(\mathbf{F}) = W(\mathbf{U}) = \hat{W}(\mathbf{C}), \qquad \forall \mathbf{F},\, \mathbf{C} = \mathbf{F}^T\mathbf{F}. \tag{1.40}$$

This property allows to write the stress-strain relation (1.35) as

$$\boldsymbol{\sigma} = -p\mathbf{1} + 2\mathbf{F}\frac{\partial \hat{W}}{\partial \mathbf{C}}\mathbf{F}^T, \tag{1.41}$$

where the hat over $\hat{W}$ may be henceforth omitted.

1.3.5 Isotropy and anisotropy

A material is said to be *isotropic* if the stress response ignores rotations preimposed on the deformation gradient, *i.e.*

$$W(\mathbf{FQ}) = W(\mathbf{F}), \qquad \forall \mathbf{F},\, \forall \mathbf{Q} \in O(3), \tag{1.42}$$

which by virtue of (1.40) can be written as

$$\hat{W}(\mathbf{Q}^T\mathbf{C}\mathbf{Q}) = \hat{W}(\mathbf{C}), \qquad \forall \mathbf{F},\, \mathbf{C} = \mathbf{F}^T\mathbf{F},\, \forall \mathbf{Q} \in O(3). \tag{1.43}$$

This condition is equivalent to W being dependent on the deformation gradient through the left Cauchy-Green deformation tensor $\mathbf{B}$,

$$W(\mathbf{F}) = W(\mathbf{V}) = \bar{W}(\mathbf{B}), \qquad \forall \mathbf{F},\, \mathbf{B} = \mathbf{F}\mathbf{F}^T = \mathbf{V}^2. \tag{1.44}$$

In terms of stress tensors, the isotropy condition reads

$$\boldsymbol{\sigma}(\mathbf{FQ}) = \boldsymbol{\sigma}(\mathbf{F}), \quad \mathbf{Q}\mathbf{S}(\mathbf{FQ})\mathbf{Q}^T = \mathbf{S}(\mathbf{F}), \qquad \forall \mathbf{F},\, \forall \mathbf{Q} \in O(3), \tag{1.45}$$

Objectivity and isotropy together imply that the strain energy can be expressed as a function of three scalar deformation invariants, defined in (1.16)-(1.18),

$$W(\mathbf{F}) = \tilde{W}(I_1, I_2, I_3), \tag{1.46}$$

and also lead to the *Rivlin-Ericksen representation theorem*,

$$\boldsymbol{\sigma} = \beta_0(I_1, I_2, I_3)\mathbf{1} + \beta_1(I_1, I_2, I_3)\mathbf{B} + \beta_2(I_1, I_2, I_3)\mathbf{B}^2. \tag{1.47}$$

Objectivity and isotropy conditions are similar in that they consider invariance of the strain energy with respect to rotations of the current and the reference configuration respectively. It is important to emphasise that isotropy (unlike objectivity) is an assumption about material properties rather than a theoretically motivated requirement. A material is said to be *symmetric* with respect to a linear transformation if the reference configuration is mapped by this transformation to another configuration, which is mechanically indistinguishable from the former. The set of all such linear transformations makes up a *symmetry group* $\mathbb{Q} \subseteq O(3)$, and the symmetry condition reads [36]

$$W(\mathbf{FQ}) = W(\mathbf{F}), \quad \forall \mathbf{F}, \forall \mathbf{Q} \in \mathbb{Q}. \tag{1.48}$$

An equivalent statement in terms of stress response functions is

$$\boldsymbol{\sigma}(\mathbf{FQ}) = \boldsymbol{\sigma}(\mathbf{F}), \quad \mathbf{QS}(\mathbf{FQ})\mathbf{Q}^T = \mathbf{S}(\mathbf{F}), \qquad \forall \mathbf{F}, \forall \mathbf{Q} \in \mathbb{Q}. \tag{1.49}$$

The maximal possible symmetry group is $O(3)$, which corresponds to an isotropic material and renders (1.48) and (1.49) identical to (1.42) and (1.45). If the symmetry group of a material is different from $O(3)$ (*i.e.* it is a proper subgroup of $O(3)$) then the material is called *anisotropic*. Although neither of the relations (1.42)-(1.47) holds for an anisotropic material, they can be replaced, in principle, by similar conditions.

Let the anisotropy of the material be associated with a finite or infinite number of unit vectors $\mathbf{a}_0^{(i)}$. Then the analog of (1.42) reads

$$W(\mathbf{FQ}, \mathbf{Qa}_0^{(i)}) = W(\mathbf{F}, \mathbf{a}_0^{(i)}), \qquad \forall \mathbf{F}, \forall \mathbf{Q} \in O(3), \tag{1.50}$$

where W can be or not be symmetric with respect to some permutations of its vector arguments. Alternatively, one can write

$$\bar{W}(\mathbf{QCQ}^T, \mathbf{QA}^{(i)}\mathbf{Q}^T) = \bar{W}(\mathbf{C}, \mathbf{A}^{(i)}), \qquad \forall \mathbf{F}, \forall \mathbf{Q} \in O(3), \tag{1.51}$$

where the anisotropy is characterized by a set of symmetric structure tensors $\mathbf{A}_0^{(i)}$, $i = 1, \ldots, k$. We note that the forward transition is provided by $\mathbf{A}^{(i)} = \mathbf{a}_0^{(i)} \otimes \mathbf{a}_0^{(i)}$. Conditions (1.50) and (1.51) , interpreted physically, assert that structure tensors $\mathbf{A}_0^{(i)}$ provide an exhaustive description of anisotropic mechanical properties. Comparison with (1.42) and (1.43) suggests that W is an isotropic function of arguments $\mathbf{C}$, $\mathbf{A}_0^{(i)}$ taken in conjunction. In other words, a rotated reference configuration is indistinguishable from the original, as long as the structure tensors are rotated with it.

Examples of material symmetries relevant to biological tissues are the orthotropic and the transversely isotropic symmetries. The minimal material symmetry group consists of just two elements, $\mathbf{1}$ and $-\mathbf{1}$. In order to define such anisotropic material it is sufficient to endow the reference configuration with two distinct and non-equivalent directions $\mathbf{a}_0^{(1)}$ and $\mathbf{a}_0^{(2)}$ (as two points are enough to define the orientation of the unit sphere). It follows that the strain energy function can be represented in a form analogous to (1.46),

$$W(\mathbf{F}, \mathbf{a}_0^{(1)}, \mathbf{a}_0^{(2)}) = \tilde{W}(I_1, \ldots, I_9),$$

where the additional scalars are known as *pseudo-invariants* and defined by [65, 66]

$$I_4 = \mathbf{C} : \mathbf{A}^{(1)} = \left|\mathbf{F}\mathbf{a}_0^{(1)}\right|^2, \quad I_5 = \mathbf{C}^2 : \mathbf{A}^{(1)} = \left|\mathbf{C}\mathbf{a}_0^{(1)}\right|^2, \tag{1.52}$$

$$I_6 = \mathbf{C} : \mathbf{A}^{(2)} = \left|\mathbf{F}\mathbf{a}_0^{(1)}\right|^2, \quad I_7 = \mathbf{C}^2 : \mathbf{A}^{(2)} = \left|\mathbf{C}\mathbf{a}_0^{(2)}\right|^2, \tag{1.53}$$

$$I_8 = \mathbf{A}^{(1)} : \mathbf{C}\mathbf{A}^{(2)}, \quad I_9 = \mathbf{A}^{(1)} : \mathbf{A}^{(2)}, \tag{1.54}$$

where $\bullet_1 : \bullet_2 = \operatorname{tr} \bullet_1 \bullet_2$. Note that I_9 does not depend on deformation.

If the directions $\mathbf{a}_0^{(1)}$, $\mathbf{a}_0^{(2)}$ are equivalent or orthogonal then the material is *orthotropic*. Tissues reinforced by two families of fibers with identical properties are modeled as orthotropic materials, in which case $\mathbf{a}_0^{(1)}$ and $\mathbf{a}_0^{(2)}$ describe the orientation of fiber families, *i.e.* the direction of reinforcing. If the directions $\mathbf{a}_0^{(1)}$, $\mathbf{a}_0^{(2)}$ coincide, or if there is only one special direction, then the material is *transversely isotropic*. The strain energy of such material depends on the reduced set of (pseudo-)invariants, $I_1, \ldots, I_5$, and is used to model a tissue reinforced in a single direction. Constitutive models for fiber reinforced materials (in particular, for orthotropic materials) are studied and discussed in Chapter 2.

1.3.6 Multiplicative decomposition for finite growth

Some materials remain stressed after removal of applied loads and body force in any physical configuration. Constitutive equations that assume the existence of a stress-free configuration cannot be directly applied to such materials. One way of adapting existing material models to residually stressed materials is to use the *multiplicative decomposition of the deformation gradient*, which was suggested in the study of finite incompatible growth in [62]. This approach assumes the existence of a *local* stress-free configuration at (almost) every material point of the body at a given time t. That is, the body in the current configuration can be represented as a union of nonintersecting parts, such that each part has a stress-free configuration if considered as a separate

isolated body. In the physical terms, this means that the residual stress can be relieved by cutting the material in pieces. By keeping track of the local deformations at each point during this "cutting" procedure, we obtain a map from the given current configuration to the *virtual configuration*, which is defined as the collection of tangent spaces. The virtual configuration can be visualised in $\mathbb{R}^3$ by removing topological constraints and allowing neighbouring parts of the body overlap or have gaps between them (Figure 1.1b). Alternatively one can consider a mapping to a 3-dimensional space equipped with a non-Euclidean metric.

In order to avoid mathematical difficulties, it is convenient to define a stress-free reference configuration $\mathcal{B}_0$ and postulate that the deformation gradient $\mathbf{F}$ can be decomposed into the product of the growth tensor $\mathbf{G}$ and the elastic deformation tensor $\mathbf{A}$,

$$\mathbf{F}(\mathbf{X},t) = \mathbf{A}(\mathbf{X},t)\mathbf{G}(\mathbf{X},t). \tag{1.55}$$

The growth tensor $\mathbf{G}$ represents the local growth deformations, which introduce incompatibility, while $\mathbf{A}$ corresponds to the elastic deformation that restores the integrity of the material (Figure 1.1b). The virtual configuration is *incompatible*, meaning that in general there exists no function $\boldsymbol{\chi}_r$ defined on the entire body such that $\mathbf{A} = \mathrm{Grad}\boldsymbol{\chi}_v$. All constitutive relations considered in the previous sections can be used for grown and residually stressed materials after replacing $\mathbf{F}$ with $\mathbf{A}$. For example, the expressions for the Cauchy stress and the incompressibility condition read

$$\begin{aligned} \boldsymbol{\sigma}(\mathbf{X},t) &= -p(\mathbf{X},t)\mathbf{1} + \frac{\partial W}{\partial \mathbf{A}}(\mathbf{A}(\mathbf{X},t),\mathbf{X})\mathbf{A}(\mathbf{X},t)^T, && (1.56)\\ \det \mathbf{A} &= 1. && (1.57) \end{aligned}$$

Continuous mechanically-induced growth can be modeled by postulating a law of the form

$$\frac{d}{dt}\mathbf{G}(\mathbf{X},t) = \dot{\mathbf{G}}(\mathbf{G},\mathbf{A},\boldsymbol{\sigma},\dots). \tag{1.58}$$

In a typical biological system the time scale of growth is larger than the time required for the material to accommodate evolving virtual configuration, therefore it is assumed that the material instantaneously responds to a change in $\mathbf{G}$. Hence biological growth can be addressed using quasi-static approach, in which all growth-related inertial effects are neglected in the Cauchy equation of motion. Although the concept of growth in biology is associated with the increase in mass or volume, *i.e.* $\det \mathbf{G} > 1$, $\mathrm{tr}\dot{\mathbf{G}} > 0$, the same framework can be applied to shrinking and resorbing materials, for which $\det \mathbf{G} < 1$, $\mathrm{tr}\dot{\mathbf{G}} < 0$.

Chapter 2

Models for fiber dispersion and fiber remodeling

2.1 Introduction

The theory of nonlinear fiber-reinforced elastic composites asserts that the strain energy is in general expressed through a set of deformation invariants and pseudo-invariants defined in (1.16)-(1.18) and (1.52)-(1.54). The number of (pseudo-)invariants required to describe the dependence of strain energy on the deformation is determined by the material symmetry and ranges from 3 for isotropic solids to 8 for general anisotropic materials. This theory can be used to model a fiber-reinforced material, in which fibers are thought as local special directions of anisotropy rather than as actual collagen fibrils. This can be illustrated by the following examples. First, consider a material in which all fibers are oriented within one plane and the probability of finding a fiber with a particular orientation is equal for all in-plane orientations. Such material is transversely isotropic with the special direction being the perpendicular to the direction of actual fibers. Now consider a material in which all fibers are parallel, that is oriented in a single direction. Such material is also transversely isotropic, however

the special direction of anisotropy here coincides with the direction of fibers. Although such difference in the structure of materials might be crutial for understanding their mechanical properties, it is disregarded by the invariants, since the materials exhibit identical symmetries.

As opposed to the general invariant-based perspective, the *structural approach* consists in making *a priori* assumptions about stress-strain relation that allow to incorporate the knowledge of internal structure of a material. A popular assumption in constitutive models of fiber-reinforced materials is that the total stress generated by the whole tissue is the sum of stresses generated by its constituents. It is tacitly implied that the stress-strain relation exists independently for each constituent, while they undergo the same deformation in a solid elastic composit. As a consequence, the components can posess different material symmetries and individual strain energy functions, which sum up to the strain energy function of the composite. Many models for collagen-rich soft tissue assume the additive split of the strain energy in the isotropic part and the parts associated with fiber families or individual fibers, see *e.g.* [43, 44], also [35] and references therein. We use the term *family* to refer to all collagen fibers that share orientation (or orientation probability) and mechanical properties at every material point and therefore can be conveniently considered as a single entity. The additive split of stresses and strain energies allows to incorporate quantitative data characterizing tissue's structure directly into the constitutive relation: fiber volume fraction or orientation-dependent density can be included as multiplicative factors in the appropriate term of the sum. In addition, the structural approach allows to formulate structurally motivated phenomenological laws for fiber remodeling and study dynamics of mechanically induced fiber reorientation [12, 29, 46, 48].

In this Chapter we review constitutive models for distributed fiber reinforcing and fiber reorientation laws.

2.2 Constitutive modeling of distributed fiber reinforcing

Many studies consider models for soft tissues in which fibers are oriented in a finite number of discrete directions (see *e.g.* [34, 28]). Continuous distribution of fiber directions was addressed by Lanir [43], who proposed a structural model for a planar collagenous tissue, where the total stress generated by fibers is given as an integral over the range of fiber directions. This approach, called the *angular integration* approach (AI), generalizes the cases of strict fiber alignment in several discrete directions, fiber dispersion around mean fiber directions and isotropic fiber distribution. The main disadvantage of this approach is that in most cases it requires repeated numerical integrations. Gasser et al. [22] proposed a material model which overcomes this drawback by using *generalized structure tensors* (GST). A similar approach was suggested by Freed et al. [20]. Models based on the GST approach were applied to many soft tissues, including human aortic valve [20], arterial wall [22, 35], cornea [57, 27], articulate cartilage [17] and bat wing membrane [72]. It has been noted that the GST and the AI approaches provide different predictions and that the error of the GST comparing to the AI model is small only for low fiber dispersion [7]. A model suggested by Pandolfi and Vasta [58] assumes that the fiber strain energy depends on the mean value and also on the variance of fiber stretch. Their "V-model" is similar to the GST model in that it is justified by the Taylor expansion of the total fiber strain energy formulated according to the AI approach, but includes an additional term in the series. This idea was further developed by Cortes and Elliott [6], who introduced so-called generalized high-order structure tensors (GHOSTs). In addition to reviewing the aforementioned models, we analyse the GST model and suggest amendments and consider a new model, which we name iGST. We also discuss some aspects of the GHOST model and suggest for consideration its variant, which is a cross-breed of the

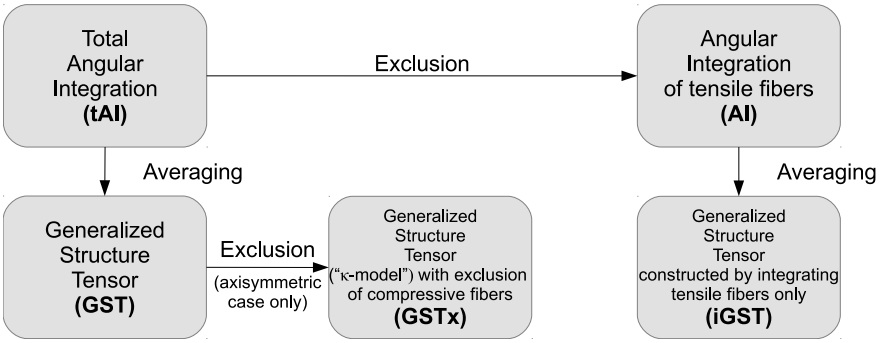

Figure 2.1: Relation between different modeling approaches for dispersed fiber reinforcement.

V-model [58] and the GHOST model proposed in [6].

2.2.1 Angular integration (AI) approach for distributed fiber reinforcing

As discussed previously, if the symmetry groups of a material contain only two elements, $\mathbf{1}$ and $-\mathbf{1}$, then no conclusions regarding the form of the strain energy function can be made from the symmetry considerations. However, if the material is described as being multiply reinforced, then some information about the structure and composition must be available and can be used in the constitutive relation under certain assumptions. The assumptions we use are: *(i)* the additive split of the strain energy function W into the isotropic part ψ_{iso} and the contributions of each fiber family $\psi_{\text{f}}^{(i)}$; *(ii)* the dependence of fibers' contribution only on one scalar, *i.e.* $\psi_{\text{f}}^{(i)} = \psi_{\text{f}}^{(i)}(I_{\text{f}}^{(i)})$. These assumptions have been used in several studies (see [35] and references therein), in which the strain energy function of a material has the form

$$W = \hat{\psi}_{\text{iso}}(\mathbf{C}) + \sum_i \rho^{(i)} \psi_{\text{f}}^{(i)}(I_{\text{f}}^{(i)}), \tag{2.1}$$

Name	Meaning	Definition
tAI	Total Angular Integration (not used in practice: AI is used instead)	$\Psi_{\mathrm{f}} = \oint\limits_{\mathbb{U}^2} \rho(\mathbf{m}_0)\psi_{\mathrm{f}}(\mathbf{m}_0 \otimes \mathbf{m}_0 : \mathbf{C})d\omega.$
AI	Angular Integration with fiber exclusion	$\Psi_{\mathrm{f}} = \oint\limits_{\mathbb{U}^2} \rho(\mathbf{m}_0)\chi(\mathbf{m}_0 \otimes \mathbf{m}_0 : \mathbf{C})\psi_{\mathrm{f}}(\mathbf{m}_0 \otimes \mathbf{m}_0 : \mathbf{C})d\omega.$
GST	Generalized Structure Tensor	$\Psi_{\mathrm{f}} = \mathrm{tr}\mathbf{H}\,\psi_{\mathrm{f}}(\frac{\mathbf{H}}{\mathrm{tr}\mathbf{H}} : \mathbf{C}), \quad \mathbf{H} = \oint\limits_{\mathbb{U}^2} \rho(\mathbf{m}_0)\mathbf{m}_0 \otimes \mathbf{m}_0 d\omega.$
GSTx	Generalized Structure Tensor with fiber exclusion	$\Psi_{\mathrm{f}} = \mathrm{tr}\mathbf{H}\,\psi_{\mathrm{f}}(\frac{\mathbf{H}}{\mathrm{tr}\mathbf{H}} : \mathbf{C}),$ $\mathbf{H} = \begin{cases} \kappa\mathbf{1} + (1-3\kappa)\mathbf{a}_0 \otimes \mathbf{a}_0, \\ \qquad (1-3\kappa)\,(\mathbf{a}_0 \otimes \mathbf{a}_0 : \mathbf{C} - 1) > 0, \\ \kappa\mathbf{1}, \\ \qquad \kappa \leq \frac{1}{3}, \quad \mathbf{a}_0 \otimes \mathbf{a}_0 : \mathbf{C} \leq 1, \\ (1-2\kappa)\mathbf{1}, \\ \qquad \kappa > \frac{1}{3}, \quad \mathbf{a}_0 \otimes \mathbf{a}_0 : \mathbf{C} \geq 1. \end{cases}$ $\kappa = \pi \int_0^\pi \tilde{\rho}(\theta)\sin^3\theta d\theta,$ where $\rho(\mathbf{m}_0) = \tilde{\rho}(\arccos \mathbf{m}_0.\mathbf{a}_0).$
iGST	Generalized Structure Tensor with selective fiber exclusion from the integrand	$\Psi_{\mathrm{f}} = \mathrm{tr}\mathbf{H}\,\psi_{\mathrm{f}}(\frac{\mathbf{H}}{\mathrm{tr}\mathbf{H}} : \mathbf{C}),$ $\mathbf{H} = \oint\limits_{\mathbb{U}^2} \rho(\mathbf{m}_0)\chi(\mathbf{m}_0 \otimes \mathbf{m}_0 : \mathbf{C})\,\mathbf{m}_0 \otimes \mathbf{m}_0 d\omega$

Table 2.1: Summary of models for dispersed fiber reinforcing.

Model	AI, tAI	GST, GSTx, iGST
Sufficient condition	$\sum_{i=1}^m \rho^{(i)}(\mathbf{m}_0) = \sum_{i=1}^m \rho^{(i)}(\mathbf{Q}\mathbf{m}_0),$ $\forall \mathbf{m}_0 \in \mathbb{U}^2, \forall \mathbf{Q} \in \mathbb{Q}.$	$\bigcup_i \rho^{(i)}(\mathbf{m}_0) = \bigcup_i \rho^{(i)}(\mathbf{Q}\mathbf{m}_0),$ $\forall \mathbf{m}_0 \in \mathbb{U}^2, \forall \mathbf{Q} \in \mathbb{Q}.$

Table 2.2: Conditions sufficient for symmetry of a material reinforced by mechanically equivalent fibers.

where $\rho^{(i)}$ is a weighting factor reflecting the amount of fibers in ith family, $I_{\mathrm{f}}^{(i)} = \mathbf{F}\mathbf{a}_0^{(i)}.\mathbf{F}\mathbf{a}_0^{(i)} = \mathbf{a}_0^{(i)} \otimes \mathbf{a}_0^{(i)} : \mathbf{C}$ is the square of fiber stretch, $\mathbf{a}_0^{(i)}$ is a unit vector in the ith family's direction and $\hat{(\bullet)}$ signifies that the quantity $(\bullet)$ is expressed as a function of $\mathbf{C}$ rather than a function of $\mathbf{F}$, which is always possible for isotropic functions.

If all fiber families are mechanically equivalent, *i.e.* $\psi_{\mathrm{f}}^{(i)}(I_{\mathrm{f}}^{(i)}) = \psi_{\mathrm{f}}(I_{\mathrm{f}}^{(i)})$, then (2.1) can be naturally generalized to the case of continuously distributed fibers

$$W = \hat{\psi}_{\mathrm{iso}}(\mathbf{C}) + \oint_{\mathbb{U}^2} \rho \psi_{\mathrm{f}}(I_{\mathrm{f}}) d\omega, \tag{2.2}$$

where $\mathbb{U}^2 = \{\mathbf{m}_0 \in \mathbb{R}^3, \text{ s.t. } |\mathbf{m}_0| = 1\}$ is the unit sphere, $d\omega$ is surface element area in the reference direction, $I_{\mathrm{f}} = \mathbf{m}_0 \otimes \mathbf{m}_0 : \mathbf{C}$ is the squared stretch in that direction, and $\rho = \rho(\mathbf{m}_0)$ is an *orientation density function* (ODF), also called a *probability density function* by other authors. When a normalization condition is imposed, we use the form

$$\oint_{\mathbb{U}^2} \rho d\omega = 1. \tag{2.3}$$

as opposed to $\oint_{\mathbb{U}^2} \rho d\omega = 4\pi$, which is used in [22, 35, 58] (with the change $\rho \to \frac{1}{4\pi}\rho$ for comparison). Without loss of generality, it can be assumed that $\rho(\mathbf{m}_0) = \rho(-\mathbf{m}_0)$ holds, since the replacement $\rho(\mathbf{m}_0) \to \frac{1}{2}\left(\rho(\mathbf{m}_0) + \rho(-\mathbf{m}_0)\right)$ does not change the strain energy (2.2).

By analogy, the strain energy function of a material reinforced by m families of distributed fibers reads

$$W = \psi_{\mathrm{iso}} + \Psi_{\mathrm{f}}, \tag{2.4}$$

with

$$\Psi_{\mathrm{f}} = \sum_{i=1}^{m} \oint_{\mathbb{U}^2} \rho^{(i)}(\mathbf{m}_0) \psi_{\mathrm{f}}^{(i)}(I_{\mathrm{f}}) d\omega, \tag{2.5}$$

where the ith fiber family is characterized by a strain energy function $\psi_{\mathrm{f}}^{(i)}$ and an ODF

$\rho^{(i)}$. The Cauchy stress is then given by

$$\boldsymbol{\sigma} = -p\mathbf{1} + \boldsymbol{\sigma}_{\text{iso}} + \boldsymbol{\sigma}_{\text{f}} = -p\mathbf{1} + 2\mathbf{F}\frac{\partial \psi_{\text{iso}}}{\partial \mathbf{C}}\mathbf{F}^T + 2\mathbf{F}\frac{\partial \Psi_{\text{f}}}{\partial \mathbf{C}}\mathbf{F}^T. \tag{2.6}$$

When applying equation (2.6) directly to the strain energy (2.5) one obtains

$$\boldsymbol{\sigma}_{\text{f}} = 2\mathbf{F}\left(\sum_{i=1}^{m}\oint_{\mathbb{U}^2}\rho^{(i)}(\mathbf{m}_0)\psi_{\text{f}}^{(i)\prime}(I_{\text{f}})\mathbf{m}_0\otimes\mathbf{m}_0 d\omega\right)\mathbf{F}^T. \tag{2.7}$$

This way of computing the Cauchy stress generated by fibers is called *angular integration* (AI) [7, 58, 64], as the total stress is given by angular integration of fiber fractions' stresses.

2.2.2 Exclusion of contracted fibers

In order to make sure that the fraction of undulated fibers does not contribute to the strain energy, one can introduce an additional multiplier χ into the integrand in (2.5), which takes values of 0 or 1 indicating whether fibers are compressed or not,

$$\chi(I_{\text{f}}) = \begin{cases} 1, & I_{\text{f}} = \mathbf{m}_0\otimes\mathbf{m}_0 : \mathbf{C} > 1, \\ 0, & I_{\text{f}} = \mathbf{m}_0\otimes\mathbf{m}_0 : \mathbf{C} \leq 1. \end{cases} \tag{2.8}$$

The total fiber strain energy and the Cauchy stress become

$$\Psi_{\text{f}} = \sum_{i=1}^{m}\oint_{\mathbb{U}^2}\rho^{(i)}(\mathbf{m}_0)\chi(I_{\text{f}})\psi_{\text{f}}^{(i)}(I_{\text{f}})d\omega, \tag{2.9}$$

$$\boldsymbol{\sigma}_{\text{f}} = 2\mathbf{F}\left(\sum_{i=1}^{m}\oint_{\mathbb{U}^2}\rho^{(i)}(\mathbf{m}_0)\chi(I_{\text{f}})\psi_{\text{f}}^{(i)\prime}(I_{\text{f}})\mathbf{m}_0\otimes\mathbf{m}_0 d\omega\right)\mathbf{F}^T. \tag{2.10}$$

The conversion of (2.5) and (2.7) into (2.9) and (2.10) is equivalent to the modi-

fication of the fiber potential

$$\psi_{\mathrm{f}}^{(i)}(I_{\mathrm{f}}) \to \chi(I_{\mathrm{f}})\psi_{\mathrm{f}}^{(i)}(I_{\mathrm{f}}), \qquad \psi_{\mathrm{f}}^{(i)\prime}(I_{\mathrm{f}}) \to \chi(I_{\mathrm{f}})\psi_{\mathrm{f}}^{(i)\prime}(I_{\mathrm{f}}), \tag{2.11}$$

which is done to exclude the response of compressed fibers. An equivalent way of thinking about this conversion is to regard χ as the characteristic function of the set of tensile directions. This would correspond to a substitution

$$\rho^{(i)}(\mathbf{m}_0) \to \chi(I_{\mathrm{f}})\rho^{(i)}(\mathbf{m}_0), \tag{2.12}$$

wherein the implicit dependence of the left-hand side on the deformation tensor $\mathbf{C}$ is assumed.

Note that in the literature the factor χ may not be explicitly included in the equations (2.9), (2.10), yet the response of compressed fibers is excluded (*e.g.* as in [7]). Following [7, 58] we refer to the model (2.9), (2.10) with fiber exclusion as "AI". In order to further avoid ambiguity, we identify the model (2.5), (2.7), which integrates contracted fibers alongside with their extended counterparts, with the acronym "tAI" standing for the *total angular integration*.

2.2.3 Generalized structure tensor approach for distributed fiber reinforcing

The generalized structure tensor (GST) approach was introduced in [22] and is based on the truncated series expansion of the anisotropic part of strain energy in the tAI approach, as noticed in [58]. We provide the derivation of the GST model from the tAI approach, similar to the derivation given in [58], but without requiring the ODFs to be normalized. This difference is key for the correct formulation of the alternative GST model, as discussed in Section 2.2.5.

We define an averaging operator induced by an ODF ρ as

$$\langle \bullet \rangle_\rho = \oint_{\mathbb{U}^2} \rho(\mathbf{m}_0) \bullet d\omega, \tag{2.13}$$

where $\bullet$ denotes a scalar or tensor quantity. The normalized counterpart of (2.13) is defined by

$$[\bullet]_\rho = \frac{\langle \bullet \rangle_\rho}{\langle 1 \rangle_\rho} = \frac{\oint_{\mathbb{U}^2} \rho(\mathbf{m}_0) \bullet d\omega}{\oint_{\mathbb{U}^2} \rho(\mathbf{m}_0) d\omega}. \tag{2.14}$$

Consider the Taylor expansion of $\psi_{\mathrm{f}}(I_{\mathrm{f}})$ about $I_{\mathrm{f}} = [I_{\mathrm{f}}]_\rho$

$$\psi_{\mathrm{f}}(I_{\mathrm{f}}) = \psi_{\mathrm{f}}([I_{\mathrm{f}}]_\rho) + \psi'_{\mathrm{f}}([I_{\mathrm{f}}]_\rho) \cdot (I_{\mathrm{f}} - [I_{\mathrm{f}}]_\rho) + O\left((I_{\mathrm{f}} - [I_{\mathrm{f}}])_\rho)^2\right). \tag{2.15}$$

By omitting higher order terms and by applying $[\bullet]_\rho$ to both sides we obtain

$$[\psi_{\mathrm{f}}(I_{\mathrm{f}})]_\rho \approx \psi_{\mathrm{f}}([I_{\mathrm{f}}]_\rho)[1]_\rho + \psi'_{\mathrm{f}}([I_{\mathrm{f}}]_\rho) \cdot [(I_{\mathrm{f}} - [I_{\mathrm{f}}]_\rho)]_\rho. \tag{2.16}$$

Using $[1]_\rho = 1$ and $[I_{\mathrm{f}} - [I_{\mathrm{f}}]_\rho]_\rho = 0$, we obtain

$$\langle \psi_{\mathrm{f}}(I_{\mathrm{f}}) \rangle_\rho \quad \approx \quad \langle 1 \rangle_\rho \cdot \psi_{\mathrm{f}}(\frac{\langle I_{\mathrm{f}} \rangle_\rho}{\langle 1 \rangle_\rho}). \tag{2.17}$$

This approximation forms the basis of the generalized structure tensor (GST) approach, where the GST is defined as

$$\mathbf{H} = \langle \mathbf{m}_0 \otimes \mathbf{m}_0 \rangle_\rho. \tag{2.18}$$

The right-hand side of (2.17) can then be written

$$\langle 1 \rangle_\rho \cdot \psi_{\mathrm{f}}(\frac{\langle I_{\mathrm{f}} \rangle_\rho}{\langle 1 \rangle_\rho}) = \mathrm{tr}\mathbf{H} \psi_{\mathrm{f}}(\frac{\mathbf{H} : \mathbf{C}}{\mathrm{tr}\mathbf{H}}),$$

whereas the left-hand side of (2.17) equals $\oint_{\mathbb{U}^2} \rho\psi_{\mathrm{f}}(I_{\mathrm{f}})d\omega$. Therefore (2.17) approximates the total angularly integrated fiber strain energy by strain energy computed via a GST.

In a material reinforced by fiber families with potentials $\psi_{\mathrm{f}}^{(i)}$ and ODFs $\rho^{(i)}$, we define for each fiber family a GST as $\mathbf{H}^{(i)} = \langle \mathbf{m}_0 \otimes \mathbf{m}_0 \rangle_{\rho^{(i)}}$. These GSTs are objective and symmetric tensors, do not depend on the deformation, and serve as an alternative representation of structural data (see Remark below). The total fiber energy reads

$$\Psi_{\mathrm{f}} = \sum_i \mathrm{tr}\mathbf{H}^{(i)} \cdot \psi_{\mathrm{f}}^{(i)}\left(\frac{\mathbf{H}^{(i)}}{\mathrm{tr}\mathbf{H}^{(i)}} : \mathbf{C}\right), \tag{2.19}$$

and the stress is given by

$$\boldsymbol{\sigma}_{\mathrm{f}} = 2\mathbf{F}\left(\sum_i \mathbf{H}^{(i)}\psi_{\mathrm{f}}^{(i)\prime}(\mathbf{H}^{(i)} : \mathbf{C}/\mathrm{tr}\mathbf{H}^{(i)})\right)\mathbf{F}^T. \tag{2.20}$$

The approach that uses (2.18) together with (2.19), (2.20) is henceforth referred to as *the GST approach*. Note that if the ODFs $\rho^{(i)}$ satisfy (2.3), the term $\mathrm{tr}\mathbf{H}^{(i)} = 1$ can be omitted in (2.19), (2.20).

Although the GST approach can be thought as an independent way to model anisotropic material behavior, we prefer to regard it, based on (2.17), as an approximation to the AI approach. For a discussion of adequacy and accuracy of the GST model see *e.g.* [7, 18, 35, 58].

It has been noted by Cortes et al. [7] that the AI and GST formulations are equivalent in the case of spherical deformations and in the absence of dispersion (*i.e.* perfect fiber alignment). They also showed a clear difference between the two approaches in the case of isotropic fiber distribution, where, unlike the AI approach, the GST approach predicts that the second Piola-Kirchhoff stress is isotropic for all deformations. This illustrates well the problem of compressed fibers: for some deformations a very small portion of fibers is extended and generates stress, whereas the majority of fibers

are compressed and relaxed (according to the AI). Nevertheless, the great tensile stress generated by the extended fibers is redistributed by the GST over all the fibers, as if the contracted fibers responded with a tensile stress.

From a computational point of view, the GST approach is vastly superior, as the angular integration has to be performed only once, to compute the GSTs, which stay constant for all deformations, as long as $\rho^{(i)}$ do not change. Also, the derivative of fiber potential $\psi_{\mathrm{f}}^{(i)\prime}$ needs to be evaluated only once for a given value of the deformation tensor $\mathbf{C}$. These two circumstances make it impossible to selectively exclude the response of compressed fraction of fibers. A mechanism that accounts for compressed fibers in the case of axisymmetrical ODFs has been suggested by Gasser et al. [22] and Holzapfel and Ogden [35]. We discuss it below and later consider an alternative approach.

Remark 1. If all the fibers are mechanically equivalent, the number of families and their split into families is somewhat arbitrary. The split does not matter in the AI model, but has an effect in the GST approach. The number of families and the distribution of fibers over them can be motivated, for example, by a desire to approximate the observed real-world structural data by transversely isotropic ODFs. Also note that the symmetric tensor $\mathbf{H}$ can be regarded as an operator, whose linear nature reduces the structural description of a fiber family from a function $\rho(\mathbf{m}_0)$ to six scalar components. The cardinality of the set of all possible $\mathbf{H}$ is less than the cardinality of the set of all admissible $\rho(\mathbf{m}_0)$, therefore the loss of information in structural data associated with the linearization (2.17) is unavoidable.

2.2.4 GST for axisymmetric dispersion and accounting for contracted fibers (GSTx)

Of particular interest are transversely isotropic, or axisymmetric, ODFs

$$\rho^{(i)}(\mathbf{m}_0) = \tilde{\rho}^{(i)}(\theta) = \tilde{\rho}^{(i)}(-\theta), \quad \theta = \arccos(\mathbf{m}_0.\mathbf{a}_0), \tag{2.21}$$

which define a fiber dispersion around the mean fiber directions $\mathbf{a}_0^{(i)}$. GSTs for such ODFs take the special form

$$\mathbf{H}^{(i)} = \kappa^{(i)}\mathbf{1} + (1 - 3\kappa^{(i)})\mathbf{a}_0^{(i)} \otimes \mathbf{a}_0^{(i)}, \tag{2.22}$$

where $\kappa^{(i)} = \pi \int_0^\pi \tilde{\rho}^{(i)}(\theta) \sin^3\theta d\theta \in [0, \frac{1}{2}]$ is the dispersion parameter [22]. The complete alignment in the direction $\mathbf{a}_0^{(i)}$, the isotropic distribution, and the complete alignment in the plane perpendicular to $\mathbf{a}_0^{(i)}$ correspond to the values $\kappa^{(i)} = 0, \frac{1}{3}, \frac{1}{2}$ respectively [35]. Apart from the case $\kappa^{(i)} = 0$ and $\frac{1}{2}$ different distributions may lead to the same parameter $\kappa^{(i)}$. For example, the value $\kappa^{(i)} = \frac{1}{3}$ also corresponds to the case when the fiber distribution forms a cone, whose generatrix and axis make an angle $\Theta^* = \arctan\sqrt{2}$, *i.e.* $\tilde{\rho}(\theta) = \delta(\Theta^* - \theta)$. This angle is known as the *magic angle* and arises in various areas, see *e.g.* [31, 24].

The form of the GST in (2.22) allows to express the mean square of fiber stretch through the invariants of a transversely reinforced material, $I_1 = \mathrm{tr}\mathbf{C}$, $I_4^{(i)} = \mathbf{a}_0^{(i)} \otimes \mathbf{a}_0^{(i)} : \mathbf{C}$,

$$\langle I_\mathrm{f} \rangle_{\rho^{(i)}} = \mathbf{H}^{(i)} : \mathbf{C} = (1 - 3\kappa^{(i)})I_4^{(i)} + \kappa I_1. \tag{2.23}$$

It also makes possible to address the issue of compressive fiber response by annihilating the anisotropic part of $\mathbf{H}$ if the stretch in the main direction is compressive ($\mathbf{a}_0 \otimes \mathbf{a}_0 : \mathbf{C} - 1 < 0$), as suggested by Gasser et al. [22] and Holzapfel and Ogden [35], in which

case we have

$$\mathbf{H}^{(i)} = \begin{cases} \kappa^{(i)}\mathbf{1} + (1-3\kappa^{(i)})\mathbf{a}_0^{(i)} \otimes \mathbf{a}_0^{(i)}, & \mathbf{a}_0^{(i)} \otimes \mathbf{a}_0^{(i)} : \mathbf{C} > 1, \\ \kappa^{(i)}\mathbf{1}, & \mathbf{a}_0^{(i)} \otimes \mathbf{a}_0^{(i)} : \mathbf{C} \leq 1, \end{cases} \tag{2.24}$$

and equations (2.19), (2.20) should be used as before.

Holzapfel and Ogden [35] observed that values of κ from $(\frac{1}{3}, \frac{1}{2}]$ yield negative pressure in an inflated thin-walled tube and concluded that these values are therefore unphysical. Similarly, in the uniaxial tension along the main fiber direction a physically meaningless combination of negative stress $\sigma < 0$ and positive strain $\lambda > 1$ can be observed for $\kappa \in (\frac{1}{3}, \frac{1}{2}]$. This can be understood by considering the following setup. Let $\mathbf{a}_0 = (1,0,0)$, $\mathbf{F} = \mathrm{diag}(\lambda, \lambda^{-1/2}, \lambda^{-1/2})$, $\boldsymbol{\sigma} = \mathrm{diag}(\sigma, 0, 0)$, and neglect the role of the ground substance other than the incompressibility. From (2.6) and (2.22) we have

$$I_\mathrm{f} = (1-2\kappa)\lambda^2 + 2\kappa\lambda^{-1}, \tag{2.25}$$

$$\sigma = \left((1-2\kappa)\lambda^2 - \kappa\lambda^{-1}\right)\psi_\mathrm{f}'(I_\mathrm{f}). \tag{2.26}$$

It follows that

$$I_\mathrm{f} - 1 \leq 0 \quad \Leftrightarrow \quad \kappa \geq \frac{\lambda + \lambda^2}{2(1+\lambda+\lambda^2)}, \tag{2.27}$$

$$\left((1-2\kappa)\lambda^2 - \kappa\lambda^{-1}\right) \leq 0 \quad \Leftrightarrow \quad \kappa \geq \frac{\lambda^3}{2\lambda^3+1}, \tag{2.28}$$

which implies that σ changes sign at both $\kappa = \lambda^3/(2\lambda^3+1)$ and $\kappa = (\lambda+\lambda^2)/(1+\lambda+\lambda^2)/2$, given that $\mathrm{sgn}(\psi_\mathrm{f}') = \mathrm{sgn}(I_\mathrm{f} - 1)$. The corresponding values of λ belong to the interval $(1, +\infty)$ if $\kappa > \frac{1}{3}$ and to the interval $(0,1)$ if $\kappa < \frac{1}{3}$. Thus, we have a region with negative stress and positive strain (Figure 2.2.a, solid line) for $\kappa > \frac{1}{3}$. For $\kappa < \frac{1}{3}$ we observe the converse situation, *i.e.* tensile stress in the contracted direction (Figure 2.2.b, solid line). However, when one computes the GST using (2.24)

instead of (2.22), contraction in the axial direction always results in compressive stress (Figure 2.2.b, dashed line). The analogy between extension or contraction in the mean fiber direction and the values $\kappa > \frac{1}{3}$ or $\kappa < \frac{1}{3}$ together with respect to the exclusion of compressed fibers suggests that the issue is not in the values $\kappa \in (\frac{1}{3}, \frac{1}{2}]$ *per se*, but rather in the GST definition (2.24), which requires different refinement to treat appropriately compressed fibers for $\kappa \in (\frac{1}{3}, \frac{1}{2}]$. We propose to correct this problem by defining the GST for transversely isotropic fiber distribution as

$$\mathbf{H}^{(i)} = \begin{cases} \kappa^{(i)}\mathbf{1} + (1-3\kappa^{(i)})\mathbf{a}_0^{(i)} \otimes \mathbf{a}_0^{(i)}, & (1-3\kappa^{(i)})\left(\mathbf{a}_0^{(i)} \otimes \mathbf{a}_0^{(i)} : \mathbf{C} - 1\right) > 0, \\ \kappa^{(i)}\mathbf{1}, & \kappa^{(i)} \leq \frac{1}{3}, \quad \mathbf{a}_0^{(i)} \otimes \mathbf{a}_0^{(i)} : \mathbf{C} \leq 1, \\ (1-2\kappa^{(i)})\mathbf{1}, & \kappa^{(i)} > \frac{1}{3}, \quad \mathbf{a}_0^{(i)} \otimes \mathbf{a}_0^{(i)} : \mathbf{C} \geq 1. \end{cases} \tag{2.29}$$

This modified GST is justified by the following proposition, which considers not only transversely symmetric but rather general isochoric deformations, defined by $\det \mathbf{C} = 1$.

Proposition 2. *Let* $\mathbf{H} = \kappa\mathbf{1} + (1-3\kappa)\mathbf{a}_0 \otimes \mathbf{a}_0$. *For* $\kappa \in [0, \frac{1}{3})$

- all isochoric deformations that extend the main fiber direction $\mathbf{a}_0$ (*i.e.* $\mathbf{a}_0 \otimes \mathbf{a}_0 : \mathbf{C} \geq 1$) result in an average extension of the fibers (*i.e.* $\mathbf{H} : \mathbf{C} \geq 1$);
- there exist isochoric deformations that contract the main fiber direction $\mathbf{a}_0$ (*i.e.* $\mathbf{a}_0 \otimes \mathbf{a}_0 : \mathbf{C} < 1$) and also contract the fibers on average (*i.e.* $\mathbf{H} : \mathbf{C} < 1$).

Contrariwise, for $\kappa \in (\frac{1}{3}, \frac{1}{2}]$

- all isochoric deformations that contract the main fiber direction $\mathbf{a}_0$ (*i.e.* $\mathbf{a}_0 \otimes \mathbf{a}_0 : \mathbf{C} < 1$) result in the fibers being extended on average (*i.e.* $\mathbf{H} : \mathbf{C} > 1$);
- there exist isochoric deformations that extend the main fiber direction $\mathbf{a}_0$ (*i.e.* $\mathbf{a}_0 \otimes \mathbf{a}_0 : \mathbf{C} > 1$) but contract fibers on average (*i.e.* $\mathbf{H} : \mathbf{C} < 1$).

Proof. We demonstrate this for $\kappa < 1/3$. To ensure that the inequality

$$\mathbf{H} : \mathbf{C} - 1 = (1 - 3\kappa)(I_4 - 1) + \kappa(I_1 - 3) \geq 0 \tag{2.30}$$

holds, we notice that $(1-3\kappa)(I_4-1) > 0$ holds by assumption, whereas $I_1-3 \geq 0$ holds by virtue of incompressibility and the inequality between geometric and arithmetic means,

$$1 = \sqrt[3]{\lambda_1^2\lambda_2^2\lambda_3^2} \leq \frac{\lambda_1^2 + \lambda_2^2 + \lambda_3^2}{3},$$

which establishes (a).

To show (b), we construct an example. We consider a tensor $\mathbf{C}$, whose first principal axis coincides with $\mathbf{a}_0 = (1, 0, 0)$. We have $I_4 = \lambda_1^2$, $I_1 = \lambda_1^2 + \lambda_2^2 + \lambda_1^{-2}\lambda_2^{-2}$ and $\mathbf{H} : \mathbf{C} = (1 - 2\kappa)\lambda_1^2 + \kappa\lambda_2^2 + \kappa\lambda_1^{-2}\lambda_2^{-2}$. Therefore,

$$[I_\mathrm{f}]_{\lambda_{1,2}=1} = 1, \tag{2.31}$$

$$\left[\frac{d}{d(\lambda_1^2)} I_\mathrm{f}\right]_{\lambda_{1,2}=1} = \left[1 - 2\kappa - \kappa\lambda_1^{-4}\lambda_2^{-2}\right]_{\lambda_{1,2}=1} > 0. \tag{2.32}$$

Hence, there exists $\epsilon > 0$ small enough, so that $\mathbf{C} = \mathrm{diag}(1-\epsilon, 1, \frac{1}{1-\epsilon})$ implies $I_4-1 < 0$ and $I_\mathrm{f} < 1$ simultaneously. □

We conclude using the Proposition 2 that definition (2.29) provides a mechanism of exclusion of compressed fibers, so that an isochoric deformation always results in an average extension of fibers ($\mathbf{H}^{(i)} : \mathbf{C} \geq 1$) for any $\kappa^{(i)}$. The approach that uses (2.29) together with (2.19), (2.20) is later referred to as the *GSTx model*, where "x" refers to "exclusion". Similarly to the GST model, it is not necessary to integrate for each deformation, and the integration can be performed only once, to compute the dispersion parameter $\kappa^{(i)}$.

Remark 3. Note that the stress-strain curves shown in Figures 2.2.a, 2.2.b (dashed lines) are not smooth at $\lambda = 1$, when the anisotropic part of the GST is being excluded.

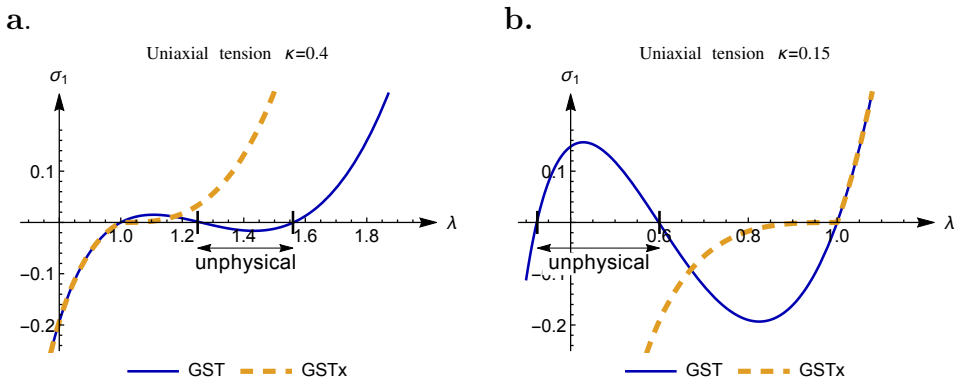

Figure 2.2: Material response in uniaxial tension as given by (2.26) with $\psi_{\rm f}(I_{\rm f}) = \frac{k_1}{2k_2}\exp\left[k_2(I_{\rm f}-1)^2\right]$, $k_1 = 4$, $k_2 = 1$. **a.** $\kappa = .4$; **b.** $\kappa = .15$. The solid lines show the response of the model where the GST is defined by (2.22). The dashed lines correspond to the GST defined by (2.29) in **a.** and by (2.24) or (2.29) in **b**.

Moreover, the fiber stress is, in general, discontinuous at $\mathbf{a}_0^{(i)} \otimes \mathbf{a}_0^{(i)} : \mathbf{C} = 1$, since both $I_{\rm f}^{(i)} = \mathbf{H}^{(i)} : \mathbf{C}/\mathrm{tr}\mathbf{H}^{(i)}$ and $\mathbf{F}\mathbf{H}^{(i)}\mathbf{F}^T$ in (2.20) suffer a jump. The reason for the absence of jump in Figure 2.2 is that the point $\lambda = 1$ corresponded to the unstrained main fiber direction ($\mathbf{a}_0 \otimes \mathbf{a}_0 : \mathbf{C} = 1$) and the unstrained fibers on average ($I_{\rm f} = 1$) at the same time, which may not happen generally, *e.g.* when a transverse direction is subject to stretch or load. In order to remove this discontinuity, one should avoid using the second and third lines of (2.29) and use a different definition for the model in the region of compressed mean fiber direction. For instance, the continuity is preserved if $\mathbf{F}\mathbf{H}^{(i)}\mathbf{F}^T$ and $I_{\rm f}^{(i)}$ are interpolated inside this region based on their values on the boundary of this region.

2.2.5 Alternative scheme for fiber exclusion in GST (iGST)

The compressed fibers in the GST definition (2.29) are taken into account after the approximation (2.17) was made. Alternatively, the contracted fibers can be excluded before the averaging takes place by replacing $\rho^{(i)}(\mathbf{m}_0)$ with $\chi(I_{\rm f})\rho^{(i)}(\mathbf{m}_0)$ in (2.13)-

(2.17). This leads to an alternative definition of the GST:

$$\mathbf{H} = \langle \mathbf{m}_0 \otimes \mathbf{m}_0 \rangle_{\chi\rho} = \oint_{\mathbb{U}^2} \rho(\mathbf{m}_0)\chi(\mathbf{m}_0 \otimes \mathbf{m}_0 : \mathbf{C})\mathbf{m}_0 \otimes \mathbf{m}_0 d\omega. \tag{2.33}$$

The approach that uses (2.33) together with (2.19), (2.20) is referred to as *iGST* (the "i" standing for "integration").

The GST defined by (2.33) differs from (2.18) in that it implicitly depends on the deformation through the factor χ. While the GST approach averages the fiber strain over all the fibers, iGST averages it only over fibers in extension, the amount of which is given by tr$\mathbf{H}$ and depends on a particular deformation. Similarly to the AI approach, integration over the unit sphere is required for each deformation, in order to compute $\mathbf{H}$. This nullifies the main computational advantage of the GST approach. However, unlike AI, this approach requires a single evaluation of the fiber potential derivative. Therefore the iGST approach is particularly useful in detecting the effect of strong fiber dispersion, as it captures correctly fibers that are in compression, yet it is very similar to the original GST model.

Remark 4. We previously mentioned that the transition from tAI to AI can be obtained using either of the substitutions (2.11) or (2.12). The iGST model is formally obtained from the GST model by (2.12). It suggests to investigate the outcome of applying (2.11) in (2.13)-(2.17). The result would be a model, identical to the GST model when the fibers are extended on average and which completely disregards fibers' presence when they are contracted on average.

2.2.6 Generalized higher-order structure tensor models (GHOST)

The idea of the GST model was further extended by Pandolfi and Vasta [58], who proposed so-called V-model, and by Cortes and Elliott [6], who introduced general-

ized high-order structure tensors (GHOSTs). Both are founded upon considering a truncated Taylor expansion of the fiber potential,

$$\psi(I_{\mathrm{f}}) = \sum_{n=0}^{\infty} \frac{1}{n!}\psi^{(n)}(\bar{I}_{\mathrm{f}}) \left(I_{\mathrm{f}} - \bar{I}_{\mathrm{f}}\right)^n \tag{2.34}$$

$$= \sum_{n=0}^{\infty}\sum_{p=0}^{n} \frac{(-1)^p}{p!(n-p)!}\psi^{(n)}(\bar{I}_{\mathrm{f}}) I_{\mathrm{f}}^{n-p}\bar{I}_{\mathrm{f}}^{p}, \tag{2.35}$$

where $\bar{I}_{\mathrm{f}} = \langle I_{\mathrm{f}}\rangle_{\rho}$, $I_{\mathrm{f}} = \mathbf{M} : \mathbf{C}$, $\mathbf{M} = \mathbf{m}_0 \otimes \mathbf{m}_0$. We have

$$\frac{\partial\psi(I_{\mathrm{f}})}{\partial\mathbf{C}} = \sum_{n=0}^{\infty}\sum_{p=0}^{n} \frac{(-1)^p}{p!(n-p)!}\frac{\partial}{\partial\mathbf{C}}\left(\psi^{(n)}(\bar{I}_{\mathrm{f}}) I_{\mathrm{f}}^{n-p}\bar{I}_{\mathrm{f}}^{p}\right) \tag{2.36}$$

$$= \sum_{n=0}^{\infty}\sum_{p=0}^{n} \frac{(-1)^p}{p!(n-p)!}\left(\psi^{(n+1)}(\bar{I}_{\mathrm{f}}) I_{\mathrm{f}}^{n-p}\bar{I}_{\mathrm{f}}^{p}\frac{\partial\bar{I}_{\mathrm{f}}}{\partial\mathbf{C}} + \right. \tag{2.37}$$

$$\left. p\psi^{(n)}(\bar{I}_{\mathrm{f}}) I_{\mathrm{f}}^{n-p}\bar{I}_{\mathrm{f}}^{p-1}\frac{\partial\bar{I}_{\mathrm{f}}}{\partial\mathbf{C}} + (n-p)\psi^{(n)}(\bar{I}_{\mathrm{f}}) I_{\mathrm{f}}^{n-p-1}\bar{I}_{\mathrm{f}}^{p}\frac{\partial I_{\mathrm{f}}}{\partial\mathbf{C}}\right). \tag{2.38}$$

In order to derive the stress-strain relation as proposed in [6], one has to neglect the dependence of the averaged stretch $\bar{I}_{\mathrm{f}}$ on the deformation by letting $\frac{\partial\bar{I}_{\mathrm{f}}}{\partial\mathbf{C}} = 0$, obtaining

$$\frac{\partial\psi(I_{\mathrm{f}})}{\partial\mathbf{C}} = \sum_{n=0}^{\infty}\sum_{p=0}^{n} \frac{(-1)^p}{p!(n-p)!}(n-p)\psi^{(n)}(\bar{I}_{\mathrm{f}}) I_{\mathrm{f}}^{n-p-1}\bar{I}_{\mathrm{f}}^{p}\mathbf{M}, \tag{2.39}$$

$$= \sum_{\tilde{n}=0}^{\infty}\sum_{p=0}^{n} \frac{(-1)^p}{p!(\tilde{n}-p)!}\psi^{(\tilde{n}+1)}(\bar{I}_{\mathrm{f}})\bar{I}_{\mathrm{f}}^{p} I_{\mathrm{f}}^{\tilde{n}-p}\mathbf{M}, \tag{2.40}$$

where we used $\tilde{n} = n - 1$ and the observation that $p = n$ produces a zero term. Applying the averaging operator yields an approximation to the 2nd Piola-Kirchhoff stress tensor,

$$\mathbf{S}_{\mathrm{f}} = 2\langle\frac{\partial\psi(I_{\mathrm{f}})}{\partial\mathbf{C}}\rangle_{\rho} = 2\sum_{n=0}^{\infty}\sum_{p=0}^{n} \frac{(-1)^p}{p!(n-p)!}\psi^{(n+1)}(\bar{I}_{\mathrm{f}})\bar{I}_{\mathrm{f}}^{p}\underbrace{\langle I_{\mathrm{f}}^{\tilde{n}-p}\mathbf{M}\rangle_{\rho}}_{\mathbf{I}_{\mathrm{f}}^{n-p+1}}, \tag{2.41}$$

where the *generalized high-order structure tensors* and the *structure stretch tensors* are defined respectively by

$$\mathbf{H}^n = \langle \underbrace{\mathbf{m}_0 \otimes \mathbf{m}_0 \otimes \cdots \otimes \mathbf{m}_0}_{2n\,\text{times}} \rangle_\rho = \langle \mathbf{m}_0^{\otimes 2n} \rangle_\rho, \tag{2.42}$$

$$\mathbf{I}_{\mathrm{f}}^{n+1} = \langle I_{\mathrm{f}}^n \mathbf{M} \rangle_\rho = \mathbf{H}^{n+1} \overset{2n}{\odot} \mathbf{C}^{\otimes n}, \tag{2.43}$$

where $\overset{l}{\odot}$ denotes the contraction of the last l indices of each argument. That is, if $\bullet$, $\star$ are tensors of orders n, m respectively, then $\bullet \overset{l}{\odot} \star$ is a tensor of order $n+m-2kl$ defined by

$$\left(\bullet \overset{l}{\odot} \star \right)_{i_1 \ldots i_{n+m-2l}} = \sum_{k_1,\ldots,k_l} \bullet_{i_1 \ldots i_{n-l} k_1 \ldots k_l} \star_{j_1 \ldots j_{m-l} k_1 \ldots k_l} . \tag{2.44}$$

Note that $\mathbf{H}^n$ is a tensor or order $2n$, while $\mathbf{I}_{\mathrm{f}}^n$ is always a second-order tensor, which expresses an oriented mean of a power of fiber stretch. The superscript of the structure stretch tensor $\mathbf{I}_{\mathrm{f}}^n$ corresponds to the order of the GHOST it is computed from. The mean $2n$th power of fiber stretch can be computed as

$$\langle I_{\mathrm{f}}^n \rangle_\rho = \mathbf{H}^n \overset{2n}{\odot} \mathbf{C}^{\otimes n} = \mathbf{I}_{\mathrm{f}}^n : \mathbf{C}.$$

The correctness of neglecting $\frac{\partial \bar{I}_{\mathrm{f}}}{\partial \mathbf{C}}$ terms in transition from (2.36) to (2.39) is questionable, as the average square of fiber stretch clearly depends on the deformation. Cortes and Elliot [6] argue that $\bar{I}_{\mathrm{f}}$ *"...is considered as a constant parameter for derivation purposes, since it was used as the center of the Taylor expansion"*. We observe that the same expressions can be obtained in a more elegant way, which avoids equating $\frac{\partial \bar{I}_{\mathrm{f}}}{\partial \mathbf{C}}$ to zero. One starts from the 2nd Piola-Kirchhoff stress generated by fibers, as provided by the AI model,

$$\mathbf{S}_{\mathrm{f}} = 2 \langle \frac{\partial \psi(I_{\mathrm{f}})}{\partial \mathbf{C}} \rangle_\rho = 2 \langle \psi'(I_{\mathrm{f}}) \frac{\partial I_{\mathrm{f}}}{\partial \mathbf{C}} \rangle_\rho, \tag{2.45}$$

where the fiber potential derivative ψ' is replaced by its Taylor expansion,

$$\psi'(I_{\rm f}) \;=\; \sum_{n=0}^{\infty}\sum_{p=0}^{n}\frac{(-1)^p}{p!(n-p)!}\psi^{(n+1)}(\bar{I}_{\rm f})I_{\rm f}^{n-p}\bar{I}_{\rm f}^{p}. \tag{2.46}$$

This yields

$$\mathbf{S}_{\rm f} \;=\; 2\sum_{n=0}^{\infty}\sum_{p=0}^{n}\frac{(-1)^p}{p!(n-p)!}\psi^{(n+1)}(\bar{I}_{\rm f})\bar{I}_{\rm f}^{p}\langle I_{\rm f}^{n-p}\mathbf{M}\rangle_{\rho}, \tag{2.47}$$

which is identical to (2.41).

In practice it is possible to use only finitely many terms in the expansion, and we define the *CE-type GHOST model* of order up to $2n_{\max}$ by the following stress-strain relation:

$$\mathbf{S}_{\rm f} = \;2\textstyle\sum_{n=0}^{n_{\max}-1}\sum_{p=0}^{n}\frac{(-1)^p}{p!(n-p)!}\psi^{(n+1)}(\bar{I}_{\rm f})\bar{I}_{\rm f}^{p}\underbrace{\mathbf{H}^{n-p+1}\overset{2(n-p)}{\odot}\mathbf{C}^{\otimes n-p}}_{\mathbf{I}_{\rm f}^{n-p+1}}. \tag{2.48}$$

For example, the case $n_{\max}=2$ is called *4ST model* [6],

$$\mathbf{S}_{\rm f} = 2\psi'(\bar{I}_{\rm f})\mathbf{H} + 2\psi''(\bar{I}_{\rm f})\left(\mathbf{H}^2:\mathbf{C} - (\mathbf{H}:\mathbf{C})\mathbf{H}\right), \tag{2.49}$$

where $\mathbf{H}^2$ is a 4th order tensor.

One consequence of expanding ψ' instead of ψ (*i.e.* neglecting $\frac{\partial \bar{I}_{\rm f}}{\partial \mathbf{C}}$) is that the resulting stress-strain relation does not in general preserve energy, at least when a finite number of terms is considered (see Remark 5), meaning that such material is not hyperelastic. To circumvent this problem a variant that preserves the $\frac{\partial \bar{I}_{\rm f}}{\partial \mathbf{C}}$ terms and ensures the hyperelastic reponse is considered here. We define the *PV-type GHOST model* by the following strain energy function,

$$\langle\psi(I_{\rm f})\rangle_{\rho} = \;\textstyle\sum_{n=0}^{n_{\max}}\sum_{p=0}^{n}\frac{(-1)^p}{p!(n-p)!}\psi^{(n)}(\bar{I}_{\rm f})\langle I_{\rm f}^{n-p}\rangle_{\rho}\bar{I}_{\rm f}^{p}. \tag{2.50}$$

The 2nd Piola-Kirchhoff stress tensor is then given by

$$\mathbf{S}_{\mathrm{f}} = 2\sum_{n=0}^{n_{\max}}\sum_{p=0}^{n}\frac{(-1)^p}{p!(n-p)!}\left(\left(\psi^{(n+1)}(\bar{I}_{\mathrm{f}})\bar{I}_{\mathrm{f}}^{p}+p\psi^{(n)}(\bar{I}_{\mathrm{f}})\bar{I}_{\mathrm{f}}^{p-1}\right)\mathbf{H}\langle I_{\mathrm{f}}^{n-p}\rangle+\right. \tag{2.51}$$

$$\left.(n-p)\psi^{(n)}(\bar{I}_{\mathrm{f}})\bar{I}_{\mathrm{f}}^{p}\langle I_{\mathrm{f}}^{n-p-1}\mathbf{M}\rangle_{\rho}\right). \tag{2.52}$$

The case $n_{\max}=2$ is the *V-model* introduced by Pandolfi and Vasta in [58]:

$$\langle\frac{\partial\psi(I_{\mathrm{f}})}{\partial\mathbf{C}}\rangle_{\rho}=\psi'(\bar{I}_{\mathrm{f}})\mathbf{H}+\psi''(\bar{I}_{\mathrm{f}})\left(\mathbf{I}_{\mathrm{f}}^{2}-\mathbf{H}\bar{I}_{\mathrm{f}}\right)+\frac{1}{2}\psi'''(\bar{I}_{\mathrm{f}})\left(\langle I_{\mathrm{f}}^{2}\rangle_{\rho}-\bar{I}_{\mathrm{f}}^{2}\right)\mathbf{H}. \tag{2.53}$$

Similarly to GSTs, GHOSTs of any order (2.42) are objective, do not depend on the deformation and need to be computed only once for a given ODF. The GHOST model does not exclude compressed fibers from the integration, and as long as the ODF ρ is normalized so are the GHOSTs, *i.e.* $\mathbf{H}^{n}\overset{2n}{\odot}\mathbf{1}^{\otimes n}=1$. In principle, variants of GHOST models with selective fiber exclusion from the integrands can be considered. In this case the normalized averaging operator $[\bullet]_{\rho}$ should be used. In the case of transversely isotropic ODFs GHOSTs have a special form and can be expressed through $n_{\max}$ scalars. We provide a simplified method of computing GHOSTs and structure stretch tensors for the case of transversely isotropic distributions in Appendix A. The general expressions for the components of GHOSTs follow from (2.42) and can be found in [6].

Remark 5. We demonstrate that the stress-strain relation predicted by the GHOST model using tensors up to the 4th order cannot be given by a fiber potential. This is proved by contradiction: if the total fiber potential Ψ_{f} exists, then mixed derivatives

must commute, $\frac{\partial}{\partial \mathrm{C}_{11}}\frac{\partial \Psi_\mathrm{f}}{\partial \mathrm{C}_{22}} = \frac{\partial}{\partial \mathrm{C}_{22}}\frac{\partial \Psi_\mathrm{f}}{\partial \mathrm{C}_{11}}$, *i.e.* $\frac{\partial}{\partial \mathrm{C}_{11}}\mathrm{S}_{22} = \frac{\partial}{\partial \mathrm{C}_{22}}\mathrm{S}_{11}$. We have

$$\begin{aligned}
\frac{1}{2}\mathrm{S}_{\mathrm{f}ii} &= \psi'(\bar{I}_\mathrm{f})\mathrm{H}_{ii} + \psi''(\bar{I}_\mathrm{f})\left(\mathrm{H}^2_{iijj}\mathrm{C}_{jj} - \mathrm{H}_{ii}\mathrm{H}_{jj}\mathrm{C}_{jj}\right), \\
\frac{1}{2}\frac{\partial \mathrm{S}_{\mathrm{f}22}}{\partial \mathrm{C}_{11}} &= \psi''(\bar{I}_\mathrm{f})\mathrm{H}_{22}\mathrm{H}_{11} + \psi'''(\bar{I}_\mathrm{f})\mathrm{H}_{11}\left(\mathrm{H}^2_{22jj}\mathrm{C}_{jj} - \mathrm{H}_{22}\mathrm{H}_{jj}\mathrm{C}_{jj}\right) \\
&\quad + \psi''(\bar{I}_\mathrm{f})\left(\mathrm{H}^2_{2211} - \mathrm{H}_{22}\mathrm{H}_{11}\right), \\
\frac{1}{2}\frac{\partial \mathrm{S}_{\mathrm{f}11}}{\partial \mathrm{C}_{22}} &= \psi''(\bar{I}_\mathrm{f})\mathrm{H}_{11}\mathrm{H}_{22} + \psi'''(\bar{I}_\mathrm{f})\mathrm{H}_{22}\left(\mathrm{H}^2_{11jj}\mathrm{C}_{jj} - \mathrm{H}_{11}\mathrm{H}_{jj}\mathrm{C}_{jj}\right) \\
&\quad + \psi''(\bar{I}_\mathrm{f})\left(\mathrm{H}^2_{1122} - \mathrm{H}_{11}\mathrm{H}_{22}\right),
\end{aligned}$$

so that the equality of derivatives would imply $\mathrm{H}_{11}\mathrm{H}^2_{22jj} = \mathrm{H}_{22}\mathrm{H}^2_{11jj}$, which does not hold for an arbitrary orientation density function.

Chapter 3

Orthotropic fiber reinforced material in uniaxial tension

3.1 Introduction

Motivated by the importance of accurate and numerically efficient constitutive models for elastic materials with distributed fiber reinforcement, we analyze the relation between the AI approach and several variants of the GST model (Figure 2.1), and compare the prediction they provide. In contrast to other authors [7, 58], who use the relative error in stress as a measure of discrepancy between the models, we look for a qualitative attribute, which is less likely to be corrected by fitting parameters to the experimental observations. As such attribute we choose the ability of an incompressible material to expand in the transverse direction when stretched. This feature is somewhat similar to having a direction-dependent Poisson's ratio, which is positive in one direction and negative in another direction. However, when a nonlinear material is being progressively stretched, the transverse extension can be followed by contraction and vice versa (Figure 3.4). These changes between contraction and extension are called the *perversion points* of the transverse strain [24]. Multiple perversion points

result from the interplay between nonlinear mechanical properties and anisotropy. The number of these perversion points depends on the choice of model for dispersed fiber reinforcement and, therefore can be used to compare different models. Thus in this Chapter we pursue two goals simultaneously: we study the effect of fiber orientation and dispersion on perversion points and use this effect to identify qualitative differences between models for fiber dispersion.

3.2 Normal homogeneous deformations of orthotropic fiber-reinforced material

In the absence of shear the deformation gradient is given by a diagonal matrix $\mathbf{F} = \text{diag}(\lambda_1, \lambda_2, \lambda_3)$, where the basis vectors $\{\mathbf{e}_1, \mathbf{e}_2, \mathbf{e}_3\}$ are defined so that they align with the principal stretch directions. For brevity, we refer to a homogeneous deformation that produces a diagonal deformation gradient simply as a diagonal deformation. Likewise, a stress state that is described by a diagonal Cauchy stress tensor in the same basis is referred to as a diagonal stress. Principal stretch directions always coincide with the principal stress directions and diagonal deformations corresponds to diagonal stresses in isotropic materials. In contrast, in an anisotropic material a diagonal deformation can give rise to non-zero shear stress components. However, a diagonal deformation always results in a diagonal stress if the material is orthotropic and the planes of symmetry are aligned with the principal stretches. In this case the Cauchy stress tensor and the left Cauchy-Green deformation tensor $\mathbf{B} = \mathbf{F}\mathbf{F}^T$ are coaxial, *i.e.* $\boldsymbol{\sigma}\mathbf{B} = \mathbf{B}\boldsymbol{\sigma}$. We note here that the the coaxiality of these tensors was analysed in detail in [60] where universal relations were obtained. Our analysis could be seen as a particular case of this study.

3.3 Sufficient symmetry conditions

As pointed out earlier, ODFs satisfy $\rho(\mathbf{m}_0) = \rho(-\mathbf{m}_0)$, therefore the fiber strain energy is invariant with respect to the transformation $\mathbf{Q} = -\mathbf{1}$ (and so is the isotropic part of the strain energy). Hence, $-\mathbf{1}$ belongs to every material symmetry group, including the minimal symmetry group, which consists of only two elements.

Next, we consider a material reinforced by m distributed families of mechanically equivalent fibers. The ith family is characterized by an ODF $\rho^{(i)}$ and a reference direction $\mathbf{a}_0^{(i)}$, which also serves as the axis of symmetry in case of a transversely isotropic distribution. For each modeling approach we formulate sufficient conditions that the ODFs must satisfy in order for the material symmetry (1.48) to hold. The sufficient symmetry condition for the AI approach is weaker than that for the iGST, GST and GSTx approaches (Table 2.2). As (1.48) is automatically satisfied for an isotropic material and the additive split of strain energy is assumed, condition (1.48) should only be applied to the anisotropic part of the strain energy.

First, consider the AI total fiber strain energy (2.9). We have

$$\begin{aligned}\Psi_{\mathrm{f}}(\mathbf{FQ}) &= \oint_{\mathbb{U}^2} \sum_i \rho^{(i)}(\mathbf{m}_0)\chi(\mathbf{Qm}_0 \otimes \mathbf{Qm}_0 : \mathbf{C})\psi_{\mathrm{f}}(\mathbf{Qm}_0 \otimes \mathbf{Qm}_0 : \mathbf{C})d\omega \\ &= \oint_{\mathbb{U}^2} \sum_i \rho^{(i)}(\mathbf{Qm}_0)\chi(\mathbf{m}_0 \otimes \mathbf{m}_0 : \mathbf{C})\psi_{\mathrm{f}}(\mathbf{m}_0 \otimes \mathbf{m}_0 : \mathbf{C})d\omega, \end{aligned} \tag{3.1}$$

where we used the identity $\mathrm{tr}\left(\mathbf{m}_0 \otimes \mathbf{m}_0 \cdot \mathbf{Q}^T\mathbf{CQ}\right) = \mathbf{Qm}_0 \otimes \mathbf{Qm}_0 : \mathbf{C}$ and then made a substitution $\mathbf{Qm}_0 \to \mathbf{m}_0$, $\mathbb{U}^2 \to \mathbf{Q}\mathbb{U}^2 = \mathbb{U}^2$. Clearly, (1.48) is satisfied for the AI model if the total orientation density is symmetric with respect to $\mathbf{Q}$, *i.e.*

$$\sum_{i=1}^{m} \rho^{(i)}(\mathbf{m}_0) = \sum_{i=1}^{m} \rho^{(i)}(\mathbf{Qm}_0), \quad \forall \mathbf{m}_0 \in \mathbb{U}^2, \forall \mathbf{Q} \in \mathbb{Q}. \tag{3.2}$$

Next, consider total fiber strain energy (2.19) for the iGST, GST and GSTx models,

$$\Psi_{\mathrm{f}}(\mathbf{FQ}) = \sum_i \mathrm{tr}\mathbf{H}^{(i)}(\mathbf{FQ}) \cdot \psi_{\mathrm{f}}(\frac{\mathbf{H}^{(i)}(\mathbf{FQ})}{\mathrm{tr}\mathbf{H}^{(i)}(\mathbf{FQ})} : \mathbf{Q}^T\mathbf{CQ}) \tag{3.3}$$

$$= \sum_i \mathrm{tr}\mathbf{QH}^{(i)}(\mathbf{FQ})\mathbf{Q}^T \cdot \psi_{\mathrm{f}}(\frac{\mathbf{QH}^{(i)}(\mathbf{FQ})\mathbf{Q}}{\mathrm{tr}\mathbf{QH}^{(i)}(\mathbf{FQ})\mathbf{Q}^T} : \mathbf{C}). \tag{3.4}$$

The equality $\Psi_{\mathrm{f}}(\mathbf{FQ}) = \Psi_{\mathrm{f}}(\mathbf{F})$ holds if

$$\bigcup_i \mathbf{QH}^{(i)}(\mathbf{FQ})\mathbf{Q}^T = \bigcup_i \mathbf{H}^{(i)}(\mathbf{F}), \quad \forall \mathbf{Q} \in \mathbb{Q}. \tag{3.5}$$

In iGST a sufficient condition for material symmetry (1.48) is that the orientation density functions are globally symmetric, *i.e.*

$$\bigcup_i \rho^{(i)}(\mathbf{m}_0) = \bigcup_i \rho^{(i)}(\mathbf{Qm}_0), \quad \forall \mathbf{m}_0 \in \mathbb{U}^2, \forall \mathbf{Q} \in \mathbb{Q}, \tag{3.6}$$

since it implies (3.5), as can be seen from

$$\mathbf{QH}^{(i)}(\mathbf{FQ})\mathbf{Q}^T = \oint_{\mathbb{U}^2} \rho^{(i)}(\mathbf{m}_0)\chi(\mathbf{Qm}_0 \otimes \mathbf{Qm}_0 : \mathbf{C})\mathbf{Qm}_0 \otimes \mathbf{Qm}_0 d\omega \tag{3.7}$$

$$= \oint_{\mathbb{U}^2} \rho^{(i)}(\mathbf{Qm}_0)\chi(\mathbf{m}_0 \otimes \mathbf{m}_0 : \mathbf{C})\mathbf{m}_0 \otimes \mathbf{m}_0 d\omega. \tag{3.8}$$

By letting $\chi \equiv 1$, one arrives at the same conclusion for the GST model (2.18). Although the GSTx approach uses the mean fiber directions $\mathbf{a}_0^{(i)}$ in the GST definition, these directions are uniquely inferred from the transversely symmetric ODFs $\rho^{(i)}$ (with the exception of an isotropic fiber distribution case) and an additional symmetry restriction on fiber directions $\mathbf{a}_0^{(i)}$ are unnecessary. Thus, the global symmetry of orientation density functions (3.6) is sufficient for the material symmetry condition (1.48) to hold in all three GST models: GST, iGST, GSTx.

Condition (3.6) is also sufficient for the GHOST models (2.48) and (2.51). A

rotation of a tensor of order n is defined by

$$\mathrm{Rot}_{\mathbf{Q}}\bullet = \mathbf{Q}^{\boxtimes n} \overset{n}{\odot} \bullet, \tag{3.9}$$

where $\boxtimes$ denotes a modified tensor product of even-order tensors according to the rule

$$(* \boxtimes \star)_{i_1 \ldots i_{2r+2s}} = *_{i_1 \ldots i_r i_{r+s+1} \ldots i_{2r+s}} \star_{i_{r+1} \ldots i_{r+s} i_{2r+s+1} i_{2r+2s}} . \tag{3.10}$$

A tensor rotated by $\mathbf{Q}$ in a given frame of reference has the same components as the original tensor in the coordinate system rotated by $\mathbf{Q}^T$, as is apparent from

$$(\mathrm{Rot}_{\mathbf{Q}}\bullet)_{i_1 \ldots i_n} = \mathbf{Q}_{i_1 j_1} \ldots \mathbf{Q}_{i_n j_n} \bullet_{j_1 \ldots j_n} . \tag{3.11}$$

Condition (3.6) implies that GHOSTs satisfy

$$\bigcup_i \{ \bigcup_n \mathrm{Rot}_{\mathbf{Q}} \mathbf{H}^{(i)n} \} = \bigcup_i \{ \bigcup_n \mathbf{H}^{(i)} \}, \quad \forall \mathbf{Q} \in \mathbb{Q}, \tag{3.12}$$

that is, a tuple consisting of all GHOSTs of one family of fibers transforms to a tuple of GHOSTs of another family under the action of rotation $\mathbf{Q}$. Note also that

$$\begin{aligned} I_{\mathrm{f}}^{(i)n}(\mathbf{FQ}) &= \mathbf{H}^{(i)n} \overset{2n}{\odot} \mathrm{Rot}_{\mathbf{Q}^T} \mathbf{C}^{\otimes n} = \mathrm{Rot}_{\mathbf{Q}} \mathbf{H}^{(i)n} \overset{2n}{\odot} \mathbf{C}^{\otimes n}, \\ \mathbf{Q}\mathbf{I}_{\mathrm{f}}^{(i)n+1}(\mathbf{FQ})\mathbf{Q}^T &= \mathbf{Q} \left(\mathbf{H}^{(i)n+1} \overset{2n}{\odot} \mathrm{Rot}_{\mathbf{Q}^T} \mathbf{C}^{\otimes n} \right) \mathbf{Q}^T = \mathrm{Rot}_{\mathbf{Q}} \mathbf{H}^{(i)n} \overset{2n}{\odot} \mathbf{C}^{\otimes n}, \end{aligned}$$

therefore (1.49) holds. Thus condition (3.6) is indeed sufficient for the material symmetry in GHOST models (2.48) and (2.51).

Note that the condition of global symmetry (3.6) does not required the ODFs to be individually symmetric, *i.e.* to satisfy

$$\rho^{(i)}(\mathbf{m}_0) = \rho^{(i)}(\mathbf{Q}\mathbf{m}_0), \quad \forall i, \forall \mathbf{m}_0 \in \mathbb{U}^2, \forall \mathbf{Q} \in \mathbb{Q}. \tag{3.13}$$

As the global symmetry of ODFs (3.6) implies the symmetry of their sum (3.2), the restriction we obtained for GST, iGST, GSTx models is stronger than the restriction obtained for the AI approach. This difference is a consequence of that the averaging (2.17) in GST approaches is done in each family individually and the result depends on how the mechanically equivalent fiber fractions are grouped into families.

3.3.1 Orthotropic material

Consider the following transformations

$$\mathbf{Q}_1 = \mathbf{1},\ \mathbf{Q}_2 = \mathrm{diag}(1,-1,1),\ \mathbf{Q}_3 = \mathrm{diag}(1,-1,-1),\ \mathbf{Q}_4 = \mathrm{diag}(1,1,-1), \tag{3.14}$$

$$\mathbf{Q}_5 = \mathrm{diag}(-1,1,1),\ \mathbf{Q}_6 = \mathrm{diag}(-1,-1,1),\ \mathbf{Q}_7 = -\mathbf{1},\ \mathbf{Q}_8 = \mathrm{diag}(-1,1,-1). \tag{3.15}$$

The orthotropic symmetry group $\mathbb{Q}_O = \{\mathbf{Q}_1, \ldots, \mathbf{Q}_8\}$ is generated by the reflections with respect to the coordinate planes, $\mathbf{Q}_2$, $\mathbf{Q}_4$, $\mathbf{Q}_5$, [67]. We number $\mathbf{Q}_k$, $k = 1, \ldots, 8$ in accordance with the numbering of octants (see Figure 3.1) and call them reflections for brevity, although the group includes proper rotations too. Some basic properties of the reflections are: *(i)* a reflection is its own inverse and transpose, *i.e.* $\mathbf{Q}_k^{-1} = \mathbf{Q}_k^T = \mathbf{Q}_k, \quad \forall k$; *(ii)* any two reflections commute, *i.e.* $\mathbf{Q}_k\mathbf{Q}_l = \mathbf{Q}_l\mathbf{Q}_k, \quad \forall k, l$; *(iii)* a reflection applied to the group bijectively maps it to itself, *i.e.* $\cup_k \mathbf{Q}_l\mathbf{Q}_k = \cup_k \mathbf{Q}_k, \quad \forall l$; *(iv)* being an orthogonal transformation, a reflection maps the unit sphere to itself, *i.e.* $\mathbf{Q}_k\mathbb{U}^2 = \mathbb{U}^2$.

In order to know if condition (1.48) holds for each element of a group, it is only necessary to check it for the generators of the group. In the case of orthotropic symmetry ($\mathbb{Q} = \mathbb{Q}_O$), it is only necessary to check condition (1.48) for $\mathbf{Q}_2$, $\mathbf{Q}_4$, as $\mathbf{Q}_5 = \mathbf{Q}_2\mathbf{Q}_4\mathbf{Q}_7$ and this condition is automatically satisfied for $\mathbf{Q}_7 = -\mathbf{1}$.

A tensor $\mathbf{A}$ is diagonal in the basis $\{\mathbf{e}_1, \mathbf{e}_2, \mathbf{e}_3\}$ if and only if $\mathbf{A} = \mathbf{Q}\mathbf{A}\mathbf{Q}^T$ for all $\mathbf{Q} \in \mathbb{Q}_O$. We show below that a diagonal deformation gradient in an orthotropic

material leads to a diagonal Cauchy stress. Thus a diagonal deformation results in a diagonal stress if condition (3.2) is satisfied when using the AI model, and condition (3.6) is satisfied when using iGST, GSTx, GST models.

Proposition 6. *Assume (1.48) holds. If the deformation gradient* $\mathbf{F}$ *satisfies* $\mathbf{F} = \mathbf{Q}_k^T\mathbf{F}\mathbf{Q}_k$, $\forall \mathbf{Q}_k \in \mathbb{Q} \subset O(3)$, *then the Cauchy stress satisfies* $\boldsymbol{\sigma} = \mathbf{Q}_k^T\boldsymbol{\sigma}\mathbf{Q}_k$, $\forall \mathbf{Q}_k \in \mathbb{Q}$.

Proof. Let $\boldsymbol{\sigma}(\mathbf{F})$ be the Cauchy stress generated by deformation gradient $\mathbf{F}$. Now consider deformation $\tilde{\mathbf{F}} = \mathbf{Q}_k^T\mathbf{F}\mathbf{Q}_k$ and the corresponding stress tensor $\tilde{\boldsymbol{\sigma}} = \boldsymbol{\sigma}(\mathbf{Q}_k^T\mathbf{F}\mathbf{Q}_k)$. By objectivity (1.38) and symmetry (1.49) we have

$$\tilde{\boldsymbol{\sigma}} = \boldsymbol{\sigma}(\mathbf{Q}_k^T\mathbf{F}\mathbf{Q}_k) = \mathbf{Q}_k^T\boldsymbol{\sigma}(\mathbf{F})\mathbf{Q}_k, \tag{3.16}$$

but since it is assumed $\mathbf{F} = \mathbf{Q}_k^T\mathbf{F}\mathbf{Q}_k$, $\forall \mathbf{Q}_k \in \mathbb{Q} \subset O(3)$, we obtain

$$\tilde{\boldsymbol{\sigma}} = \boldsymbol{\sigma}(\mathbf{F}) = \mathbf{Q}_k^T\boldsymbol{\sigma}(\mathbf{F})\mathbf{Q}_k, \tag{3.17}$$

which holds $\forall \mathbf{Q}_k \in \mathbb{Q} \subset O(3)$. □

3.3.2 An example of orthotropically symmetric fiber arrangement

Consider a material reinforced by $m = 4$ families of fibers. We pick a characteristic direction $\mathbf{a}_0^{(1)}$ for the first family of fibers. Let $\mathbf{R}_1 \in SO(3)$ be a rotation, which transforms $\mathbf{e}_1$ to $\mathbf{a}_0^{(1)}$, *i.e.* $\mathbf{a}_0^{(1)} = \mathbf{R}_1\mathbf{e}_1$. We define rotations $\mathbf{R}_i$ and fiber directions $a_0^{(i)}$ (see Figure 3.1.a) by

$$\mathbf{R}_i = \mathbf{Q}_i\mathbf{R}_1\mathbf{Q}_i, \tag{3.18}$$

$$\mathbf{a}_0^{(i)} = \mathbf{R}_i\mathbf{e}_1, \qquad i = 2, 3, 4. \tag{3.19}$$

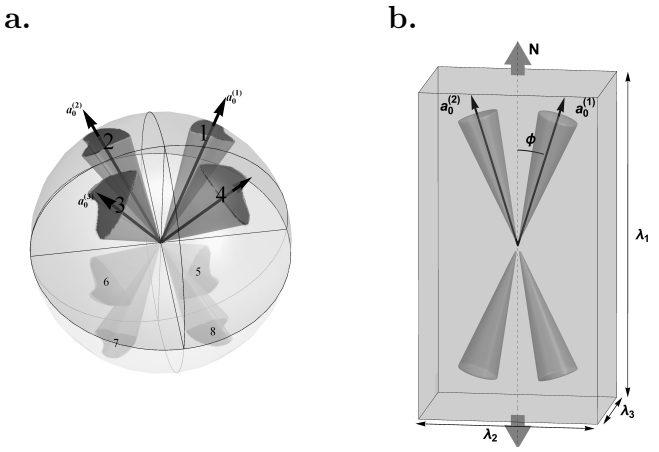

Figure 3.1: **a.** A schematic representation of an orthotropically symmetric fiber-reinforcement in a material with four families of fibers. Each family is characterized by its reference direction $\mathbf{a}_0^{(i)}$ and orientation density function $\rho^{(i)}(\mathbf{m}_0)$. The ODFs $\rho^{(i)}(\mathbf{m}_0)$ do not have to define transversely isotropic distributions, but must be symmetrically arranged (depicted as irregular shapes). Single digits number the octants. Fibers in the lower hemisphere (pale) are the extensions of the fibers in the upper hemisphere beyond the center of the sphere, the former can be obtained from the latter by applying transformation $\mathbf{Q}_7 = -\mathbf{1}$. The related identity $\rho^{(i)}(\mathbf{m}_0) = \rho^{(i)}(-\mathbf{m}_0)$ holds for each fiber family. **b.** A material reinforced by two families of mechanically equivalent fibers is in uniaxial tension, subject to the axial load N. Both fiber families are transversely isotropic and described by the von Mises distribution with the concentration parameter b. The mean fiber directions $\mathbf{a}_0^{(i)}$ are aligned symmetrically with respect to the principal directions, making angle ϕ with the direction of applied load. The material is orthotropic, and transverse isotropy is only observed for $\phi = 0, \pi/2$.

That is,

$$\mathbf{a}_0^{(1)} = (\cos\alpha, \sin\alpha\cos\beta, \sin\alpha\cos\beta), \tag{3.20}$$

$$\mathbf{a}_0^{(2)} = (\cos\alpha, -\sin\alpha\cos\beta, \sin\alpha\cos\beta), \tag{3.21}$$

$$\mathbf{a}_0^{(3)} = (\cos\alpha, -\sin\alpha\cos\beta, -\sin\alpha\cos\beta), \tag{3.22}$$

$$\mathbf{a}_0^{(4)} = (\cos\alpha, \sin\alpha\cos\beta, -\sin\alpha\cos\beta). \tag{3.23}$$

The rotation $\mathbf{R}_i$ also relates the ODFs in families' coordinates (*i.e.* relatively to $\mathbf{a}_0^{(i)}$) and in material coordinates (*i.e.* relatively to $\mathbf{e}_1$), we have

$$\rho^{(i)}(\mathbf{m}_0) = \rho_i(\mathbf{R}_i^T\mathbf{m}_0), \qquad i = 1, \ldots, 4. \tag{3.24}$$

Furthermore, the ODFs in families' coordinates are also symmetric, *i.e.*

$$\rho_i(\mathbf{m}_0) = \rho(\mathbf{Q}_i\mathbf{m}_0). \tag{3.25}$$

As a result, conditions (3.6) and (3.2) are satisfied for this material. Indeed, we have

$$\bigcup_{i=1}^{m} \rho^{(i)}(\mathbf{Q}_k\mathbf{m}_0) = \bigcup_{i=1}^{m} \rho(\mathbf{Q}_i\mathbf{R}_i^T\mathbf{Q}_k\mathbf{m}_0) = \bigcup_{i=1}^{m} \rho(\mathbf{Q}_i\mathbf{Q}_i\mathbf{R}_1^T\mathbf{Q}_i\mathbf{Q}_k\mathbf{m}_0) = \bigcup_{p=1}^{m} \rho(\mathbf{R}_1^T\mathbf{Q}_p\mathbf{m}_0), \quad \forall i, \tag{3.26}$$

and

$$\bigcup_{i=1}^{m} \rho^{(i)}(\mathbf{m}_0) = \bigcup_{i=1}^{m} \rho(\mathbf{Q}_i\mathbf{R}_i^T\mathbf{m}_0) = \bigcup_{i=1}^{m} \rho(\mathbf{Q}_i\mathbf{Q}_i\mathbf{R}_1^T\mathbf{Q}_i\mathbf{m}_0) = \bigcup_{i=1}^{m} \rho(\mathbf{R}_1^T\mathbf{Q}_i\mathbf{m}_0), \qquad \forall i. \tag{3.27}$$

We conclude that condition (3.6) holds and condition (3.2) follows from it. Thus, this material is orthotropically symmetric for all the dispersion models.

3.4 Uniaxial tension of a material with two families of fibers

3.4.1 Fiber-reinforced material with two families of fibers

An important example of a fiber reinforced material is a material with two families of fibers. This type of material has been used to model various soft biological tissues, including human annulus fibrosus [73], cornea [1] and arterial wall [35]. Among materials reinforced by axisymmetrically distributed fibers, this is the simplest case of an orthotropic material: a material with one family is always transversely isotropic, whereas two equivalent fiber families guarantee that a material is orthotropic and not transversely isotropic, unless the characteristic fiber directions coincide or fibers are distributed isotropically.

In order to keep the analysis as simple as possible, yet to avoid the limitations of the transverse isotropy, for the remainder of this Chapter we restrict our attention to an incompressible material reinforced by two mechanically equivalent families of fibers with mean directions $\mathbf{a}_0^{(1)} = (\cos\phi, \sin\phi, 0)$, $\mathbf{a}_0^{(2)} = (\cos\phi, -\sin\phi, 0)$ (see Figure 3.1.b). We assume that the ODFs are transversely isotropic and defined by

$$\rho^{(1)}(\mathbf{m}_0) = \rho(\mathbf{R}_1^T\mathbf{m}_0) = \tilde{\rho}\left(\arccos(\mathbf{e}_1 \cdot \mathbf{R}_1^T\mathbf{m}_0)\right), \tag{3.28}$$

$$\rho^{(2)}(\mathbf{m}_0) = \rho(\mathbf{R}_1\mathbf{m}_0) = \tilde{\rho}\left(\arccos(\mathbf{e}_1 \cdot \mathbf{R}_1\mathbf{m}_0)\right), \tag{3.29}$$

where $\mathbf{R}_1$ is the rotation matrix by angle ϕ about the axis $\mathbf{e}_3$ and $\tilde{\rho}(\theta)$ is the von Mises distribution [22]

$$\tilde{\rho}(\theta) = \frac{\sqrt{2b}}{2\pi\sqrt{\pi}} \frac{\exp\left[b(\cos 2\theta + 1)\right]}{\operatorname{erfi}(\sqrt{2b})}, \tag{3.30}$$

with $\operatorname{erfi}(x) = \int_0^x \exp(t^2)dt$. The degree of fiber dispersion is defined by the concentration parameter b. As noted in [34], there is a one-to-one correspondence between

the concentration parameter b and the dispersion parameter κ. Note also that $\tilde{\rho}(\theta) = \tilde{\rho}(-\theta) = \tilde{\rho}(\pi + \theta)$ and that $\oint_{\mathbb{U}^2} \tilde{\rho}(\theta) d\omega = 1$.

We further assume that the matrix is *an incompressible neo-Hookean* material,

$$\psi_{\text{iso}}(\mathbf{C}) = \frac{\mu}{2}(\text{tr}\mathbf{C} - 1), \tag{3.31}$$

where μ is the shear modulus, and that the constitutive model for fibers is either the *standard reinforcing model* [69]

$$\psi_{\text{std}}(I_{\text{f}}) = \frac{\gamma}{2}(I_{\text{f}} - 1)^2, \tag{3.32}$$

or the *exponential model* proposed in [34]

$$\psi_{\text{exp}}(I_{\text{f}}) = \frac{k_1}{2k_2} \exp[k_2(I_{\text{f}} - 1)^2], \tag{3.33}$$

where γ, k_1 are fiber stiffness parameters of the dimension of stress and k_2 is a dimensionless parameter. As can be seen from the derivatives of (3.32) and (3.33)

$$\frac{\partial}{\partial I_{\text{f}}}\psi_{\text{std}}(I_{\text{f}}) = \gamma(I_{\text{f}} - 1), \qquad \frac{\partial}{\partial I_{\text{f}}}\psi_{\text{exp}}(I_{\text{f}}) = k_1(I_{\text{f}} - 1)\exp[k_2(I_{\text{f}} - 1)^2], \tag{3.34}$$

the standard reinforcing model is a special case of the exponential model for which $k_1 = \gamma$, $k_2 = 0$.

Here we choose to study the standard reinforcing and exponential models as they have been widely studied and used in different contexts [50, 37, 35, 25, 23]. However, more recently it has been pointed out that a model that only includes the invariant I_4 is not suitable in the limit of small deformations as it does not match the expected behaviour of linear anisotropic elasticity [9, 52]. However, the standard reinforcing and exponential model are simple enough so that analytical progress can be achieved. We

also expect that the generic features of perversions presented here will also be observed in more complicated systems as it is mainly due to a balance between nonlinearity, anisotropy and large deformations [9, 52].

Conditions (3.2) and (3.6) hold for the material, therefore the homogeneous diagonal deformations $\mathbf{F} = \mathrm{diag}(\lambda_1, \lambda_2, \lambda_3)$ correspond to a diagonal Cauchy stress $\boldsymbol{\sigma} = \mathrm{diag}(\sigma_1, \sigma_2, \sigma_3)$. The constitutive relation (2.6) can now be written as

$$\sigma_i(\lambda_1, \lambda_2, \lambda_3) = -p + \mu\lambda_i^2 + \sigma_{\mathrm{f}\,i}(\lambda_1, \lambda_2, \lambda_3), \quad i = 1, 2, 3, \tag{3.35}$$

where the principal stretches obey the incompressibility restriction

$$\lambda_1\lambda_2\lambda_3 = 1. \tag{3.36}$$

The fiber stress contribution $\sigma_{\mathrm{f}\,i} = 2\lambda_i^2 \partial W/\partial(\lambda_i^2)$ includes the response of both families and depends on the choice of the model that accounts for fiber distribution.

For the AI model we have

$$\sigma_{\mathrm{f}\,i} = 4\lambda_i^2 \oint_{\mathbb{U}^2} \rho(\mathbf{m}_0)\chi(\mathbf{R}_1\mathbf{m}_0 \otimes \mathbf{R}_1\mathbf{m}_0 : \mathbf{C})\psi_{\mathrm{f}}'(\mathbf{R}_1\mathbf{m}_0 \otimes \mathbf{R}_1\mathbf{m}_0 : \mathbf{C})(\mathbf{R}_1\mathbf{m}_0)_i^2 d\omega, \tag{3.37}$$

where $(\mathbf{R}_1\mathbf{m}_0)_i$ denotes ith component of vector $\mathbf{R}_1\mathbf{m}_0$.

For the GST, GSTx and iGST approaches, the fiber stress reads

$$\sigma_{\mathrm{f}\,i} \;=\; 4\lambda_i^2 \mathrm{H}_{ii}\psi_{\mathrm{f}}'\left(\frac{\mathbf{H} : \mathbf{C}}{\mathrm{tr}\mathbf{H}}\right), \tag{3.38}$$

where $\mathbf{H} = (\mathbf{H}^{(1)} + \mathbf{H}^{(2)})/2$ is a diagonal tensor, whose exact form depends on the variant of GST approach considered. For the GST model, we have

$$\mathrm{H}_{11} = \kappa + (1 - 3\kappa)\cos^2\phi, \quad \mathrm{H}_{22} = \kappa + (1 - 3\kappa)\sin^2\phi, \quad \mathrm{H}_{33} = \kappa. \tag{3.39}$$

In the GSTx approach the components of $\mathbf{H}$ are given by

$$\begin{aligned} &\mathrm{H}_{11} = \kappa + (1-3\kappa)\cos^2\phi, \quad \mathrm{H}_{22} = \kappa + (1-3\kappa)\sin^2\phi, \\ &\mathrm{H}_{33} = \kappa, \qquad\qquad \text{if } (1-3\kappa)\left(\lambda_1\cos^2\phi + \lambda_2\sin^2\phi - 1\right) > 0, \\ &\mathrm{H}_{11} = \kappa, \quad \mathrm{H}_{22} = \kappa, \quad \mathrm{H}_{33} = \kappa, \qquad\qquad \text{otherwise.} \end{aligned} \tag{3.40}$$

In the iGST approach $\mathbf{H}$ is given through the integral over the unit sphere

$$\mathrm{H}_{ii} \;=\; \oint_{\mathbb{U}^2} \rho(\mathbf{m}_0)\chi(\mathbf{R}_1\mathbf{m}_0 \otimes \mathbf{R}_1\mathbf{m}_0 : \mathbf{C})(\mathbf{R}_1\mathbf{m}_0)_i^2 d\omega. \tag{3.41}$$

3.4.2 Comparison of the models in uniaxial tension

We apply a reference load $N > 0$ to the material in the direction $\mathbf{e}_1$ and leave the lateral faces traction free (Figure 3.1.b). That is, we have the following equations for the principal stresses

$$\sigma_1 = N\lambda_1, \quad \sigma_2 = 0, \quad \sigma_3 = 0, \tag{3.42}$$

where the unknowns are the Lagrangian multiplier p and any two principal stretches (*e.g.* λ_1, λ_3), while the remaining principal stretch is determined by them via (3.36). After eliminating the Lagrangian multiplier p from the system using $\sigma_3 = 0$, equations (3.42) become

$$N\lambda_1 \;=\; \sigma_1(\lambda_1, \lambda_3), \tag{3.43}$$

$$0 \;=\; \sigma_2(\lambda_1, \lambda_3). \tag{3.44}$$

3.4.2.1 Transversely isotropic case

As a preliminary step in the comparison of the models, we neglect the ground substance response ($\mu = 0$) and consider the transversely isotropic case $\phi = 0$, when the two fiber families are aligned and can be regarded as a single family. The symmetry

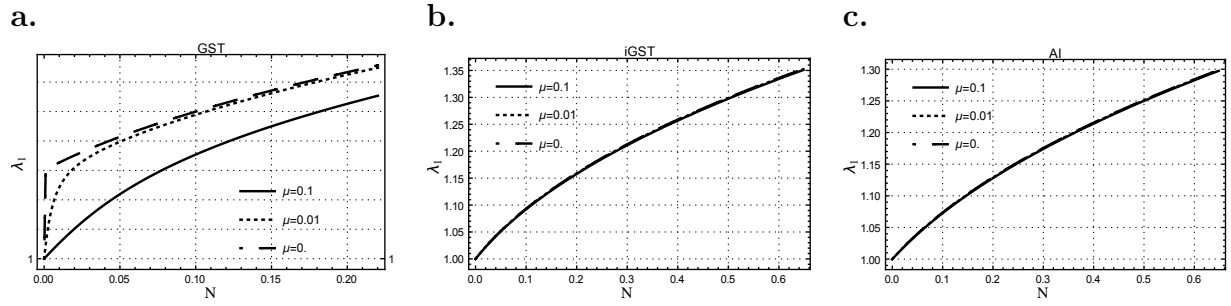

Figure 3.2: Response of a material (orthotropically, but not transversely symmetric) in uniaxial tension, $\phi = \pi/4$, $b = 2$, $k_2 = 0$, **(a)** GST, **(b)** iGST, **(c)** AI. If the elastic response of the ground substance is neglected, then the GST model predicts finite strain for infinitesimal load (**a**, case $\mu = 0$).

implies $\lambda_2 = \lambda_3 = \lambda_1^{-1/2}$, and the deformation is completely defined by a stretch in one direction. We plot the axial Cauchy stress component as a function of the engineering strain $\varepsilon = \log \lambda_1$ for axial fiber alignment (Figure 3.3.a) [58]. In order to focus on the effect of fiber dispersion, we ignore the strain energy component of the ground substance, whose only contribution to the material behavior is the incompressibility. We also plot the relative error of various models with respect to AI as a function of fiber dispersion parameter (Figure 3.3.b, c).

Remark. If the ground substance is neglected then equation (3.44) for the GST model becomes $(\lambda_1^{-2}\lambda_3^{-2}\mathrm{H}_{22} - \lambda_3^2\mathrm{H}_{33})\psi_{\mathrm{f}}'(\mathbf{H} : \mathbf{C}) = 0$. It follows that the solution continuously passes through the unstrained state $\lambda_1 = \lambda_3 = 1$ only if $\mathrm{H}_{22} = \mathrm{H}_{33}$, *i.e.* the material is transversely isotropic with respect to the direction of loading. The stress-strain curves for various values of μ are shown in Figure 3.2. This unrealistic behavior, consisting in instantaneous large deformation for small applied loads, is only peculiar to the GST model, while the nonlinearities in the AI and iGST models allow for continuous deformation at high fiber dispersions.

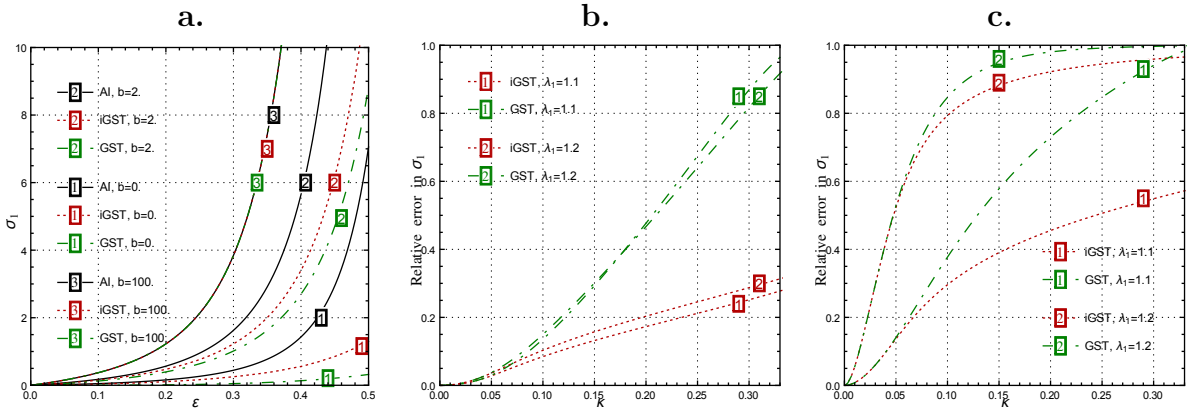

Figure 3.3: The comparison of different models in uniaxial tension along the mean fiber direction. (**a**) The stress in uniaxial tension versus the logarithm of the stretch. (**b**,**c**) Error in the response provided by the iGST and GST models relative to the response of the AI model as a function of fiber dispersion for constant axial stretch values $\lambda_1 = 1.1$ and $\lambda_1 = 1.2$: (**b**) soft fiber response, $k_2 = 1$; (**c**) stiff fiber response $k_2 = 30$. (Compare to Fig. 3, 4 in [58])

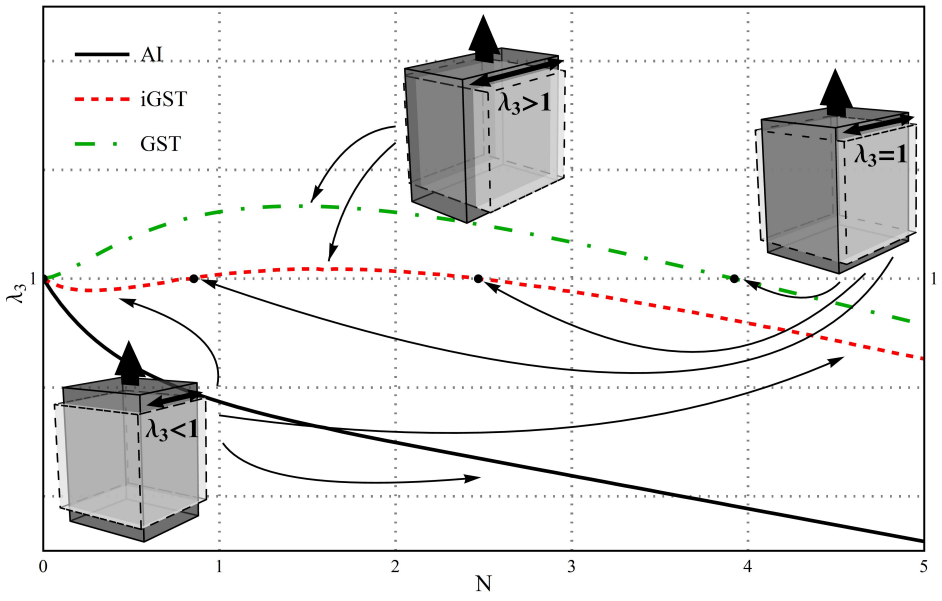

Figure 3.4: The dependence of the transverse stretch λ_3 on the axial load N in uniaxial tension. The perversion points are indicated with black. Different models for fiber dispersion result in qualitatively different material behavior (*i.e.* different number of perversion points), although the difference in stretch λ_3 does not exceed 6%.

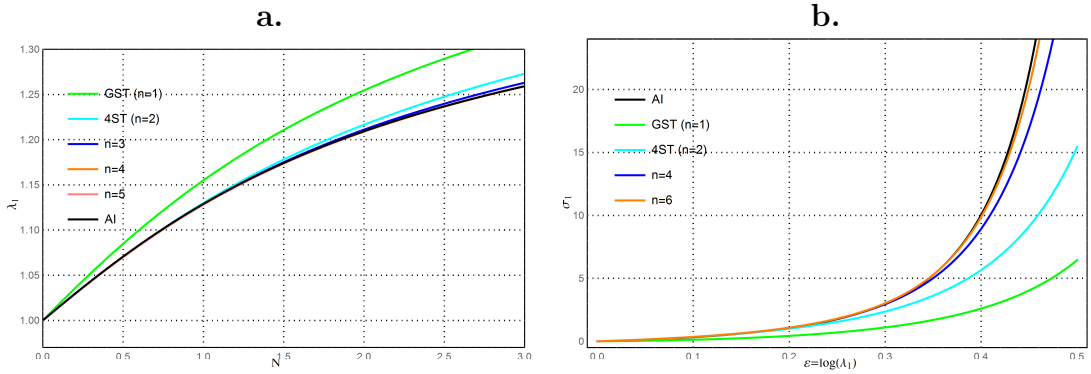

Figure 3.5: The response of transversely isotropic material as predicted by the CE-type GHOST model $n_{\max} = n$ (2.48) compared to the AI model: (**a**) $k_2 = 2$, $b = 2$, $\mu = 1$; (**b**) $k_2 = 1$, $b = 1$, $\mu = 0$.

3.4.2.2 Perversion points of the transverse strain

Extension in the transverse direction under positive axial load N is not possible in isotropic and transversely isotropic (axially symmetric) incompressible materials. That is, generically we have $\lambda_1 > 1 > \lambda_2, \lambda_3$. However, if the transverse isotropy is broken, the tensile axial load may cause the material to extend in the transverse direction $\mathbf{e}_3$, so that the principal stretches satisfy $\lambda_1, \lambda_3 > 1 > \lambda_2$. Moreover, the same material can switch between extension and contraction in this direction as the load increases. We refer to such qualitative change as a *perversion point*, which is defined in [24] as a point at which a strain passes through a distinguished value. In our case the distinguished value of stretch is $\lambda_3 = 1$, as it corresponds to the undeformed and unloaded state. As illustrated in Figure 3.4, the material can have multiple perversion points. The existence and number of perversion points depends on the amount of fibers, fiber stiffness, fiber dispersion and the approach chosen to model the distributed fibers. That is, different models can predict different numbers of perversion points for the same set of material parameters (Figure 3.4). This suggests that the number of perversion points can be used as a qualitative measure of agreement between various models, which is specific to the case when the material symmetry is weaker than transverse isotropy.

Equations (3.43), (3.44) at a perversion point ($\lambda_3 = 1$) can be written as

$$N\lambda_1 = \sigma_1(\lambda_1), \tag{3.45}$$

$$0 = \sigma_2(\lambda_1), \tag{3.46}$$

which can be solved for the axial stretch λ_1 and the load N. Note that there always exists a trivial solution $\lambda_1 = 1$, $N = 0$, which is ignored and not counted, and that equation (3.46) is decoupled from (3.45) and can be solved independently. Given that the material obeys the tension-extension inequalities, the number of perversion points when $N > 0$ equals to the number of roots of (3.46) that satisfy $\lambda_1 > 1$.

Since rescaling the stress will not affect the number of perversion points, we let $k_1 = \gamma = 1$ in the fiber potentials (3.32), (3.33). The role of shear modulus μ is then to control the relative amount of fibers with respect to the ground substance. The values $\mu = +\infty$ and $\mu = 0$ correspond, respectively, to an isotropic Neo-Hookean material and an incompressible material composed entirely of fiber.

We first focus on the case of the standard reinforcing model ($k_2 = 0$). The three remaining material parameters form the parametric space (ϕ, μ, b), which is divided into regions corresponding to different numbers of perversion points. The algebraic multiplicity of perversion points is at least two at the borders between these regions. Therefore the borders are given by

$$\sigma_2(\lambda_1) = 0, \tag{3.47}$$

$$\sigma_{21}(\lambda_1) = 0, \tag{3.48}$$

where $\sigma_{21}(\lambda_1) = \frac{d\sigma_2(\lambda_1)}{d\lambda_1}$, $\sigma_{22}(\lambda_1) = \frac{1}{2}\frac{d^2\sigma_2(\lambda_1)}{d\lambda_1^2}$ are the coefficients in the Taylor expansion

$$\sigma_2(\lambda_1 + \triangle\lambda_1) = \sigma_2(\lambda_1) + \triangle\lambda_1\sigma_{21}(\lambda_1) + \triangle\lambda_1^2\sigma_{22}(\lambda_1) + O(\triangle\lambda_1^3). \tag{3.49}$$

As mentioned previously, the stress in the GSTx model can have discontinuities when $\lambda_1 = \tan\phi$. If the jump occurs across the λ_1-axis then it is counted as a perversion point, therefore the condition

$$\sigma_2(\tan\phi + 0) = 0 \quad \text{or} \quad \sigma_2(\tan\phi - 0) = 0, \tag{3.50}$$

must be used instead of the equation (3.48) at $\lambda_1 = \tan\phi$.

The computations for the GST model are simple and can be done analytically. With the help of (3.38), (3.47) becomes

$$\eta^2 \mathrm{H}_{22}^2 + \eta(\frac{\mu}{4} - \mathrm{H}_{11}\mathrm{H}_{22} - \mathrm{H}_{33}\mathrm{H}_{22}) + \mathrm{H}_{11}\mathrm{H}_{33} = 0, \tag{3.51}$$

where $\eta = \lambda_1^{-2}$ and H_{ii} are constants given by (3.39). The number of perversions is exactly the number of roots $0 < \eta < 1$ of the quadratic polynomial in η in (3.51). One can formulate the conditions on the coefficients of the polynomial to have precisely 0, 1 or 2 suitable roots and obtain relations between parameters μ and ϕ. The analysis for GSTx requires to take into account some additional conditions, but is otherwise similar. The details are provided in the Appendix and the results are shown in Figure 3.6.a, d, f.

The analysis of the AI and iGST models is more complicated. As can be seen from (3.37) or (3.38) and (3.41), equations (3.45) and (3.46) contain integrals that cannot be solved analytically. A numerical root finding algorithm is required to solve the non-linear system (3.45), (3.46), see Appendix for the exact expressions used in this system.

The results for various models are shown for selected values of b in Figure 3.6. The diagrams for high degree of fiber alignment (*i.e.* low dispersion) are almost identical for all models and consist of three simply connected regions on the (μ, ϕ) plane, whose borders are parabola-like curves (Figure 3.6.a). High values of shear modulus μ indicate low fiber content and result in no perversion points, as expected for a nearly

isotropic material. At lower values of μ the number of perversion points depends on the fiber orientation angle ϕ. The region of one perversion is situated predominantly in the half-plane $\phi < \pi/4$, whereas two perversion points can be observed for all angles. We note that some dispersion of fibers is required for the existence of two perversion points, since both axial stretch λ_1 and load N at the second perversion point tend to infinity in the limit of strict fiber alignment ($b \to +\infty$, $\kappa \to 0$).

The difference between the modeling approaches is apparent when the fiber dispersion is significant. As the dispersion increases (concentration b decreases), the regions corresponding to one and two perversion points shrink. This process occurs faster for the AI approach and slower for the GST and GSTx approaches (see Figures 3.6.b, c, d). The behavior of the iGST model is intermediate between AI and GST models. The range of fiber orientation angles ϕ corresponding to at least one perversion shrinks in AI and iGST models, but remains $(0, \pi/2)$ in the GST model. Also unlike the iGST and AI models, the GST model does not allow for a single perversion point when $\phi > \pi/4$. Two perversion points become impossible in AI and iGST models at high values of dispersion (Figure 3.6.e). At some higher degree of dispersion the material has zero perversion points for all values of shear modulus μ and fiber orientation angle ϕ. This is in contrast to the GST model (Figure 3.6.f), which allows the regions of one and two perversions for arbitrarily high fiber dispersion, unless the material is ideally isotropic or transversely isotropic. This difference between the models is also demonstrated in Figure 3.7, where the minimum and maximum values of μ that allow to have one or two perversion points are plotted as a function of the concentration parameter b.

We also considered the case of exponential fiber potential (3.33) for the GST model. We show in Figure 3.7 that in this case the number of perversion points is not limited to two and there exists a region corresponding to three perversion points.

Remark 7. With regard to numerics, we observe that an adaptive scheme for accurate

numerical integration is required when investigating the number of perversions. Fixed grids can result in oscillations of the computed numerical value of $\sigma_2(\lambda_1)$ around the true value. These oscillations occur when a node of the grid enters the tensile region (as λ_1 increases) and the finite portion of fibers associated with the node is taken into consideration. This leads to the overestimation of the amount of tensile fibers, which is later followed by the underestimation, and then the cycle repeats with another node as the deformation proceeds. The fluctuations of numerical values of σ_2 can have a sufficiently large magnitude to cause multiple false perversion points to appear. These artifacts are associated with high fiber dispersion and are especially noticeable in the iGST approach, where (unlike the AI model) the integrand is discontinuous at the boundary of the tensile region on the unit sphere. For instance, when we use the Lebedev quadrature scheme of the 131st order of accuracy [59, 45] with 5810 nodes, the described artifacts take place for a reasonable choice of step $\triangle\lambda_1$. Skacel and Bursa [64] compared various schemes of numerical integration on the unit sphere and concluded that Lebedev quadrature achieved the best results, surpassing adaptive quadratures, yet the latter are required for the analysis of perversion points.

3.5 Conclusion

The angular integration model (AI) allows to incorporate fiber orientation density functions into the strain energy function of a material [43]. The main disadvantage of this model is that it requires repeated numerical integrations. The generalized structure tensor model (GST) [22] does not have this problem, since numerical integration is only required to compute the GST from a given fiber distribution. Thus, the GST model presents an attractive approach, which has been used to model fiber dispersion in various studies [20, 22, 57, 27, 17, 72]. However, the GST model approximates the AI model well only for low values of fiber dispersion [7]. The weighted averaging of

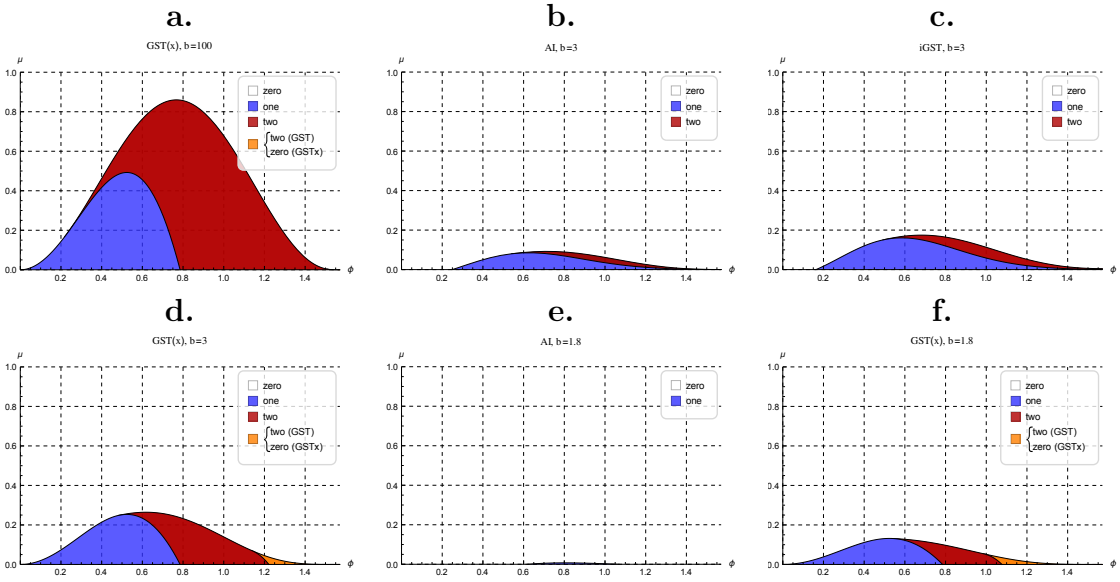

Figure 3.6: The number of perversion points as a function of fiber orientation angle ϕ and relative stiffness of the ground substance μ, using the standard reinforcing model ($k_2 = 0$). (**a**) Predictions of GST, iGST and AI models are very similar for high degree of fiber alignment, $b = 100$. The diagram is plotted for the GST approach. If fiber dispersion is significant, then the differences between the approaches become clear. The diagrams are shown for $b = 3$ as predicted by (**b**) AI, (**c**) iGST, (**d**) GST. For higher degrees of fiber dispersion the regions of two and one perversions shrink until they disappear from the diagram, as shown for the AI model for $b = 1.7$, (**e**). In contrast, the GST model predicts the existence of regions for $b = 1.7$ (**f**), and these regions persist for any $b > 0$.

the square of the fiber stretch over all directions as well as the inability to selectively exclude the response of compressed fiber fractions contribute to the error in the GST model. We introduced the iGST model, which disregards the contracted fiber fractions and averages the fiber stretch only over tensile directions. A comparison of the models for distributed fibers is given in Figure 2.1 and Table 2.1.

We used the problem of perversion points of the transverse strain in uniaxial tension as a qualitative measure of agreement between models for distributed fiber reinforcement, namely, the AI, GST, GSTx and iGST models. These perversion points correspond to the critical values at which a stretched rectangular slab expands in the direction perpendicular to the direction of applied load (Figure 3.4). As expected from the relative errors in stress predictions (Figure 3.3), the behavior of the iGST model is

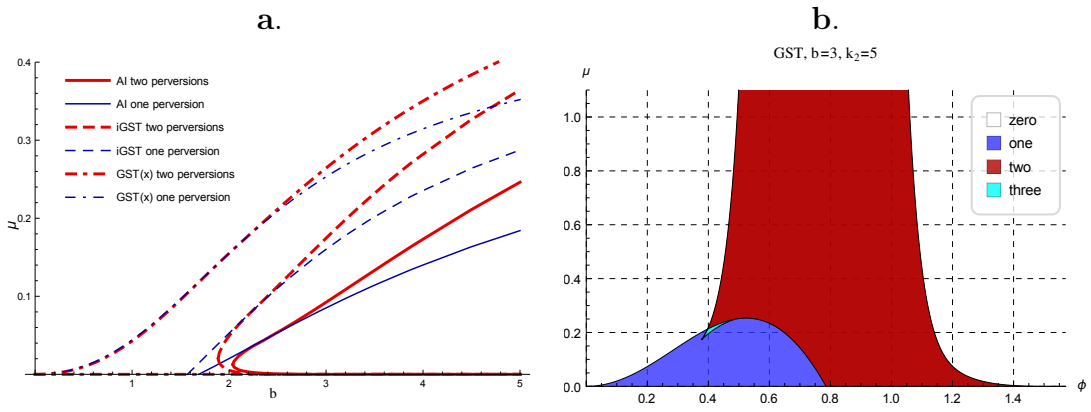

Figure 3.7: **a**. Extremal values of μ in the regions of one or two perversion as a function of the concentration parameter b. **b**. The number of perversion points as a function of fiber orientation angle ϕ and relative stiffness of the ground substance μ as predicted by the GST model for $b = 3$. Exponential fiber potential is used ($k_2 = 5$). In contrast to the case $k_2 = 0$, three perversion points are possible.

in between the AI and GSTx models, but is much closer to the AI model. The iGST model also possesses several distinctive features of the AI model, such as the shrinkage of the range of fiber orientation angles (Figure 3.6) and the existence of the maximum fiber dispersion that allows perversion points (Figure 3.7). The difference between the GSTx and iGST models consists in that the latter correctly addresses contracted fibers by excluding them from consideration, while the GST and GSTx models average fiber strain over both contracted and extended fibers. The largest fraction of fibers in extension is obtained when the mean fiber direction is aligned with the maximum principal stretch, hence, the accuracy of the GSTx model depends not only on the extent of dispersion, but also on the number and the arrangement of fiber families and the deformation regime. The former circumstance has been discussed *e.g.* in [18, 58], while the latter is evident from the comparison of the predictions of the GST and iGST models (Figure 3.6 c and f respectively) for small fiber angles ϕ and when the angle is $\phi > \frac{\pi}{4}$ or larger. Based on this argument, we advocate that the GSTx model is inaccurate compared to the AI model when the fiber dispersion is significant, primarily because it is unable to selectively disregard compressed fibers, which suggests that the

GSTx model should be used only when the dispersion is low, or, at least, when most of the fibers are in extension.

Chapter 4

Simple model for fiber reorientation

4.1 Introduction

The aim of this Chapter is to study the coupling between material elastic properties and mechanically induced fiber reorientation. Recently there were several studies of fiber reorientation dynamics in elastic tissues (*e.g.* [29, 11, 42]), where the main focus was on reproduction of structures in numerical simulations that resemble the arrangement of real soft biological tissues. In order to match models to real tissues these studies considered sophisticated geometry and a number of tunable parameters that allowed for the adjustment of the models. In contrast, we do not consider any particular organ or tissue, but aim to understand the generic behaviour of a material undergoing mechanically induced fiber reorientation. Our intention is to conduct a thorough study of a simple model and understand the implications of choosing a particular phenomenological law for mechanically coupled fiber reorientation.

We assume that fiber reorientation is a quasi-static process, that is a material instantaneously responds to the changes in its properties. Therefore inertial terms and explicit time dependence are neglected in the Cauchy momentum equation, which can be decoupled from the equation for evolution of material properties. Hence the

model consists of the static and the time-dependent parts. The static part incorporates the constitutive equation,

$$\boldsymbol{\sigma} = \boldsymbol{\sigma}(\mathbf{F}), \tag{4.1}$$

the Cauchy equation of equlibrium where no body force assumed,

$$\mathrm{div}\boldsymbol{\sigma} = 0, \tag{4.2}$$

and suitable boundary conditions. The time-dependent part consists of phenomenological equations defining mechanically induced evolution of fiber directions and initial data. In the simplest case the fiber configuration at each material point is described by a single parameter, fiber angle ϕ, whose evolution equation is of the form

$$\dot{\phi}(t) = \dot{\phi}(\phi, \mathbf{F}, \boldsymbol{\sigma}, \dots). \tag{4.3}$$

The right-hand side of equation (4.3) defines the change of fiber angle as a function of current local mechanical state, *i.e.* the values of deformation gradient $\mathbf{F}$, Cauchy stress $\boldsymbol{\sigma}$ etc at the material point considered. Equations (4.1), (4.2), (4.3) constitute an autonomous differential-algebraic equation.

The particular setting we are considering involves a subcase of a material defined in Chapter 3. We consider an incompressible neo-Hookean material reinforced by two families of fibers whose directions in the reference configuration are given by

$$\mathbf{a}_0^{(1)} = (\cos\phi, \sin\phi, 0), \qquad \mathbf{a}_0^{(2)} = (\cos\phi, -\sin\phi, 0). \tag{4.4}$$

As in Chapter 3, we consider a homogeneous deformation that produces a diagonal deformation gradient

$$\mathbf{F}{=}\mathrm{diag}(\lambda_1, \lambda_2, \lambda_3), \tag{4.5}$$

and due to the symmetrical arrangement of fibers a diagonal Cauchy stress tensor

$$\boldsymbol{\sigma} = \mathrm{diag}(\sigma_1, \sigma_2, \sigma_3) = -p\mathbf{1} + 2\mathbf{F}\frac{\partial W}{\partial \mathbf{C}}\mathbf{F}. \tag{4.6}$$

The incompressibility condition reads

$$\lambda_1\lambda_2\lambda_3 = 1. \tag{4.7}$$

Note that this deformation regime is consistent with boundary conditions that prescribe uniform normal traction at the boundaries of a rectangular slab and also with the boundary conditions that prescribe fixed displacement at the boundary. In the latter case an additional condition on stress is required to eliminate incompressibility-related Lagrangian multiplier p. So to make the model more visual, we define the reference configuration as a cuboid $\mathcal{B}_0 = [0, L_1] \times [0, L_2] \times [0, L_3] \in \mathbb{R}^3$ (Figure 4.1). Accordingly, the current configuration is also a cuboid, $\mathcal{B}_t = [0, l_1] \times [0, l_2] \times [0, l_3]$, with $l_i = L_i\lambda_i$, $i = 1, 2, 3$. Note that the Cauchy equilibrium equation (4.2) is automatically satisfied, since the mechanical state is homogeneous.

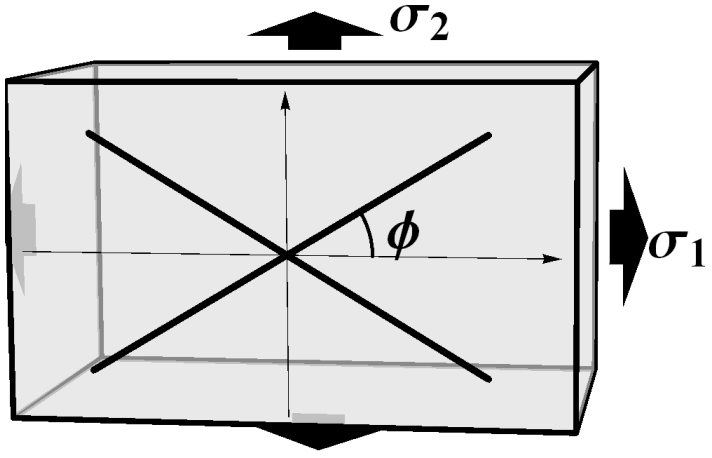

Figure 4.1: The cuboid is subject to external loading, which maintains the constant normal stress on each face of the cuboid. The material is reinforced by two families of fibers, which are in-plane, aligned symmetrically and make an angle ϕ with the X_1-axis in the reference configuration.

The boundary conditions can be given by a constant load or by a constant deformation. The reorientation law (4.3) can also be a function of the stress or the strain. If the boundary conditions and the reorientation law are prescribed by different fields (one by stress, another by strain), then the constitutive equation plays an important role in defining the value of the right-hand side of (4.3) and thus the resulting fiber arrangement. Conversely, if the boundary conditions and the reorientation law are both given by the same field, then the final fiber orientation is directly determined by the boundary conditions and the constitutive equation has little or no effect on the dynamics.

4.2 Strain-induced fiber reorientation subject to constant stress

In this section we prescribe Cauchy stress as the boundary conditions for Equation (4.2). That is, the principal stresses σ_i are given and constant, while the principal stretches λ_i are regarded as unknowns.

4.2.1 The case of strict fiber alignment

We assume that the material defined above is reinforced by two fiber families with no fiber dispersion. We use the the *standard reinforcing model* (3.32) for fibers. The total strain energy reads

$$W(\mathbf{F}) = \frac{\mu}{2}(I_1 - 3) + \frac{\gamma}{2}\left[(I_4 - 1)^2 + (I_6 - 1)^2\right], \tag{4.8}$$

where $I_4 = \mathbf{a}_0^{(1)} \cdot \mathbf{C}\mathbf{a}_0^{(1)}$, $I_6 = \mathbf{a}_0^{(2)} \cdot \mathbf{C}\mathbf{a}_0^{(2)}$. In the presence of fibers one can assume $\gamma = 1$ without loss of generality, since as long as $\gamma \neq 0$, the unit of force can be chosen to

ensure $\gamma = 1$. The constitutive equation becomes

$$\sigma_1 = -p + \mu\lambda_1^2 + 4\lambda_1^2\cos^2\phi(\lambda_1^2\cos^2\phi + \lambda_2^2\sin^2\phi - 1), \tag{4.9}$$

$$\sigma_2 = -p + \mu\lambda_2^2 + 4\lambda_2^2\sin^2\phi(\lambda_1^2\cos^2\phi + \lambda_2^2\sin^2\phi - 1), \tag{4.10}$$

$$\sigma_3 = -p + \mu\lambda_3^2, \tag{4.11}$$

where p is the Lagrangian multiplier associated with the incompressibility. Therefore, the solution to the static part of our problem reduces to inverting the constitutive function, *i.e.* finding λ_i, p from (4.7), (4.9)-(4.11).

We use the reorientation law suggested in [47],

$$\frac{d\mathbf{a}_0^{(i)}}{dt} = \frac{1}{\tau}\left(\mathbf{n}_{max}^{\mathbf{C}} - (\mathbf{n}_{max}^{\mathbf{C}} \cdot \mathbf{a}_0^{(i)})\mathbf{a}_0^{(i)}\right), \tag{4.12}$$

where $\mathbf{n}_{max}^{\mathbf{C}}$ is the unit vector in the reference configuration in the direction of maximum principal stretch and τ is a relaxation parameter. If the maximum principal stretch is not unique, then we assume that $d\mathbf{a}_0^{(i)}/dt = 0$. Since the fibers are symmetric and confined in the X_1X_2-plane and remain such in the course of reorientation, one can express (4.12) in terms of the orientation angle ϕ

$$\dot{\phi} = \begin{cases} -\frac{\sin\phi}{\tau}, & \lambda_1 > \lambda_2, \\ 0, & \lambda_1 = \lambda_2, \\ \frac{\cos\phi}{\tau}, & \lambda_1 < \lambda_2. \end{cases} \tag{4.13}$$

One can also simplify equations (4.7), (4.9)-(4.11) and obtain

$$A = \mu(x - y) + 4(x\cos^2\phi - y\sin^2\phi)(x\cos^2\phi + y\sin^2\phi - 1), \tag{4.14}$$

$$B = \mu(x + y - \frac{2}{xy}) + 4(x\cos^2\phi + y\sin^2\phi)(x\cos^2\phi + y\sin^2\phi - 1), \tag{4.15}$$

where $x = \lambda_1^2$, $y = \lambda_2^2$, $A = \sigma_1 - \sigma_2$, $B = \sigma_1 + \sigma_2 - 2\sigma_3$. Equation (4.14) is the difference of (4.10) and (4.9); Equation (4.15) is obtained from their sum using $p = \mu\lambda_3^2 - \sigma_3$, which is equivalent to (4.11). The state of the system (4.13)-(4.15) at time t is uniquely described by $(x(t), y(t), \phi(t))$, that is we have a 3-dimensional phase space. The initial conditions,

$$\phi_{|t=0} = \phi_0, \quad x_{|t=0} = x_0, \quad y_{|t=0} = y_0 \tag{4.16}$$

must satisfy equations (4.14) and (4.15).

The system can be interpreted geometrically: Equations (4.14), (4.15) define, for given A and B, two level sets in the phase space (x, y, ϕ). The intersection of these level sets is a curve, each point of which corresponds to a state of the system at some time t. As the system evolves, the point $(x, y, \phi)(t)$ moves along the curve, the direction and the velocity is defined by (4.13). Since the system is autonomous, we are only interested in the direction, and the behaviour of the system is exhaustively described by one or several oriented curves in the phase space (x, y, ϕ), see *e.g.* Figure 4.5.

An important aspect of the system's evolution is related to the fact that typical fibers do not support compressive loads. Therefore, we assume that the fibers can be completely disregarded when they are compressed and no reorientation takes place in this case. In other words, we further restrict the dynamics in our model to the *fiber-tensile region*, defined by

$$\begin{aligned} &I_{\mathrm{f}} = x\cos^2\phi + y\sin^2\phi > 1, \\ &\phi \in [0, \pi/2]. \end{aligned} \tag{4.17}$$

The boundary of region (4.17) corresponds to the unstrained state of fibers, whereas the material behaves as a classical Neo-Hookean isotropic material in the fiber-compressive region, *i.e.* when $x\cos^2\phi + y\sin^2\phi < 1$, $\forall\phi \in [0, \pi/2]$.

4.2.1.1 Analysis

In order to determine the behaviour of system (4.13)-(4.15) in the fiber-tensile region (4.17), we first find all equilibria in that region and determine their local stability (by an equilibrium we mean a stationary point of (4.13)-(4.15)). Then, we identify all points at which a trajectory in the phase space (x, y, ϕ) can enter or leave the fiber-tensile region, that is, we find all unstrained fibers states. Finally, we conclude from continuity considerations that any curve defined by (4.14), (4.15) connects a unique equilibrium state to two points, which are on the boundary of the fibre-tensile region and correspond either to an unstrained fibers state or to a non-equilibrium state with $\phi = 0, \pi/2$. The analysis of the global behaviour of the system is accomplished by defining the directions in which the evolution occurs along the curve using Equation (4.13).

We start from the observation that a steady state of system (4.13)-(4.15) satisfies one of the following conditions:

1. $\phi = 0$, $x > y$ (ϕ achieves its minimum and λ_1 is the predominant stretch);
2. $\phi = \frac{\pi}{2}$, $x < y$ (ϕ achieves its maximum and λ_2 is the predominant stretch);
3. $\phi = \phi^* \in (0; \frac{\pi}{2})$, $x = y = \lambda^2$ (there is no predominant stretch in X_1X_2-plane).

Equilibria of the first and second type are called *extreme equilibria*, whereas the third type are *intermediate equilibria*. In the latter case the value of the equilibrium fiber angle ϕ^* is unknown and has to be computed using the constitutive law. Borderline cases $x = y$, $\phi = 0 \,\text{or}\, \pi/2$ can be considered as either type of equilibria.

Equations (4.13)-(4.15) are invariant with respect to the change of variables: $x \mapsto y$, $y \mapsto x$, $\phi \mapsto \frac{\pi}{2} - \phi$, $A \mapsto -A$. Thus, we may only consider extreme equilibria for $x > y$, intermediate equilibria for $A \geq 0$, and extend the results to remaining cases via this symmetry.

4.2.1.2 Extreme equilibrium states

At a extreme equilibrium, ($\phi = 0$, $x > y$) equations (4.14), (4.15) and inequalities $x > y$, $y > 0$, (4.17) become respectively

$$A = \mu(x - y) + 4x(x - 1), \tag{4.18}$$

$$B = \mu(x + y - \frac{2}{xy}) + 4x(x - 1), \tag{4.19}$$

$$-\left(4x^2 - 4x - A\right) > 0, \tag{4.20}$$

$$4x^2 - 4\alpha x - A > 0, \tag{4.21}$$

$$x > 1, \tag{4.22}$$

where $\alpha = 1 - \frac{\mu}{4}$.

Proposition 8. *System (4.18)-(4.22) has at most one solution, and the criterion for its existence is given by*

$$\begin{cases} B_{cr2} < B < B_{cr1}, & \text{if} \quad 0 < A < \mu, \\ B < B_{cr1}, & \text{if} \quad A \geq \mu, \end{cases} \tag{4.23}$$

where

$$B_{cr1} = A + \mu\left(1 + \sqrt{1 + A} - \frac{8}{\left(1 + \sqrt{1 + A}\right)^2}\right) \tag{4.24}$$

$$B_{cr2} = -A - \frac{2\mu A}{\mu - A}. \tag{4.25}$$

Proof. Inequalities (4.20)-(4.22) are equivalent to

$$\frac{1}{2}\left(1-\sqrt{1+A}\right) < x < \frac{1}{2}\left(1+\sqrt{1+A}\right), \tag{4.26}$$

$$\frac{1}{2}\left(\alpha+\sqrt{\alpha^2+A}\right) < x, \tag{4.27}$$

$$1 < x, \tag{4.28}$$

since $x < \frac{1}{2}\left(\alpha-\sqrt{\alpha^2+A}\right)$ is incompatible with $1 < x$ as $\alpha < 1$. Note also that $1-\sqrt{1+A} < \alpha+\sqrt{\alpha^2+A}$. By considering two cases, and $\alpha+\sqrt{\alpha^2+A} < 2$ and $\alpha+\sqrt{\alpha^2+A} > 2$, we can write (4.20)-(4.22) as

$$\frac{1}{2}\left(\alpha+\sqrt{\alpha^2+A}\right) < x < \frac{1}{2}\left(1+\sqrt{1+A}\right) \quad \text{if } \mu < A, \tag{4.29}$$

$$1 < x < \frac{1}{2}\left(1+\sqrt{1+A}\right) \quad \text{if } 0 < A < \mu. \tag{4.30}$$

Assume that A, μ are fixed and $y = \frac{1}{\mu}\left(x^2-\alpha x-A\right)$ is expressed from (4.18). Now regard the right-hand side of (4.19) as a function of x and denote it $\bar{B}(x)$, so that, (4.19) becomes

$$B = \bar{B}(x), \tag{4.31}$$

where

$$\bar{B}(x) = \mu(x+y-\frac{2}{xy}) + 4x(x-1). \tag{4.32}$$

It is easy to see that $\bar{B}(x)$ is strictly increasing in x, unbounded for $x > 1$, $y > 0$, and has a vertical asymptote at $y = 0$, since

$$\frac{d}{dx}\bar{B}(x) = \mu\left(1+y'+\frac{2y+2xy'}{x^2y^2}\right) + 8x - 4 > 0, \tag{4.33}$$

where $y' = \frac{1}{\mu}(2x-\alpha) > 0$. It follows from monotonicity of $\bar{B}(x)$, that at most one value of x (such that $y > 0$) satisfies (4.32) for any constant B. Therefore, (4.18)-(4.22) has

at most one solution. Moreover, this solution exists if and only if

$$B < \bar{B}(\frac{1}{2}\left(1+\sqrt{1+A}\right)) \quad \text{if } 1-\alpha < A, \tag{4.34}$$

$$\bar{B}(1) < B < \bar{B}(\frac{1}{2}\left(1+\sqrt{1+A}\right)) \quad \text{if } 0 < A < 1-\alpha, \tag{4.35}$$

which is obtained by applying $\bar{B}(\cdot)$ to (4.29) and (4.30). The left inequality in (4.29) vanished, since $\bar{B}(\alpha+\sqrt{\alpha^2+A}+0) = -\infty$. Also, this asymptote and strict monotonicity of $\bar{B}(x)$ guarantee that no extra positive solutions x, y have been acquired by transition from (4.29) to (4.34). After substituting expressions for $\bar{B}(\cdot)$ in (4.34), (4.35) leads to (4.23). □

By Proposition 8, a unique extreme equilibrium exists if and only if the parameters A, B, μ satisfy (4.23). The local stability of this steady state is given by the following proposition.

Proposition 9. *Any positive solution of (4.13)-(4.15) with $\phi = 0$ is a locally stable equilibrium if and only if $x > y$.*

Proof. Consider an equilibrium point $(\tilde{x}, \tilde{y}, 0)$ in the space (x, y, ϕ). Equations (4.14), (4.15) become polynomial in x and y after multiplying by $xy > 0$. These two equations have a finite number of zeros (x, y), which depend on ϕ continuously. Inequality $\tilde{x}¿\tilde{y}$ holds as follows from (4.13), then there exist $\varepsilon > 0$ and a neighborhood $\Omega = \{(x, y, \phi) \in \mathbb{R}^3 | \, |(x-\tilde{x}, y-\tilde{y}, \phi)| < \varepsilon\}$, in which $x > y$ also holds and which contains no equilibrium apart from $(\tilde{x}, \tilde{y}, 0)$. Since $x > y$ implies $d\phi/dt < 0$ and due to the continuous dependence of the right-hand side of (4.13) on ϕ, any state (x, y, ϕ) in this neighborhood that satisfies (4.13)-(4.15) will be attracted to $(\tilde{x}, \tilde{y}, 0)$. □

4.2.1.3 Intermediate equilibrium states

At an intermediate equilibrium ($x = y$) Eqs. (4.13)-(4.15) reduce to

$$A = 4x(x-1)\cos 2\phi, \tag{4.36}$$

$$B = \mu(2x - \frac{2}{x^2}) + 4x(x-1), \tag{4.37}$$

$$x > 1, \tag{4.38}$$

where the last inequality comes from (4.17).

Proposition 10. *System (4.36)-(4.38) for $A \geq 0$ has at most one solution and the criterion for its existence is given by*

$$B > B_{cr1} = A + \mu\left(1 + \sqrt{1+A} - \frac{8}{\left(1+\sqrt{1+A}\right)^2}\right), \tag{4.39}$$

Proof. Similarly to Proposition 8, we introduce the notation $\tilde{B}(x)$ for the right-hand side of (4.37). Using $A \geq 0$ and the fact that the range of $\cos 2\phi$ is $(-1, 1)$, system (4.36)-(4.38) can be written as

$$A < x(x-1),$$

$$B = \tilde{B}(x),$$

$$x > 1,$$

and further simplified to

$$x > \frac{1}{2}\left(1 + \sqrt{1+A}\right), \tag{4.40}$$

$$B = \tilde{B}(x), \tag{4.41}$$

where

$$\tilde{B}(x) = \mu(2x - \frac{2}{x^2}) + 4x(x-1).$$

$\tilde{B}(x)$ is an unbounded and strictly increasing function for $x > 0$, as can be seen from

$$\frac{d}{dx}\tilde{B}(x) = \mu(2 + \frac{4}{x^3}) + 8x - 4.$$

We apply $\tilde{B}(\cdot)$ to (4.40) and use (4.41) to obtain

$$B > \tilde{B}(\frac{1}{2}\left(1 + \sqrt{1+A}\right)),$$

which is equivalent to (4.39). □

By Proposition 10, the unique intermediate equilibrium exists if and only if the parameters A, B, μ satisfy (4.39).

In order to investigate the local stability of the intermediate equilibrium, we introduce the change of variables $g = \frac{1}{2}(x+y)$, $h = \frac{1}{2}(x-y)$ and aim to examine the derivative $\frac{dh}{d\phi}$ at $h = 0$, whose sign characterizes the stability as illustrated on Figure 4.2. The geometric meaning of $\frac{dh}{d\phi}$ is the slope of the curve, defined by (4.14), (4.15) at its intersection with the plane $h = (x-y)/2 = 0$, where all possible intermediate equilibria are situated. This slope determines via equation (4.13) whether a solution in the vicinity of the equilibrium is attracted to it or repelled from it.

The following proposition demonstrates that the derivative $\frac{dh}{d\phi}$ is positive in the fiber-tensile region. Therefore, we conclude that the intermediate equilibrium is locally stable.

Proposition 11. *Equations (4.14), (4.15) imply that for* $x > 1$

$$\left[\frac{dh}{d\phi}\right]_{h=0} = \left[\frac{d(x-y)/2}{d\phi}\right]_{x=y} > 0. \tag{4.42}$$

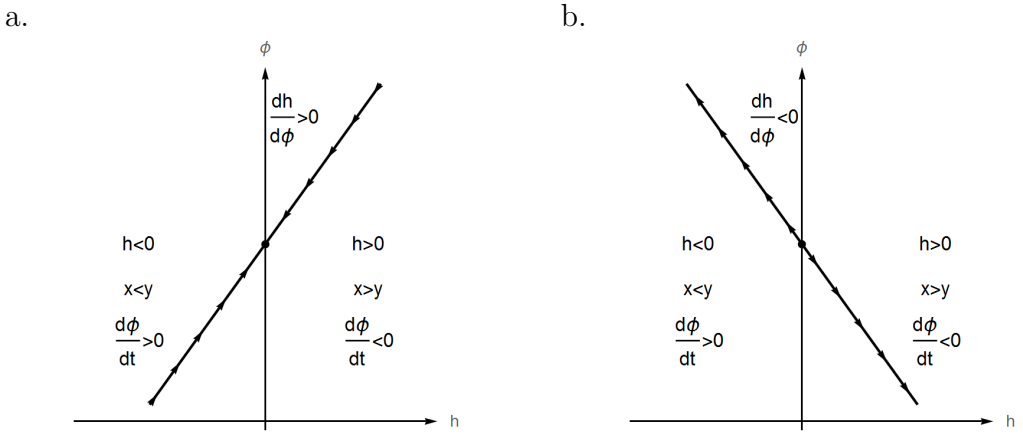

Figure 4.2: **a**. Locally stable intermediate equilibrium. **b**. Locally unstable intermediate equilibrium.

Proof. Equations (4.14) and (4.15) are

$$\begin{aligned} A &= 2\mu h + 4\left(\cos 2\phi(h^2+g^2) + (\cos^2 2\phi + 1)gh - g\cos 2\phi - h\right), \\ B &= 2\mu g + 4\left(h^2\cos^2 2\phi + g^2 + 2gh\cos 2\phi - h\cos 2\phi - g\right), \end{aligned}$$

where $g = \frac{1}{2}(x+y)$, $h = \frac{1}{2}(x-y)$. We differentiate these two equations with respect to ϕ and evaluate the result at $h = 0$ to obtain

$$\begin{aligned} \frac{dg}{d\phi}\cos 2\phi\,(2g-1) + \frac{dh}{d\phi}\left(g\left(\frac{3}{2}+\frac{1}{2}\cos 4\phi\right) + \frac{\mu}{2} - 1\right) - 2\sin 2\phi\left(g^2 - g\right) = 0, \\ \frac{dg}{d\phi}\left(2g + \frac{\mu}{g^3} + \frac{\mu}{2} - 1\right) + \frac{dh}{d\phi}\cos 2\phi\,(2g-1) = 0. \end{aligned} \tag{4.43}$$

Then by solving these linear algebraic equations and using $x = g|_{h=0}$ we obtain

$$\frac{dh}{d\phi}|_{h=0} = \frac{x\,(1-x)\,f_3(x)\sin 2\phi}{(\cos 4\phi + 1)f_1(x) + (1-\cos 4\phi)f_2(x)}, \tag{4.44}$$

where

$$
\begin{aligned}
f_1(x) &= -\left(x^4 - \left(\frac{1}{2} - \frac{\mu}{8}\right)x^3 + x - \left(\frac{1}{2} - \frac{\mu}{4}\right)\right), \\
f_2(x) &= -\frac{1}{\mu}\left(x - \left(1 - \frac{\mu}{2}\right)\right)\left(x^4 - \left(\frac{1}{2} - \frac{\mu}{4}\right)x^3 + \frac{\mu}{2}\right) = -\frac{1}{\mu}\left(x - \left(1 - \frac{\mu}{2}\right)\right) f_3(x), \\
f_3(x) &= x^4 - \left(\frac{1}{2} - \frac{\mu}{4}\right)x^3 + \frac{\mu}{2}.
\end{aligned}
$$

It follows from the form of $f_1(x)$, $f_2(x)$, $f_3(x)$ and from $\frac{1}{2} - \frac{\mu}{4} < 1$, $\frac{1}{2} - \frac{\mu}{8} < 1$ that $f_1(x) > 0$, $f_2(x)$, $f_3(x) < 0$ for any $x > 1$. Hence, the numerator of the right-hand side in (4.44) is negative, so is the denominator as a convex combination of $2f_1(x)$ and $2f_2(x)$ parametrized by $\cos 4\phi \in [-1, 1]$. Therefore, (4.42) holds. □

4.2.1.4 Unstrained fibers states

We have previously shown that extreme and intermediate equilibria are unique whenever they exist in the fiber-tensile region. We now question whether solutions of system (4.13)-(4.15) can enter or leave this region. The unstrained fibers states are those that satisfy

$$
\begin{aligned}
& x\cos^2\phi + y\sin^2\phi = 1, \\
& \phi \in [0, \pi/2].
\end{aligned}
\tag{4.45}
$$

Equation (4.45) is equivalent to

$$
\phi = \mathrm{ArcTan}\sqrt{\frac{x-1}{1-y}}, \tag{4.46}
$$

$$
0 \geq (x-1)(y-1). \tag{4.47}
$$

Inequality (4.47) means that x and y are on opposite sides of the unity. We investigate only the case $y < 1 < x$ and extend the results to the case $x < 1 < y$ using the

symmetry mentioned above. Thus, the unstrained fibers states are given by

$$A = \mu(x - y), \tag{4.48}$$

$$B = \mu(x + y - \frac{2}{xy}), \tag{4.49}$$

$$y > 0, \tag{4.50}$$

$$y \leq 1, \tag{4.51}$$

$$x \geq 1. \tag{4.52}$$

Proposition 12. *System (4.48)-(4.52) has a solution if and only if the parameters A, B, μ satisfy*

$$\begin{cases} B_{cr2} \leq B \leq B_{cr3}, & 0 < A < \mu, \\ B \leq B_{cr3}, & A \geq \mu, \end{cases} \tag{4.53}$$

where

$$B_{cr3} = A + \frac{2\mu A}{\mu + A}, \tag{4.54}$$

and B_{cr2} is defined by (4.25). The solution is unique, whenever it exists.

Proof. We express y as a function of x using (4.48) and introduce, as before, the notation $\hat{B}(x)$ for the right-hand side of (4.49). System (4.48)-(4.52) then becomes

$$y = x - \frac{A}{\mu}, \tag{4.55}$$

$$B = \hat{B}(x), \tag{4.56}$$

$$x > \frac{A}{\mu}, \tag{4.57}$$

$$x \leq 1 + \frac{A}{\mu}, \tag{4.58}$$

$$x \geq 1. \tag{4.59}$$

Inequalities (4.57)-(4.59) are in turn equivalent to

$$1 \leq x \leq 1 + \frac{A}{\mu}, \quad \text{if} \quad 0 < A < \mu,$$
$$\frac{A}{\mu} < x \leq 1 + \frac{A}{\mu}, \quad \text{if} \quad A \geq \mu.$$

It is easy to see, that

$$\hat{B}(x) = \mu(x + y - \frac{2}{xy}) = 2\mu x - A - \frac{2\mu}{x(x - A/\mu)})$$

is a strictly increasing unbounded function for $x \geq y > 0$, and has a vertical asymptote at $y = 0$ ($x = A/\mu$). Based on the same arguments as in Proposition 8, we conclude that system (4.48)-(4.52) has a unique solution if

$$\hat{B}(1) \leq B \leq \hat{B}(1 + \frac{A}{\mu}) \quad \text{if} \quad 0 < A < \mu,$$
$$B \leq \hat{B}(1 + \frac{A}{\mu}), \quad \text{if} \quad A \geq \mu,$$

and no solution otherwise. Thus, we obtained condition (4.53). □

By Proposition 12, there is at most one unstrained fibers state, whose existence is given by (4.53).

4.2.1.5 Singularities

System (4.14)-(4.13) includes algebraic and ordinary differential equations, and therefore, its solutions cannot be continuously extended in time at certain points, which are called singularities. In order to investigate where such singularities occur, we take a time derivative of (4.14) and (4.15) to obtain

$$\mathbf{M}\begin{pmatrix} \dot{x} \\ \dot{y} \end{pmatrix} = \mathbf{f}, \tag{4.60}$$

where $\mathbf{M} = \mathbf{M}(x, y, \phi)$ is a 2×2 matrix, and $\mathbf{f} = \mathbf{f}(x, y, \phi)$ is a column-vector, whose entries are

$$\mathbf{M}_{11} = \mu - 4\cos^2\phi + 8x\cos^4\phi, \quad \mathbf{M}_{21} = \mu + \frac{2\mu}{x^2 y} - 4\cos^2\phi + 8x\cos^4\phi + 2y\sin^2 2\phi, \tag{4.61}$$

$$\mathbf{M}_{12} = -\mu + 4\sin^2\phi - 8y\sin^4\phi, \quad \mathbf{M}_{22} = \mu + \frac{2\mu}{xy^2} - 4\sin^2\phi + 8y\sin^4\phi + 2x\sin^2 2\phi, \tag{4.62}$$

$$\mathbf{f}_1 = -4\dot{\phi}\sin 2\phi\left(x + y - 2x^2\cos^2\phi - 2y^2\sin^2\phi\right), \tag{4.63}$$

$$\mathbf{f}_2 = 4\dot{\phi}\sin 2\phi(x - y)\left(x + y - 1 + (x - y)\cos 2\phi\right). \tag{4.64}$$

Equation (4.60) together with (4.13) form a system of 3 autonomous ODEs, equivalent to the differential-algebraic system (4.13)-(4.15), provided initial conditions for the former satisfy (4.14) and (4.15). A solution of (4.60), (4.13) or (4.13)-(4.15), cannot be continuously extended in time at the points where the matrix $\mathbf{M}$ is singular, *i.e.* $\det\mathbf{M} = 0$.

Geometrically, a singularity corresponds to a point at which the tangent to the trajectory in phase space (x, y, ϕ) is parallel to the xy-plane, hence, the derivative of ϕ along the the trajectory is zero. A curve defined by equations (4.14), (4.15) has local minima or maxima of ϕ at simple (unrepeated) singularities. Therefore, the value of ϕ cannot increase or decrease locally, as prescribed by equation (4.13), see Remark 13.

Here $\mathbf{M}$ depends only on x, y, ϕ and on the shear modulus μ, hence, the set $\det\mathbf{M} = 0$ in phase space (x, y, ϕ) depends only on μ, which captures relative fiber content or stiffness. This set is depicted on Figure 4.3 for various values of μ. It can be clearly seen from Figure 4.3 that the surface $\det\mathbf{M} = 0$ is contained in the fiber-

compressive region, and we conclude that there are no singularities in the fiber-tensile region (4.17).

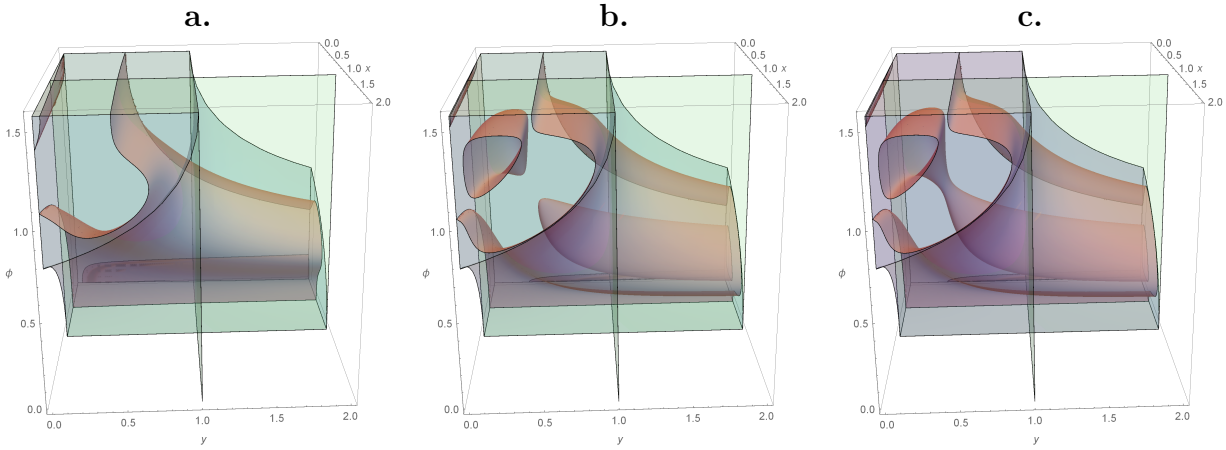

Figure 4.3: Zeros of det$\mathbf{M}$ in the phase space (x, y, ϕ) for various parameters. **a**. $\mu = 0.1$. **b**. $\mu = 1/75$. **c**. $\mu = 1/80$. The fiber-compressive region $x\cos^2\phi + y\sin^2\phi < 1$ (blue), planes $x = 1$, $y = 1$ (light green).

4.2.1.6 Global behaviour

Criteria (4.23), (4.39), (4.53) are summarized on bifurcation diagrams in Figure 4.4. We now comment on the solutions of dynamical system (4.14)-(4.13).

It has been already mentioned, that equations (4.14), (4.15) define a curve or a set of curves in phase space (x, y, ϕ). Due to the polynomial nature of (4.14) and (4.15), branching and coalescence of trajectories are associated with singularities, which are absent in the fiber-tensile region (4.17). The existence of a cycle also implies a singularity due to Rolle's Theorem, which applied to $\oint \frac{d\phi}{dl} dl = 0$ requires $\frac{d\phi}{dl} = 0$. Constant applied stresses (A, B = const) imply that any solution $(x, y, \phi)(t)$ is bounded, as can be seen from (4.14), (4.15). Thus, equations (4.14), (4.15) define a single curve connecting two points on the boundary of the fiber-tensile region, which can be an extreme equilibrium $\phi = 0, \pi/2$, a non-equilibrium solution $\phi = 0, \pi/2$ or an unstrained fibers state $\phi \neq 0, \pi/2$. If there exists an intermediate equilibrium $\phi \neq 0, \pi/2$, then the curve has to pass through it. Equation (4.13) prescribes the orientation of the curve,

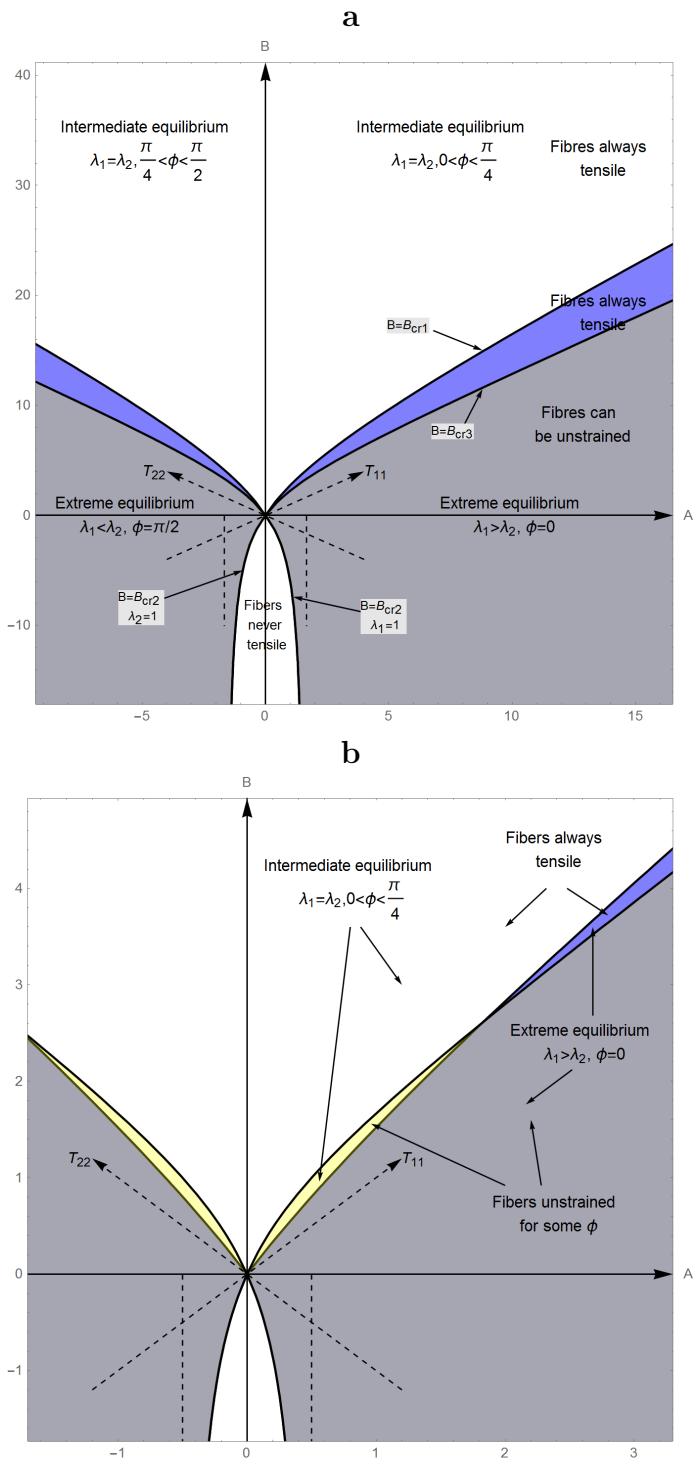

Figure 4.4: Bifurcation diagram of the system (4.13)-(4.15) for fiber stiffness **a**. $\mu > \frac{4}{3}$, **b**. $\mu < \frac{4}{3}$. In the upper white region a unique stable intermediate equilibrium exists and fibers are tensile for any orientation. In the yellow region a unique stable tensile intermediate equilibrium exists, whereas fibers are compressed for some orientations. In the blue region a unique stable extreme equilibrium exists and fibers are tensile for any orientation. In the grey dashed region a unique stable tensile extreme equilibrium exists, whereas fibers are compressed for some orientations.

which can change only at the stable intermediate equilibrium. The initial conditions for system (4.13)-(4.15) define the point on the curve where the evolution begins and hence the part of the curve it involves.

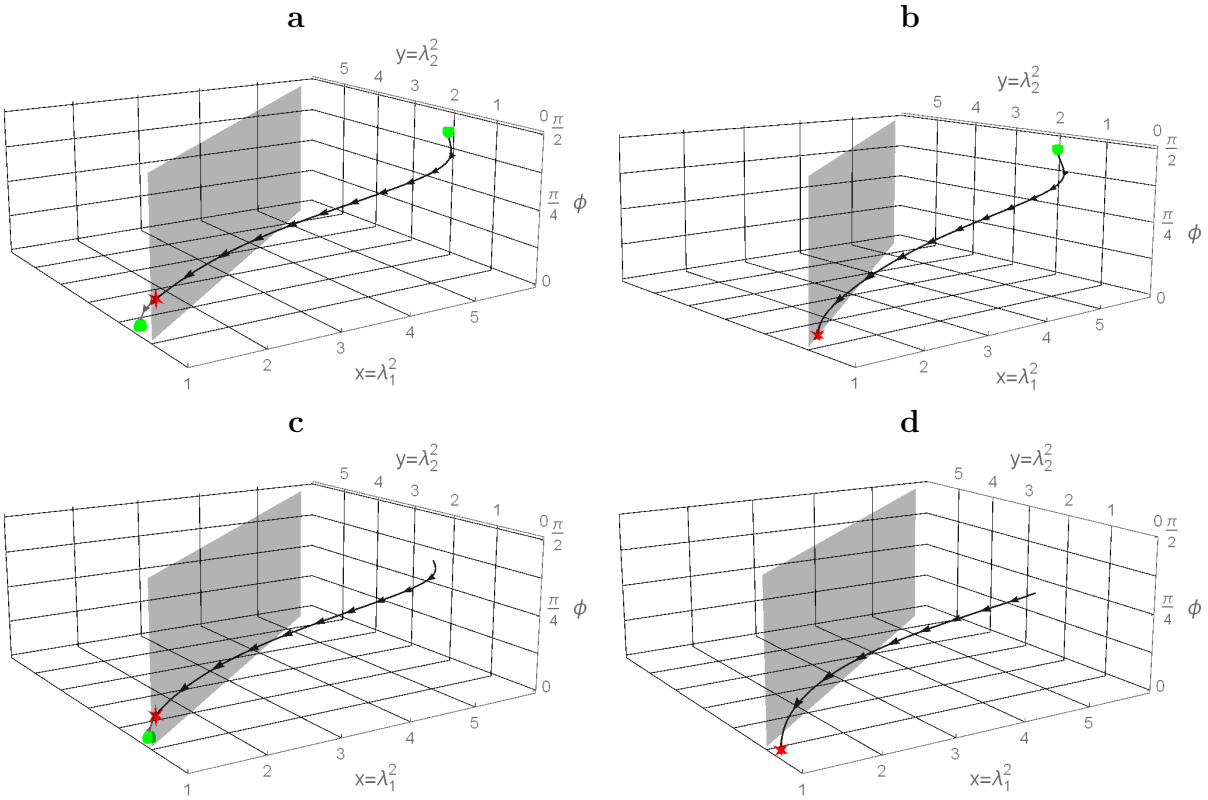

Figure 4.5: Solutions of system (4.14)-(4.13) in the fiber-tensile region as oriented curves in the space $(x = \lambda_1^2, y = \lambda_2^2, \phi)$, stable equilibria (red stellate), extreme fiber orientation points at $\phi = 0, \pi/2$ that are not steady states (green spheres), unstrained fibers points (loose ends), plane $\lambda_1^2 = \lambda_2^2$ (grey). **a.** Intermediate equilibrium and two non-equilibrium points, $\mu = 0.1$, $A = 0.4$, $B = 0.4$. **b.** Extreme equilibrium and one non-equilibrium point, $\mu = .5$, $A = 2$, $B = 2.82$. **c.** Intermediate equilibrium, non-equilibrium point and unstrained fibers point, $\mu = .1$, $A = 0.4$, $B = 0.52$. **d.** Extreme equilibrium and unstrained fibers point, $\mu = 0.1$, $A = 0.4$, $B = 0.24$.

If $B > B_{cr1}$, $B > B_{cr3}$ (Figure 4.4.a, Figure 4.4.b, upper white region; Figure 4.5.a), then the trajectory connects one non-equilibrium point ($\phi = \pi/2$) to another non-equilibrium point ($\phi = 0$), passing through a unique stable intermediate equilibrium in the middle ($0 < \phi < \pi/2$), towards which it is oriented. The fiber angle value ϕ at the intermediate equilibrium depends smoothly on the parameters A, B.

When point (A, B) crosses $B = B_{cr1}(A)$ on the bifurcation diagram, one non-equilibrium point coalesces with an intermediate equilibrium at $\phi = 0$ (if $A > 0$) or at $\phi = \pi/2$ (if $A < 0$).

When (A, B) crosses $B = B_{cr3}(A)$, the second non-equilibrium point ($\phi = 0$, $\lambda_1 < \lambda_2$ or $\phi = \pi/2$, $\lambda_1 > \lambda_2$) leaves the fiber-tensile region and is replaced by a point of unstrained fibers at the end of the trajectory.

Accordingly, if $B_{cr1} < B < B_{cr3}$ (Figure 4.4.a, Figure 4.4.b, blue region; Figure 4.5.b), the trajectory connects a non-equilibrium point to an extreme equilibrium, which are at $\phi = \pi/2$ and $\phi = 0$ respectively for $A > 0$ and vice versa for $A < 0$. Both ends of the curve are on the same side from the plane $\lambda_1 = \lambda_2$.

If $B_{cr3} < B < B_{cr1}$ (Figure 4.4.b, yellow region; Figure 4.5.c), the trajectory connects a non-equilibrium point and a point of unstrained fibers to an intermediate stable equilibrium between them.

If $B < B_{cr1}$, $B < B_{cr2}$ (Figure 4.4.a, Figure 4.4.b, grey region; Figure 4.5.d), the trajectory connects an unstrained fibers point to the stable extreme equilibrium.

When (A, B) crosses $B = B_{cr3}(A)$ on the bifurcation diagram, a stable equilibrium coalesces with an unstrained fibers point and leaves the fiber-tensile region. There is no solution in the fiber-tensile region, if $B < B_{cr2}$ (lower white region on Figure 4.4.a, Figure 4.4.b). Under the assumption that no fiber reorientation happens when the fibers are not stretched and that fibers do not support compressive loads, the behaviour of the material in this region is identical to the behaviour of a neo-Hookean material without reinforcement and reorientation.

It follows from the above considerations that for constant loads satisfying $B > B_{cr3}(A)$, a unique configuration (λ_1, λ_2) corresponds to each value of fiber angle $\phi \in [0, \pi/2]$. In addition, $B > B_{cr2}(A)$ ensures at most one configuration (λ_1, λ_2) for each ϕ, while there are no fiber-tensile solutions for extreme fiber orientations ($[\phi^\circ, \pi/2]$ if $A > 0$ or $[0, \phi_\circ]$ if $A < 0$, where ϕ° is an angle at which fibers are unstrained for given

parameters A, B, μ).

Although a curve defined by (4.14) and (4.15) can cross the boundary of the fiber-tensile region (4.17), the solutions do not leave it, that is, the system is persistent in the fiber-tensile region (4.17), within which it is attracted to a unique stable equilibrium. We also notice that the final fiber orientation angle ϕ can take any value from $[0, \pi/2]$ and is controlled by the applied loads according to the diagrams (Figure 4.4.a, Figure 4.4.b).

Remark 13. A singularity of matrix $\mathbf{M}$ in (4.60) indicates that multiple deformations satisfy the boundary conditions for some orientation angles. The corresponding trajectory in $(\lambda_1, \lambda_2, \phi)$ space has local extrema of ϕ (Figure 4.6). Enforcing fiber reorientation law leads in some cases to unphysical hysteresis-like behaviour, which consists in cyclic non-monotonic evolution of fiber angle accompanied by discontinuous evolution of deformation (Figure 4.6b).

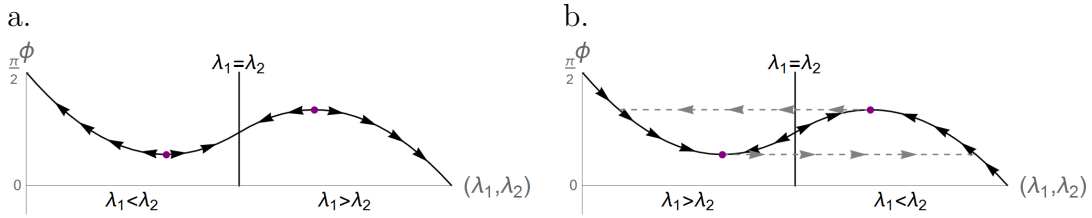

Figure 4.6: Schematic representation of a trajectory that has two singularity points (purple). (**b**) Unphysical hysteresis-like evolution.

4.2.2 The case of fiber dispersion captured by the GST model.

Next, we study the effect of fiber dispersion on the model considered above. We tacitly keep in force all assumptions made in Section 4.2.1, unless explicitly stated otherwise. The main change is the introduction of fiber dispersion as provided by the GST model, which was defined and discussed in details in Chapter 2. Equations (4.9)-(4.11) are

replaced by

$$\sigma_1 = -p + \mu\lambda_1^2 + 4\mathrm{H}_{11}\lambda_1^2(\lambda_1^2\mathrm{H}_{11} + \lambda_2^2\mathrm{H}_{22} + \lambda_3^2\mathrm{H}_{33} - 1), \tag{4.65}$$

$$\sigma_2 = -p + \mu\lambda_2^2 + 4\mathrm{H}_{22}\lambda_2^2(\lambda_1^2\mathrm{H}_{11} + \lambda_2^2\mathrm{H}_{22} + \lambda_3^2\mathrm{H}_{33} - 1), \tag{4.66}$$

$$\sigma_3 = -p + \mu\lambda_3^2, \tag{4.67}$$

where H_{ii} are components of the average generalized structure tensor

$$\mathbf{H} = \frac{1}{2}(\mathbf{H}^{(1)} + \mathbf{H}^{(2)}) = \kappa\mathbf{1} + (1 - 3\kappa)\mathrm{diag}(\cos^2\phi, \sin^2\phi, 0), \tag{4.68}$$

where $\kappa \in [0, \frac{1}{3}]$ is the dispersion parameter. One can observe that $\kappa = 0$ corresponds to the case of strict fiber alignment considered in the previous subsection. Using incompressibility, equations (4.65)-(4.67) can be reduced to

$$\begin{aligned} A &= A(x, y, \phi) \qquad (4.69)\\ &:= \mu(x - y) + 4\left(\kappa(x - y) + (1 - 3\kappa)(x\cos^2\phi - y\sin^2\phi)\right)(I_\mathrm{f} - 1), \\ B &= B(x, y, \phi) \qquad (4.70)\\ &:= \mu(x + y - \frac{2}{xy}) + 4\left(\kappa(x + y - \frac{2}{xy}) + (1 - 3\kappa)(x\cos^2\phi + y\sin^2\phi)\right)(I_\mathrm{f} - 1), \end{aligned}$$

where $x = \lambda_1^2$, $y = \lambda_2^2$, $A = \sigma_1 - \sigma_2$, $B = \sigma_1 + \sigma_2 - 2\sigma_3$, $I_\mathrm{f} = \mathbf{H} : \mathbf{C} = \kappa I_1 + (1 - 3\kappa)I_4$. The evolution of the fiber orientation angle is described by exactly the same phenomenological law

$$\dot{\phi} = \begin{cases} -\frac{\sin\phi}{\tau_{rel}}, & \lambda_1 > \lambda_2, \\ 0, & \lambda_1 = \lambda_2, \\ \frac{\cos\phi}{\tau_{rel}}, & \lambda_1 < \lambda_2. \end{cases} \tag{4.71}$$

The fiber tensile region is defined by

$$\begin{aligned} I_4 &= x\cos^2\phi + y\sin^2\phi > 1, \\ \phi &\in [0, \pi/2], \end{aligned} \tag{4.72}$$

and we note that $I_4 > 1$ implies $I_\mathrm{f} > 1$ as discussed in Proposition 2 of Chapter 2. In other words, the fiber evolution consists in the reorientation of the main fiber direction at constant fiber dispersion. If the strain in the main fiber direction is negative then there is no evolution and the material is isotropic.

4.2.2.1 Analysis

Similarly to the case of no dispersion, the steady states of system (4.69)-(4.71) are defined by the right-hand side of (4.71): extreme equilibria are given by $\phi = 0$, $\lambda_1 > \lambda_2$ and $\phi = \pi/2$, $\lambda_2 > \lambda_1$, an intermediate equilibrium state is defined by $\lambda_1 = \lambda_2$. We investigate regions in the space of parameters (A, B) corresponding to each type of equilibria.

4.2.2.2 Extreme equilibrium states

Without loss of generality we consider the case $x > y$. An extreme equilibrium must satisfy equations (4.69)-(4.71), wherein $\phi = 0$, and inequalities $x > y > 0$, $x > 1$, *i.e.* it is a solution of the system

$$A = A(x, y, 0), \tag{4.73}$$

$$B = B(x, y, 0), \tag{4.74}$$

$$x > y, \tag{4.75}$$

$$y > 0, \tag{4.76}$$

$$x > 1. \tag{4.77}$$

We assume that a root of (4.73), (4.74) exists and depends continuously on the parameters A, B. This root ceases to be an extreme equilibrium if and only if at least one of the inequalities (4.75)-(4.77) ceases to be valid. Hence the boundaries of the corresponding region in (A, B) are defined by $x = y$, $x = 1$ or $y = 0$. These boundaries can be expressed in a parametric form from (4.73) and (4.74),

$$A_{\mathrm{cr1}} = A(x, x, 0), \tag{4.78}$$

$$B_{\mathrm{cr1}} = B(x, x, 0), \tag{4.79}$$

where $x \in (1, +\infty)$, and

$$A_{\mathrm{cr2}} = A(1, y, 0), \tag{4.80}$$

$$B_{\mathrm{cr2}} = B(1, y, 0), \tag{4.81}$$

where $y \in (0, 1)$. The condition $y = 0$ leads to $\|(A, B)\| \to \infty$, which can be considered as a natural boundary of the region at infinity.

The stability of an extreme equilibrium follows from the assumption of continuous dependence on the parameters and Proposition 9.

4.2.2.3 Intermediate equilibrium state

At the intermediate equilibrium state we have

$$A = A(x, x, \phi), \tag{4.82}$$

$$B = B(x, x, \phi), \tag{4.83}$$

$$x > 1. \tag{4.84}$$

$$0 < \phi < \frac{\pi}{2}. \tag{4.85}$$

As the original system (4.69)-(4.71) is symmetric with respect to the change of variables $x \mapsto y$, $y \mapsto x$, $\phi \mapsto \frac{\pi}{2} - \phi$, $A \mapsto -A$, we consider the case $\phi < \pi/4$ without loss of generality. If Equations (4.82)-(4.83) have a root depending continuously on A, B, then it ceases to be an intermediate equilibrium if and only if $x = 1$ or $\phi = 0$. Condition $x = 1$ corresponds to a single point $A = B = 0$, whereas condition $\phi = 0$ results in a parametric curve previously defined by (4.78)-(4.79).

Numerical solutions of the system suggest that the intermediate equilibrium state is stable whenever it exists, however a proof of stability is not provided here.

4.2.2.4 Unstrained fibers states

Consider the case $x > y$. According to (4.72), the main fiber direction is positively strained if and only if

$$0 < y < 1 < x \tag{4.86}$$

$$\phi = \mathrm{ArcTan}\sqrt{\frac{x-1}{1-y}}, \tag{4.87}$$

hold in addition to (4.69)-(4.70). If a root of Equations (4.69)-(4.70) exists and depends continuously on A, B, then, as we vary A and B, this root will correspond to zero strain in the main fiber direction if any of the inequalities in (4.86) no longer holds. Condition $y = 0$ leads to $\|(A, B)\| \to \infty$, condition $x = 1$ implies $\phi = 0$ and leads to the curve defined in (4.80), (4.81). The last option, $y = 1$, implies $\phi = \pi/2$ and leads to a curve

$$A_{\mathrm{cr3}} = A(1, y, \pi/2), \tag{4.88}$$

$$B_{\mathrm{cr3}} = B(1, y, \pi/2). \tag{4.89}$$

4.2.2.5 Singularities

Taking the time derivative of equations of (4.69), (4.70) yields

$$\mathbf{M}\begin{pmatrix} \dot{x} \\ \\ \dot{y} \end{pmatrix} = \mathbf{f}, \tag{4.90}$$

where $\mathbf{M} = \mathbf{M}(x, y, \phi)$ is a 2×2 matrix, and $\mathbf{f} = \mathbf{f}(x, y, \phi)$ is a column-vector, whose entries are

$$\begin{aligned}
\mathbf{M}_{11} &= -4\kappa + \mu + \frac{4\kappa^2 - 4\kappa(3\kappa-1)\sin^2\phi}{x^2} + 8\kappa^2 x + 8(1-3\kappa)^2 x\cos^4\phi \quad (4.91)\\
&\quad -4(3\kappa-1)(4\kappa x - 1)\cos^2\phi,\\
\mathbf{M}_{12} &= 4\kappa - \mu + \frac{4\kappa(3\kappa-1)\cos^2\phi - 4\kappa^2}{y^2} - 8\kappa^2 y - 8(1-3\kappa)^2 y\sin^4\phi \quad (4.92)\\
&\quad +4(3\kappa-1)(4\kappa y - 1)\sin^2\phi,\\
\mathbf{M}_{21} &= \mu + \frac{2\mu}{x^2 y} + 4\left((1-3\kappa)\cos^2\phi + \kappa + \frac{2\kappa}{x^2 y}\right) \quad (4.93)\\
&\quad \left((1-3\kappa)\left(x\cos^2\phi + y\sin^2\phi\right) + \kappa\left(\frac{1}{xy} + x + y\right) - 1\right)\\
&\quad +4\left((1-3\kappa)\cos^2\phi + \kappa - \frac{\kappa}{x^2 y}\right)\\
&\quad \left((1-3\kappa)\left(x\cos^2\phi + y\sin^2\phi\right) + \kappa\left(-\frac{2}{xy} + x + y\right)\right),\\
\mathbf{M}_{22} &= \mu + \frac{2\mu}{xy^2} + 4\left((1-3\kappa)\sin^2\phi + \kappa + \frac{2\kappa}{xy^2}\right) \quad (4.94)\\
&\quad \left((1-3\kappa)\left(x\cos^2\phi + y\sin^2\phi\right) + \kappa\left(\frac{1}{xy} + x + y\right) - 1\right)\\
&\quad +4\left((1-3\kappa)\sin^2\phi + \kappa - \frac{\kappa}{xy^2}\right)\\
&\quad \left((1-3\kappa)\left(x\cos^2\phi + y\sin^2\phi\right) + \kappa\left(-\frac{2}{xy} + x + y\right)\right),
\end{aligned}$$

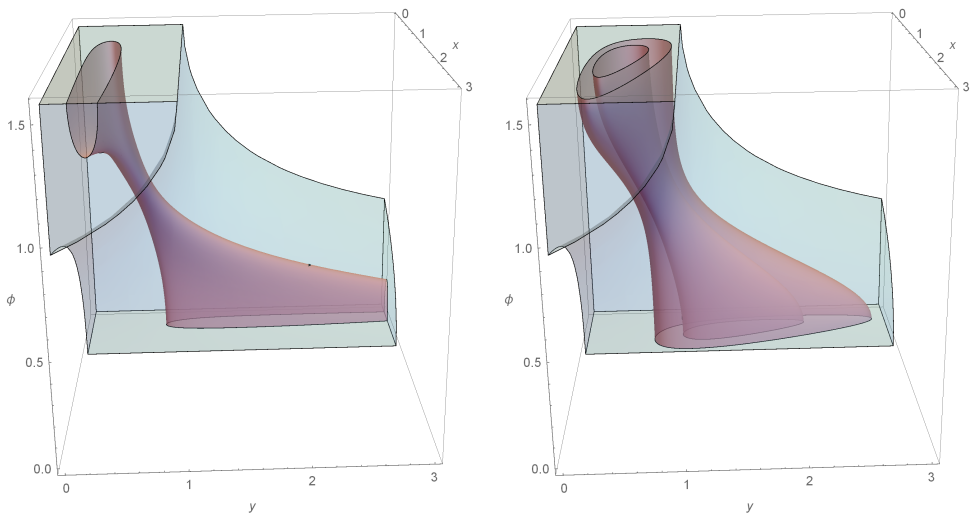

(a) (b)

Figure 4.7: Zeros of $\det \mathbf{M}$ (yellow) inside the fiber compressiv region (blue) in the phase space (x, y, ϕ) for various parameters: (a) $\kappa = 0.3$, $\mu = 0.1$; (b) $\kappa = 0.3$, $\mu = 0.02$.

$$\mathbf{f}_1 = -\ 4\dot{\phi}(1-3\kappa)\sin 2\phi \left((3\kappa-1)\left(x^2-y^2\right)\cos 2\phi - (1-\kappa)\left(x^2+y^2\right) - \frac{\kappa(x+y)}{xy} + x + y\right), \tag{4.95}$$

$$\mathbf{f}_2 = -4\dot{\phi}(1-3\kappa)(x-y)\sin 2\phi \left(2(3\kappa-1)x\cos^2\phi + 2(3\kappa-1)y\sin^2\phi + 1 - 2\kappa(x+y+\frac{1}{xy})\right). \tag{4.96}$$

Numerical evaluation of $\det \mathbf{M}$ shows that similarly to the case of strict fiber alignment, matrix $\mathbf{M}$ is nondegerate in the tensile region of phase space (x, y, ϕ) for all parameters $\mu > 0$, $\kappa \in [0, 1/3]$, Figure 4.7.

4.2.2.6 Global behaviour

The global behaviour of system (4.69)-(4.71) is similar to that of system (4.13)-(4.15). The diagram in Figure 4.8 shows the correspondence between parameters A, B, which express the constant applied loads and the behavior of the system. If the loads allow for a state of tensile fibers, then there exists a unique steady state, which is stable in the tensile region (4.72). The equilibrium direction of fiber reinforcement corresponds

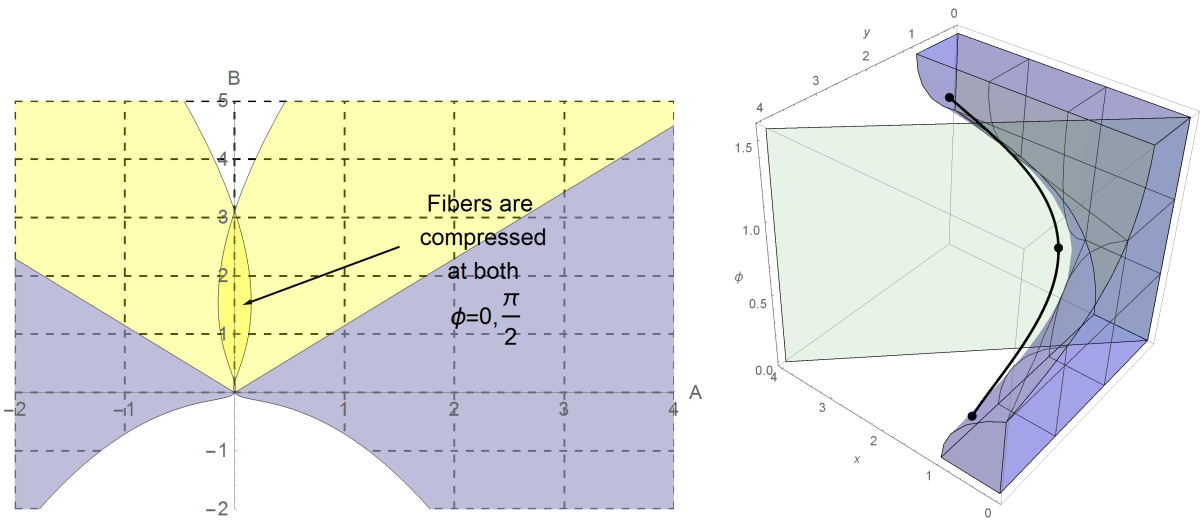

(a) (b)

Figure 4.8: (**a**) Bifurcation diagram computed for parameter values $\mu = 0.07$, $\kappa = 0.05$ showing the existence and type of steady states depending on the applied loads. A unique stable intermediate equilibrium exists in the upper white and yellow regions. A unique stable extreme equilibrium exists in the blue region. Fibers are tensile for all orientations in the upper white region and are compressive for all orientations in the lower white region. In the lighter yellow precisely one extreme orientation $\phi = 0$ or $\pi/2$ results in compressed fibers, while in the darker yellow region both extreme orientations result in compressed fibers. (**b**) A trajectory in the phase space computed for parameter values $\mu = 0.07$, $\kappa = 0.05$ and constant loads $A = 0.04$, $B = 0.6$, which corresponding to the darker tellow region in (a). The trajectory intersects the plane $x = y$, where it has a stable intermediate equilibrium, and is only defined in the fiber-tensile region (blue) for $\phi \in [\phi_{\min}, \phi_{\max}]$, $0 < \phi_{\min}$, $\phi_{\max} < 0$.

either to an extreme value, $\phi = 0, \pi/2$ (extreme equilibrium), or to an intermediate value $\phi \in (0, \pi/2)$ (intermediate equilibrium). The fiber angle changes monotonically as prescribed by (4.71) until it reaches the equilibrium state.

The only qualitative difference between the cases of strict fiber alignment and dispersed fiber reinforcing is that the range of fiber angles resulting in positively strained fibers may contain neither of extreme values $\phi = 0, \pi/2$. In other words, for certain fixed loads the main fiber direction is compressed if it is aligned in the direction of principal stretch λ_1 or λ_2. However at some intermediate orientations between the principal direction, $\phi \in (0, \pi/2)$, the main fiber direction is tensile for the same applied loads.

4.2.3 The case of fiber dispersion captured by the AI model.

The angular integration model treats each portion of fibers independently and allows for selective exclusion of compressed fibers. Thereby the reorientation law can be applied to each fiber individually. However in this case there is no guarantee that the form the orientation density function is preserved, since this would impose a relation between the ODF, the fibre reorientation law and current mechanical state. We assume here that the reorientation law applies to the entire family rather than to individual fibers. The constitutive equations are

$$\begin{aligned}\sigma_{\mathrm{i}} &= -p + \mu\lambda_i^2 \\ &\quad +4\lambda_i^2 \oint_{\mathbb{U}^2} \rho(\mathbf{m}_0)\chi(\mathbf{R}_1\mathbf{m}_0 \otimes \mathbf{R}_1\mathbf{m}_0 : \mathbf{C})\psi_{\mathrm{f}}'(\mathbf{R}_1\mathbf{m}_0 \otimes \mathbf{R}_1\mathbf{m}_0 : \mathbf{C})(\mathbf{R}_1\mathbf{m}_0)_i^2 d\mathbb{U}^2,\end{aligned} \tag{4.97}$$

where $\mathbf{m}_0 \in \mathbb{U}^2$ is the direction of integration, $(\mathbf{R}_1\mathbf{m}_0)_i$ denotes ith component of vector $\mathbf{R}_1\mathbf{m}_0$, $\mathbf{R}_1$ is the rotation matrix by angle ϕ from the axis $\mathbf{E}_1$ about $\mathbf{E}_3$, $\rho(\mathbf{R}_1^T\mathbf{m}_0) = \tilde{\rho}\left(\arccos(\mathbf{E}_1 \cdot \mathbf{R}_1^T\mathbf{m}_0)\right)$, and $\tilde{\rho}(\theta)$ is the von Mises distribution (3.30). The system is defined by constitutive equations

$$A = A(x, y, \phi), \tag{4.98}$$

$$B = B(x, y, \phi), \tag{4.99}$$

and the phenomenological reorientation equation

$$\dot{\phi} = \begin{cases} -\frac{\sin\phi}{\tau_{rel}}, & \lambda_1 > \lambda_2, \\ 0, & \lambda_1 = \lambda_2, \\ \frac{\cos\phi}{\tau_{rel}}, & \lambda_1 < \lambda_2, \end{cases} \tag{4.100}$$

where we define

$$A(x,y,\phi) = \mu(x-y) + 4\oint_{\mathbb{U}^2} \rho(\mathbf{R}_1^T\mathbf{m}_0)\chi(I_\mathrm{f})\psi_\mathrm{f}'(I_\mathrm{f})\left(\lambda_1^2(\mathbf{m}_0)_1^2 - \lambda_2^2(\mathbf{m}_0)_1^2\right)d\omega, \quad (4.101)$$

$$B(x,y,\phi) = \mu(x+y-\frac{2}{xy}) + 4\oint_{\mathbb{U}^2} \rho(\mathbf{R}_1^T\mathbf{m}_0)\chi(I_\mathrm{f})\psi_\mathrm{f}'(I_\mathrm{f})\left(\lambda_1^2(\mathbf{m}_0)_1^2 + \lambda_2^2(\mathbf{m}_0)_1^2 - \frac{2}{\lambda_1^2\lambda_2^2}(\mathbf{m}_0)_3^2\right)d\omega, \quad (4.102)$$

with $I_\mathrm{f} = \mathbf{m}_0 \otimes \mathbf{m}_0 : \mathbf{C}$.

Numerical solutions of (4.98)-(4.100) showed that its solutions act similar to that of systems (4.69)-(4.71) or (4.13)-(4.15). Therfore we use the same method to plot the bifurcation diagram as we used in case of the GST model. The comparison of bifurcation diagrams for strict fiber alignment, GST and AI models are shown on Figure 4.9.

4.3 Stress-induced reorientation subject to constant stresses

Consider a model that is obtained from (4.9)-(4.12) by replacing the strain-induced reorientation law (4.12) with a similar stress-induced law. Such model is described by equations (4.14), (4.15) and fiber reorientation equation

$$\dot{\phi} = \begin{cases} -\frac{\sin\phi}{\tau_{rel}}, & \sigma_1 > \sigma_2, \\ 0, & \sigma_1 = \sigma_2, \\ \frac{\cos\phi}{\tau_{rel}}, & \sigma_1 < \sigma_2. \end{cases} \quad (4.103)$$

As before, we assume that the time evolution takes place only if the fibers are under tension, *i.e.* we restrict the dynamics to the fibre-tensile region (4.17). Since the

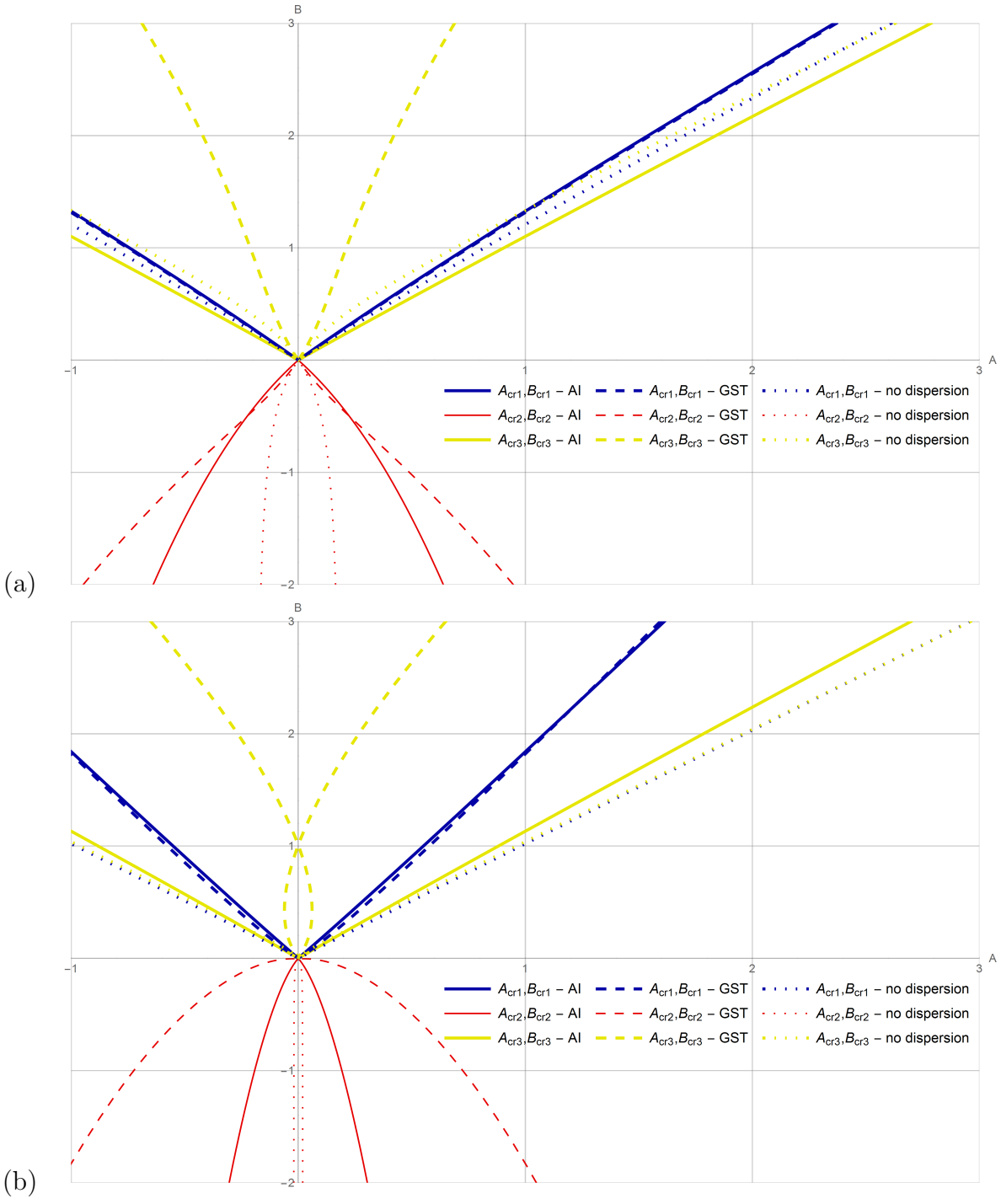

Figure 4.9: Comparison of bifurcation diagrams for the cases of strict fiber alignment, fiber dispersion modelled by GST and AI models. (**a**) mild dispersion and low relative fiber content $\kappa = 0.05$, $\mu = .02$; (**b**) significant dispersion and high fiber content $\kappa = 0.2$, $\mu = 0.02$.

reorientation equation (4.103) only incorporates constant principal stresses, but not the changing principal stretches, it is decoupled from the stress-strain relation (4.14), (4.15). As a result, the evolution of fiber angle $\phi(t)$ is almost fully determined by an initial orientation $\phi(0) = \phi_0$ and parameters A, B. The role played by the constitutive equation in the dynamics is limited to defining what orientation angles result in unstrained fibers for given stresses.

It follows from (4.103) that there exists a unique stable steady state $\phi = 0$, if $\sigma_1 > \sigma_2$, and a unique stable steady state $\phi = \frac{\pi}{2}$, if $\sigma_1 < \sigma_2$. The convergent stability of these extreme fiber alignment steady states follows from the fact that the right-hand side of (4.103) is zero at the respective equilibrium and of appropriate constant sign elsewhere. There is no time evolution at all if $\sigma_1 = \sigma_2$. In this case any fiber orientation ϕ can be considered as a neutrally stable steady state.

The behaviour of the system can be described as follows. If the loads applied to the material compress the fibers then there is no dynamics. If the loads result in fibers being in tension then the fibers realign asymptotically approaching the direction of the maximum principal stress (Fig. 4.10a). The arguments presented in Subsection 4.2.1.5 are valid here and imply that the deformation depends continuously on the fiber angle ϕ, since Equations (4.14), (4.15) define the same curves in phase space (x, y, ϕ). Note also that once the fibers are tensile, they cannot become unstrained in the course of fiber reorientation, that is, a trajectory can only enter the fiber-tensile region. An example of a trajectory is depicted in Fig. 4.10b.

4.4 Strain-induced reorientation subject to constant strains

Consider a fixed displacement boundary condition for the material described in the previous section. We assume that the constant principal stretches λ_i are given and

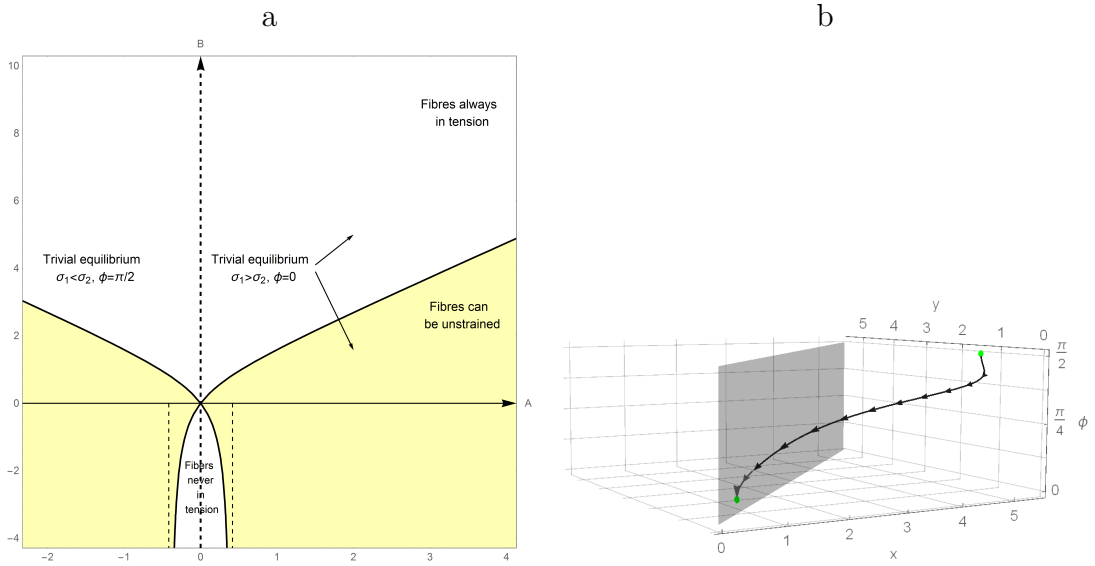

Figure 4.10: a. Bifurcation diagram for system (4.14), (4.15), (4.103); b. an example of solution for (4.14), (4.15), (4.103).

satisfy the incompressibility condition (4.7). The Cauchy stress in an incompressible material is determined by the deformation only up to an isotropic part, which is represented by the Lagrange multiplier p in (4.9)-(4.11). We take $\sigma_3 = 0$ as an additional condition, which is used to compute the value of the stress. Thus, the static part of the model is given by

$$A = \mu(x - y) + 4(x\cos^2\phi - y\sin^2\phi)(x\cos^2\phi + y\sin^2\phi - 1), \tag{4.104}$$

$$B = \mu(x + y - \frac{2}{xy}) + 4(x\cos^2\phi + y\sin^2\phi)(x\cos^2\phi + y\sin^2\phi - 1), \tag{4.105}$$

where $A = \sigma_1 - \sigma_2$, $B = \sigma_1 + \sigma_2$ are regarded as uknowns, which can be computed from given $x = \lambda_1^2$, $y = \lambda_2^2$ and fiber angle ϕ. The only difference between equations (4.104)-(4.105) and (4.14)-(4.15) is that different sets of variables are considered as given constants or unknowns. The dynamical part of the model consists in strain-induced fiber reorientation described by (4.13).

Similarly to the case of constant loads and stress-driven fiber reorientation, a combination of constant strain and strain-induced reorientation results in a trivial beha-

viour. If the principal stretches and initial value of fiber angle belong to the fiber-tensile region (4.17) then $\phi(t)$ monotonically and asymptotically approaches its equilibrium value, which is $\phi = 0$, if $\lambda_1 > \lambda_2$, and $\phi = \frac{\pi}{2}$, if $\lambda_1 > \lambda_2$. If $\lambda_1 = \lambda_2$ then there is no reorientation and any fiber angle can be regarded as a neutrally stable steady state.

It is convenient to identify a solution of system (4.104), (4.105), (4.13) with an oriented curve in a 3-dimensional phase space $(\sigma_1, \sigma_2, \phi)$. A trajectory $(\sigma_1, \sigma_2, \phi)(t)$ is continuous and can be parametrized by fiber angle ϕ. In fact, this parametrization is given by (4.9), (4.10), where the Lagrange multiplier p can be expressed from (4.11). A curve $(\sigma_1(\phi), \sigma_2(\phi), \phi)$ connects a non-equilibrum state with extreme fiber alignment $\phi = 0, \frac{\pi}{2}$ or an unstrained fibers state $I_\mathrm{f} = 1$ to the unique equilibrium. Unstrained fiber states repel trajectories into the fiber tensile region, as can be seen from

$$\frac{d}{dt}(I_\mathrm{f} - 1) = -\dot{\phi} \sin 2\phi (x - y) > 0, \tag{4.106}$$

where we use the fact that $(\sigma_1 - \sigma_2)$, $(x - y)$ and $-\dot{\phi}$ are of the same sign at $I_\mathrm{f} = 1$. The behaviour of the system for various parameters is summarized in Figure 4.11a. An example of solution is depicted in Figure 4.11b.

4.5 Stress-induced reorientation subject to constant strains

Now consider a combination of fixed displacement boundary conditions and stress-driven fiber reorientation. Such system is described by Equations (4.103)-(4.105), where $x = \lambda_1^2$, $y = \lambda_2^2$, $\sigma_3 = 0$ are given constants and $A = \sigma_1 - \sigma_2$, $B = \sigma_1 + \sigma_2$ change in the course of evolution. We assume that the fiber reorientation only takes place if (4.17) holds, *i.e.* if the direction of fibers is positively strained. This model displays an interesting dynamics due to the part that the stress-strain relation plays

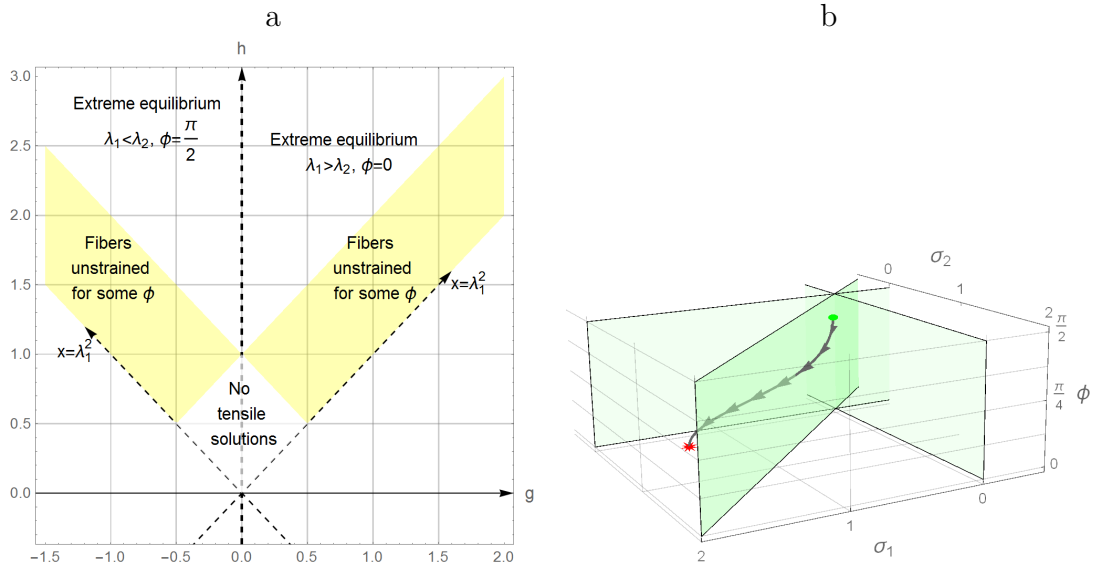

Figure 4.11: a. Bifurcation diagram for system (4.104), (4.105), (4.13); b. An example of solution for system (4.104), (4.105), (4.13).

in determining the reorientation. As before, the system is invariant with respect to change of variables $x \mapsto y$, $y \mapsto x$, $\phi \mapsto \frac{\pi}{2} - \phi$, $A \mapsto -A$, hence without loss of generality we only consider the case $x \geq y$.

The right-hand side of (4.103) provides three possibilities for steady states:

1. $\phi = 0$, $\sigma_1 > \sigma_2$;

2. $\phi = \frac{\pi}{2}$, $\sigma_1 < \sigma_2$;

3. $\phi = \phi^* \in (0; \frac{\pi}{2})$, $A = \sigma_1 - \sigma_2 = 0$.

Contrary to the model considered in Section 4.2.1, the unknowns σ_1, σ_2 can be found without inverting the constitutive relation. Therefore, a choice of constant stretches λ_i defines a curve $(\sigma_1(\phi), \sigma_2(\phi), \phi)$ in 3-dimensional space $(\sigma_1, \sigma_2, \phi)$, where $\sigma_i(\phi)$ can be found from (4.9)-(4.10). A trajectory starts from an initial state $(\sigma_1(\phi_0), \sigma_2(\phi_0), \phi_0)$ and covers a part of this curve, which can be parametrized by time.

4.5.1 Singularities

A trajectory $(\sigma_1, \sigma_2, \phi)(t)$ can be parametrized by ϕ, where the stresses σ_i are continuous functions of the fiber angle ϕ. Therefore a small increment in ϕ results in a small increment in σ_1, σ_2. That property can be seen from differentiating (4.9)-(4.11) assuming constant principal stretches λ_i,

$$\frac{d\sigma_1}{d\phi} = -4x \sin 2\phi(\cos 2\phi(x-y) + x - 1), \tag{4.107}$$

$$\frac{d\sigma_2}{d\phi} = -4y \sin 2\phi(\cos 2\phi(y-x) + 1 - y), \tag{4.108}$$

wherein the right-hand side is bounded. That means that a trajectory in $(\sigma_1, \sigma_2, \phi)$ space is nowhere parallel to $\phi = \text{const}$ and that the solution of system (4.103)-(4.105) can always be continuously extended in time. In other words, the reorientation law (4.103) is compatible with the constitutive equations (4.104), (4.105) and the constant displacement boundary conditions.

4.5.2 Extreme equilibrium states

From (4.104) we have

$$(\sigma_1 - \sigma_2)_{|\phi=0} = \mu(x-y) + 4x(x-1), \tag{4.109}$$

$$(\sigma_1 - \sigma_2)_{|\phi=\frac{\pi}{2}} = \mu(x-y) - 4y(y-1). \tag{4.110}$$

It follows that

$$(\sigma_1 - \sigma_2)_{|\phi=0} > 0, \tag{4.111}$$

since $x > 1$ at $\phi = 0$ in the fiber-tensile region (4.17). Therefore, the extreme equilibrium state $\phi = 0$ always exists.

The existence of the equilibrium state at $\phi = \frac{\pi}{2}$ is subject to the condition

$$(\sigma_1 - \sigma_2)_{|\phi=\frac{\pi}{2}} < 0. \tag{4.112}$$

A breach of this last condition corresponds to a point $(\sigma_1, \sigma_2, \frac{\pi}{2})$ crossing the $\sigma_1 = \sigma_2$ in phase space and ceasing to be a steady state.

Extreme equilibrium states are always locally stable due to (4.103). One can make an argument similar to Proposition 9, based on the continuity of the stress-strain relation (4.104), (4.105).

4.5.3 Unstrained fibers states

The unstrained fiber state is characterized by an angle ϕ°, given by

$$\phi^\circ = \arctan\sqrt{\frac{x-1}{1-y}}, \qquad \cos 2\phi^\circ = \frac{2-x-y}{x-y}. \tag{4.113}$$

There exists exactly one unstrained fibers state if $x > 1 > y$ and no such states if $x > y > 1$. At $\phi = \phi^\circ$ we have

$$(\sigma_1 - \sigma_2)_{|\phi=\phi^\circ} = \mu(x-y) > 0. \tag{4.114}$$

An unstrained fibers state repels the trajectory passing through it inside the fiber-tensile region, hence trajectories cannot leave the fiber-tensile region. The argument made in Section 4.4 based on (4.106) applies here.

4.5.4 Intermediate eqiulibrium states

Equation (4.104) can be written as a quadratic polynomial in $\cos 2\phi$,

$$\sigma_1 - \sigma_2 = \cos^2 2\phi(x^2 - y^2) + 2\cos 2\phi(x^2 + y^2 - x - y) + (x-y)(x+y+\mu-2). \tag{4.115}$$

It follows that an intermediate equilibrium state corresponds to a root of Equation (4.115) satisfying

$$-1 \leq \cos 2\phi \leq 1, \qquad \text{if } x, y > 1, \tag{4.116}$$

$$\cos 2\phi^{\circ} \leq \cos 2\phi \leq 1, \qquad \text{if } x > 1 > y. \tag{4.117}$$

The number of roots can be inferred from the sign of this quadratic function at the endpoints and at the critical point

$$\cos 2\phi_{\text{crit}} = \frac{x^2 + y^2 - x - y}{y^2 - x^2}. \tag{4.118}$$

The stability of an intermediate equilibrium state is determined by the derivative

$$\frac{d}{d\phi}(\sigma_1 - \sigma_2) = -4 \sin 2\phi \left(\cos 2\phi (x^2 - y^2) + (x^2 + y^2 - x - y) \right). \tag{4.119}$$

The sign of the right-hand side of (4.119) changes at $\phi = \phi_{\text{crit}}$. The intermediate eqiulibrium is stable if $\phi > \phi_{\text{crit}}$ and unstable $\phi < \phi_{\text{crit}}$ due to (4.119) and (4.103). The argument here is similar to the one made in Proposition 11, Fig. 4.2.

Proposition 14. *There exist two stable extreme equilibria $\phi = 0, \frac{\pi}{2}$, one unstable intermediate equilibrium $\phi \in (0, \frac{\pi}{2})$ and no other steady states in the fiber-tensile region if x, y satisfy*

$$y < x < y + \frac{4y}{\mu}(y - 1). \tag{4.120}$$

Proof. Inequality (4.120) implies (4.112), as can be seen from (4.110). Condition (4.111) is automatically satisfied. Note that $x > y > 1$ holds and the fibers are in tension for all $\phi \in [0, \frac{\pi}{2}]$. Therefore $\phi = 0$ and $\phi = \frac{\pi}{2}$ are locally stable steady states. Inequalities (4.112), (4.111) also imply that the quadratic function (4.115) changes sign from negative (at $\cos 2\phi = -1$, $\phi = \frac{\pi}{2}$) to positive (at $\cos 2\phi = 1$, $\phi = 0$), therefore it

has exactly one root. Due to continuity we necessarily have

$$\frac{d}{d\phi}(\sigma_1 - \sigma_2) < 0, \tag{4.121}$$

that is, the intermediate steady state is unstable. □

Proposition 15. *There exists one extreme locally stable equilibrium $\phi = 0$, two intermediate equilibria $\phi_{1,2} \in (0, \frac{\pi}{2})$, $\phi_1 < \phi_2$ and no other steady state if the following condition holds*

$$x > y + \frac{4y}{\mu}(y-1), \tag{4.122}$$

$$x - y < \sqrt{(x+y)(x+y+\mu-1) - (x+y)\sqrt{(x+y+\mu-1)^2 - (x+y-1)^2}}. \tag{4.123}$$

Moreover, the intermediate equilibrium ϕ_1 is locally unstable, while the intermediate equilibrium ϕ_2 is locally stable.

Proof. First, we show that the system evolves along a curve $(\sigma_1, \sigma_2, \phi)(\phi)$, whose endpoints lie in the $\sigma_1 > \sigma_2$ half space and which intersects $\sigma_1 - \sigma_2 = 0$. The endpoint at $\phi = 0$ is in fiber-tensile region and satisfies $\sigma_1 > \sigma_2$, as (4.111) holds. The other endpoint is at $\phi = \frac{\pi}{2}$, if $y \geq 1$, or corresponds to unstrained fibers at $\phi = \phi^\circ$, if $y < 1$. In the first case it belongs to half space $\sigma_1 > \sigma_2$ because condition (4.122) is the negation of (4.112). In the second case the endpoint belongs to half space $\sigma_1 > \sigma_2$ due to (4.114). Therefore ends of the curve are in $\sigma_1 > \sigma_2$, while the curve intersects $\sigma_1 - \sigma_2 = 0$, as condition (4.123) implies that

$$(\sigma_1 - \sigma_2)_{|\phi=\phi_{\text{crit}}} < 0. \tag{4.124}$$

We will explain the implication (4.123) $\Longrightarrow$ (4.124) in details. From (4.115) and

(4.118) we have

$$(\sigma_1 - \sigma_2)_{\text{crit}} = \mu(x - y) + \frac{(x + y - 2xy)^2}{y^2 - x^2}. \tag{4.125}$$

Condition $(\sigma_1 - \sigma_2)_{\text{crit}} < 0$ is equivalent to

$$-h^4 + 2h^2 g(\mu + g - 1) + g^2(g - 1) < 0, \tag{4.126}$$

which can be written as

$$-(h^2 - h_-^2)(h^2 - h_+^2) < 0, \tag{4.127}$$

where $x = g + h$, $y = g - h$, and the roots of the biquadratic equation are

$$h_\pm^2 = g(\mu + g - 1) \pm g\sqrt{(\mu + g - 1)^2 - (g - 1)^2}. \tag{4.128}$$

Inequality (4.123) is the same as $h^2 < h_-^2$ and implies (4.124). As we do not claim equivalence, there is no need to investigate the case $h^2 > h_-^2$, which will be considered in Proposition 16.

It remains to demonstrate for the case $y < 1$ that $0 < \phi_{\text{crit}} < \phi^\circ$, *i.e.* $\cos 2\phi^\circ < \cos 2\phi_{\text{crit}} < 1$. By changing variables in (4.118) we obtain

$$\cos 2\phi_{\text{crit}} = \frac{g^2 + h^2 - g}{-2gh} < 0, \tag{4.129}$$

since $g, h > 0$. Inequality $\cos 2\phi^\circ < \cos 2\phi_{\text{crit}}$ yields

$$\frac{1 - g}{h} < \frac{g^2 + h^2 - g}{-2gh}, \tag{4.130}$$

which is equivalent to

$$h^2 < g^2 - g. \tag{4.131}$$

This is automatically satisfied since

$$h_-^2 = g^2 - g + g\mu\left(1 - \sqrt{1 + \frac{2g-2}{\mu}}\right) < g^2 - g,$$

where $g > 1$ is used. □

Proposition 16. *There exists an extreme stable equilibrium $\phi = 0$, which is the only steady state, if*

$$x - y > \sqrt{(x+y)(x+y+\mu-1) - (x+y)\sqrt{(x+y+\mu-1)^2 - (x+y-1)^2}}. \tag{4.132}$$

Proof. Note that (4.132) is equivalent to $h^2 > h_-^2$. First, we demonstrate by contradiction that (4.132) implies (4.122): condition (4.132) and the negation of (4.122) mean that the minimum of quadratic function (4.115) is positive, while it takes a negative value at $\cos\phi = 0$. Therefore (4.122) holds, and both endpoints of the curve $(\sigma_1, \sigma_2, \phi)(\phi)$ are in $\sigma_1 > \sigma_2$.

Now we show that the curve does not intersects $\sigma_1 = \sigma_2$. If it does, then $(\sigma_1 - \sigma_2)_{\text{crit}} < 0$, or equivalently (4.126), must hold. But it can only be satisfied for $h^2 > h_+^2$, as we excluded the possibility $h^2 < h_-^2$. However,

$$h^2 > h_+^2 = g^2 - g + g\mu\left(1 + \sqrt{1 + \frac{2g-2}{\mu}}\right) > g^2 - g, \tag{4.133}$$

implies that the vertex of the parabola defined by (4.115) is in the fiber-compressive region, since $\cos 2\phi^\circ > \cos 2\phi_{\text{crit}}$ is equivalent to $h^2 > g^2 - g$. Therefore function (4.115) takes only positive values for $1 \geq \cos 2\phi > \cos 2\phi^\circ$. Thus there are no intermediate steady states in the fiber-tensile region. □

Global behaviour The statements of Propositions 14-16 are summarized in Figure 4.12.a. The system (4.103)-(4.105) can have different number and stability of steady states depending on the value of constant stretches, unlike the model considered in Section 4.2.1, which always has a unique globally attractive equilibrium. Another notable difference is that the dynamics and the outcome of reorientation depends on the initial fiber orientation.

For instance, in the parameter region corresponding to the upper white region in Fig. 4.12.a, the system has one intermediate unstable equilibrium and two extreme stable equilibria (Fig. 4.12.b). The range of fiber angles $[0, \frac{\pi}{2}]$ is split into two intervals, $[0, \phi^*]$, $[\phi^*, \frac{\pi}{2}]$ which are the basins of attraction of the stable equilibria. When the point (g, h) crosses the border of white and red regions in the parametric space, one stable equilibrium moves from the extreme to an intermediate fiber orientation. In the red region the system still has two stable equilibria (one extreme, one intermediate) and an unstable intermediate equilibrium (Fig. 4.12.c). In this case the remaining extreme fiber alignment is either a non-steady state or is in the fiber-compressive region.

When the point (g, h) crosses the border of red and blue regions in the parametric space, the system undergoes a saddle-node bifurcation at which two intermediate equilibria (one stable, one unstable) merge and disappear. In the blue region in the diagram the system has a unique stable extreme equilibrium state (Fig. 4.12.d).

4.6 Conclusions and discussion

We considered several simple models for anisotropic remodeling in a fiber reinforced material. All models consider homogeneous deformations and mechanically induced fiber reorientation. We assume that the material specimen is an incompressible elastic cuboid reinforced by two families of fibers, whose directions lie parallel to a face of

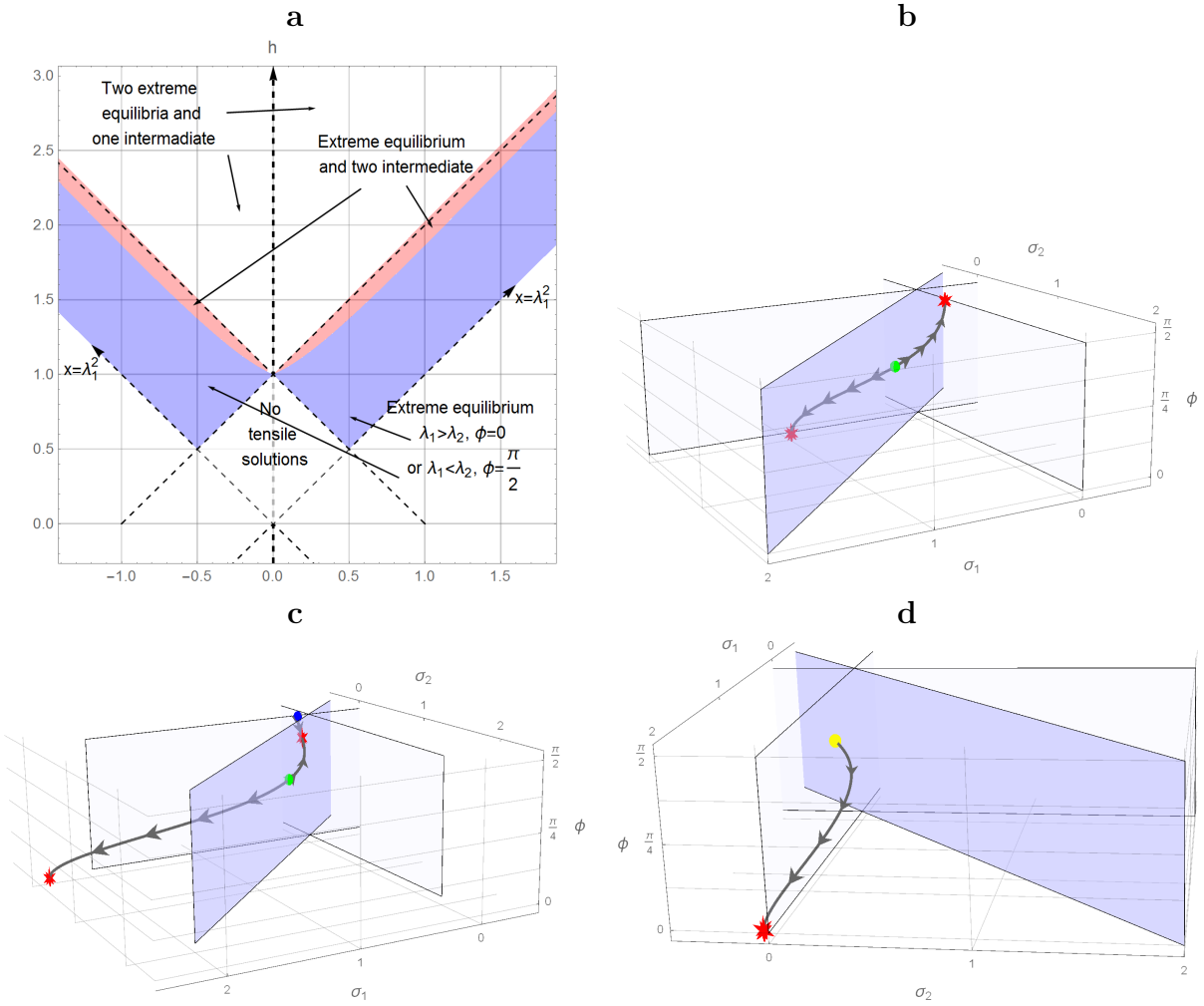

Figure 4.12: **a**. Bifurcation diagram for system (4.103)-(4.105). **b**. A trajectory corresponding to the upper white region in the diagram: the system has two stable extreme equilibria (red stellates) and one repelling intermediate equilibrium (green sphere). **c**. A trajectory corresponding to the red region: the system has one stable extreme equilibrium and one stable intermediate equilibrium (red stellates) and also an unstable intermediate equilibrium (green sphere). The blue sphere denotes either a non-steady state $\phi = \frac{\pi}{2}$ (if $y > 1$) or a unstrained fibers point (if $y \leq 1$). **d**. A trajectory corresponding to the blue region on the diagram: the system has a unique globally attractive extreme equilibrium state. The trajectry starts at the border of the fiber-tensile region (yellow sphere).

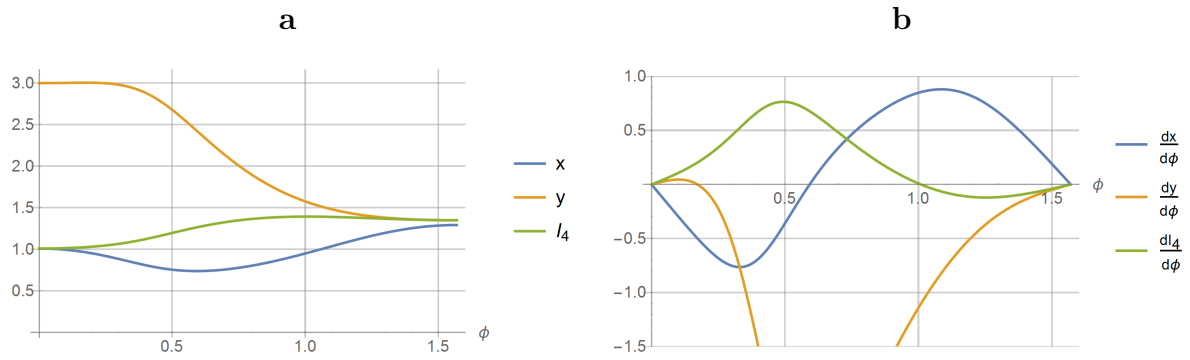

Figure 4.13: A solution of system (4.14), (4.15), no dispersion, $\mu = 1$.

cuboid and are symmetrical with respect to the remaining faces. We used a Neo-Hookean strain-energy function for the bulk material and a standard model for fiber reinforcement. The models differ in boundary conditions and phenomenological laws for fiber reorientation.

If the boundary conditions and the reorientation law are both defined in terms of principal stretches, then the dynamical behaviour of the system is trivial and the final fiber orientation does not depend on the constitutive equation (Fig. 4.11).

If the boundary conditions and the reorientation law are both defined in terms of principal stresses, then the constitutive equation defines whether the fibers are tensile and the reorientation is induced, yet it has no effect on the final fiber orientation (Fig. 4.10).

If the boundary conditions are given in terms of loads and the reorientation law prescribes fiber realignment in the direction of the maximum principal stretch, then the constitutive equation has an effect in determining the outcome of remodeling. Depending on the parameters, the fibers reorient towards one of the extreme angles $\phi = 0, \frac{\pi}{2}$ or an intermediate angle $\phi \in (0, \frac{\pi}{2})$, at which the principal stretches in fiber plane are equal (Fig. 4.4). We also considered variants of this model that take into account fiber dispersion (Figs. 4.8, 4.9).

If the boundary conditions are given in terms of fixed displacement and the reori-

entation law prescribes fiber realignment in the direction of the maximum principal stress, then the constitutive equation plays a role in determining the outcome of remodeling. Unlike the previous case, this model can exhibit multiple equilibria including a combination of stable and unstable steady states (Fig. 4.12a). The resulting fiber angle depends not only on the material parameters and boundary conditions, but also on the initial orientation. In the most probable setting, the fibers reorient to the direction $\phi = 0$ if the initial angle is close enough to it, and to the direction $\phi = \frac{\pi}{2}$ otherwise.

The difference in the dynamical behaviour of the last two models can be explained by the concept of "reinforcing", which can be formulated as follows: the reinforcing of a particular direction in the material tends to increase the stress in this direction if the deformation is fixed or decrease the strain if the loads are held constant. In the fixed loads scenario, the reorientation towards the greater principal stretch decreases the value of this principal stretch thereby forming a negative feedback loop. Hence we always observe a unique equilibrium in Fig. 4.4. Conversely, in the fixed deformation scenario, the reorientation towards the maximum principal stress increases it thereby forming a positive feedback loop, which results in two stable equilibria separated by an unstable steady-state in Fig. 4.12.a. Note that this description is invalid in the strict sense. For example, the realignment in the most stretched direction under constant loads may (i) increase the stretch in the most stretched direction, (ii) decrease the stretch in the other direction, (iii) decrease the fiber stretch, see Fig. 4.13. Such counterintuitive behaviour is due to the interplay between nonlinearity and anisotropy - similar to the one observed in the study of perversion points of Chapter 3.

Chapter 5

Coupled growth and remodeling in a fiber-reinforced elastic disk

5.1 Introduction and motivation

This Chapter is dedicated to the study of the interplay between different aspects of the dynamics of anisotropic remodeling. In addition to fiber reorientation, studied separately in Chapter 4, here we consider dynamical inhomogeneous growth, which is another substantial factor contributing to the change of anisotropic material properties. The inclusion of inhomogeneous growth into a model implies that neither deformation nor stress fields are uniform in general. If the remodeling laws in question are mechanically induced, then the non-uniformity of material properties, stress and deformation fields is generically persistent. The compatibility of the current configuration and the balance of linear momentum require global coherence between local mechanical states, thereby facilitating interactions between distant parts of the body and coupling their mechanical state and evolution with the overall geometry. A possible outcome of such interactions is mechanically driven self-organisation and pattern formation. Pattern formation associated with elastic instabilities in growing tissues and mechanochemical

coupling was addressed in several studies, *e.g.* [51, 4, 8, 53].

The model we formulate in this Chapter is motivated by a particular example of *in vitro* tissue self-organisation, namely the experiment conducted by Dhimolea et al. [10]. Here we summarize its relevant aspects. A cell culture containing non-tumorigenic human breast epithelial cells MCF10A was suspended in a type 1 collagen gel and seeded into plastic wells. Upon solidification, the gels were detached from the bottom and sides of the wells. The cultures were maintained for 1-4 weeks, within which samples were harvested for morphological and histochemical examination. The following changes and processes were observed during the course of experiment. Gel specimens were contracted by the cells within first 10 days by up to 85% of the initial surface area, the contraction started on the second and third days. The cells proliferated and formed epithelial structures, represented by spherical organoids (acini and alveoli) and elongated structures (tubules and ducts). The presence of these organoids varied both in space and time. Initially the cells were evenly distributed and were found alone or as small aggregates. The formation of structures started on the second and third days. Elongated ducts and tubules were found in the upper layer of the gel, while the lower layer contained only or mostly acini. Three regions were distinguished in the horizontal direction: the centre, the intermediate region and the periphery. During the first week, the tubular structures were oriented circumferentially in the periphery, radially in the intermediate region and had no preferred orientation in the central region. During the second week, these elongated structures started branching and transforming into ductal network in central and intermediate regions, while in the periphery they gradually shifted to the intermediate region during the end of the first week. After the second week the organoids began to disintegrate. It was observed that the elongated and tubular structures modified the collagen, facilitated formation of thick fibers parallel to the direction of elongation and interacted with neighbouring structures using the fibers. The authors argue that the morphogenesis appears

	Central region	Intermediate region	Periphery
Week 1	No defined orientation.	Radial orientation.	Circumferential orientation. Shifting to the intermediated region.
Week 2	Extensive branching forming elaborate ductal network.	Branching and crossing forming a network	No elongated structures. Only acini.
Weeks 3, 4	The organoids were losing cohesion and disintegrated by the end of the fourth week.		

Table 5.1: Orientation of elongated structures (tubules and ducts) in the upper layer of the gel depending on the location. Summary of the experiment conducted by Dhimolea et al. [10].

to be regulated by inhomogeneous spatio-temporal distribution of biochemical and/or biomechanical factors, including collagen matrix rigidity, the capability to contract it (provided by the detachment from the wells) and the shape of the wells [10].

We note that the orientation of thick collagen fibers, which were aligned with respect to the direction of elongated structures, depends on the spatial position. Although it is not known to which extent mechanical factors control the observed self-organisation, we investigate the possibility of pattern formation that is driven and determined by tissue mechanics and remodeling. We hypothesise that morphogenesis can be coordinated solely by mechanical signals, which arise from material remodeling and are mediated by the stress and deformation fields. These signals enable cells to determine their orientation and position within the gel, starting from a homogeneous isotropic state and using the overall geometry of the material as the only clue. This hypothesis could be supported by a material model in which the action of local and objective phenomenological remodeling laws results in symmetry breaking and robust formation of global patterns.

In our approach the cell-populated collagen gel is modelled as a hyperelastic material reinforced by two families of fibers. Although one can distinguish at least three different constituents in the real gel (collagen fibers, cells and the medium), here we

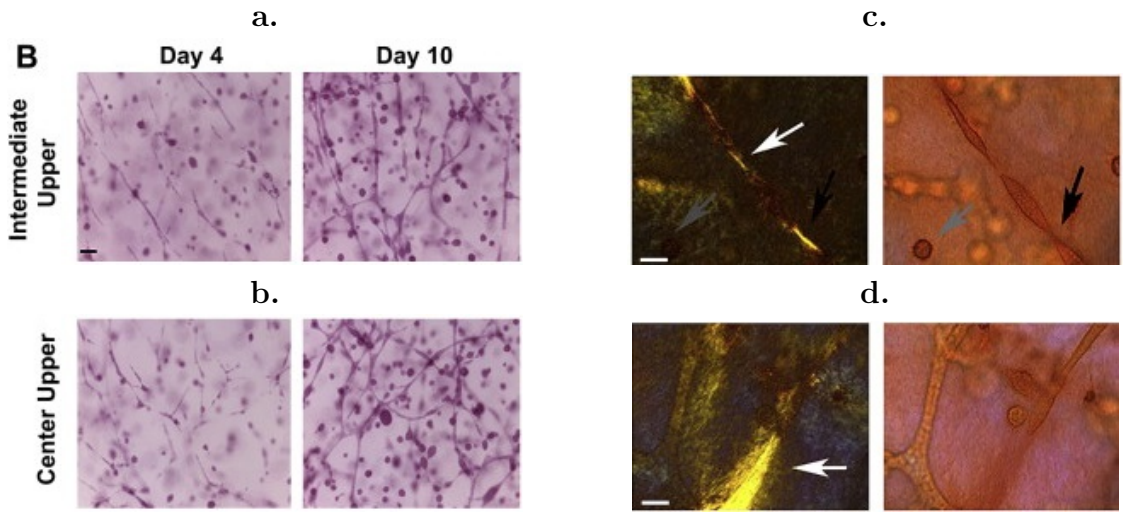

Figure 5.1: Morphology of co-culture of MCF10A and RMF (reduction mammoplasties fibrocytes). Epithelial structures in the intermediate upper (**a**) and central upper (**b**) regions of the gel. Whole mount picrosirius red staining (**c,d**) under polarised (left) and non-polarised (right) light. Collagen fibers modified by cells form bundles (white arrows) aligned along the axes of elongated structured. Scale bar 50μ. [10] Reprinted from *Biomaterials* 31 (2010) 3622-3630, Dhimolea at al. "The role of collagen reorganization on mammary epithelial morphogenesis in a 3D culture model", Copyright (2010), with permission from Elsevier.

consider technically a single-phase fiber-reinforced material. The orientations of elongated cellular structures and thick collagen fibers strongly correlate in the experiment and are represented in our model by a single parameter, the fiber angle ϕ. Getting ahead of the detailed presentation of the model, we have to mention that the value $\phi = \frac{\pi}{4}$ corresponds to isotropic collagen distribution associated with tubules and ducts of no defined orientation. The values $\phi = 0, \frac{\pi}{2}$ correspond to radial and circumferential orientations respectively. Our goal is to study anisotropic pattern formation analogous to the one observed in the experiment, whose interpretation in terms of fiber angle is depicted in Fig.5.3.

The quasi-static remodeling consists of mechanically induced growth and fiber reorientation. In order to model inhomogeneous growth, we adopt the framework of morphoelasticity, summarised in Section 1.3.6, and use the multiplicative decomposition of the total deformation gradient $\mathbf{F}$ into growth tensor $\mathbf{G}$ and elastic deformation

tensor $\mathbf{A}$,

$$\mathbf{F}(\mathbf{X},t) = \mathbf{A}(\mathbf{X},t)\mathbf{G}(\mathbf{X},t). \tag{5.1}$$

The elastic response is given by

$$\boldsymbol{\sigma}(\mathbf{X},t) = \boldsymbol{\sigma}(\mathbf{A}) = -p(\mathbf{X},t)\mathbf{1} + \frac{\partial W(\mathbf{X},t)}{\partial \mathbf{A}}(\mathbf{A}(\mathbf{X},t),\mathbf{X})\mathbf{A}(\mathbf{X},t)^T, \tag{5.2}$$

where p is the Lagrangian multiplier associated with the incompressibility and W is the strain energy function. The incompressibility condition reads

$$\det \mathbf{A}(\mathbf{X},t) = 1. \tag{5.3}$$

Since all inertial effects arising from the dynamics of remodeling are neglected, the balance of linear momentum is given by the Cauchy equation of equilibrium,

$$\mathrm{div}\boldsymbol{\sigma} = 0, \tag{5.4}$$

where no body force is present. Equations (5.1)-(5.4) with given W, $\mathbf{G}$ and suitable boundary conditions (5.4) form the static part of our model.

The dynamical part consists of the remodeling laws, namely the equations for mechanically induced growth and fiber reorientation,

$$\frac{d}{dt}\phi = \dot{\phi}(\phi, \mathbf{A}, \boldsymbol{\sigma}, \dots), \tag{5.5}$$

$$\frac{d}{dt}\mathbf{G} = \dot{\mathbf{G}}(\mathbf{G}, \mathbf{A}, \boldsymbol{\sigma}, \dots), \tag{5.6}$$

which describe the evolution of fiber angle ϕ and growth tensor $\mathbf{G}$ as a function of the local mechanical state. Note that in (5.5), (5.6) there is no explicit dependence on time or position, meaning that the remodeling is defined as a local, autonomous and uniform process.

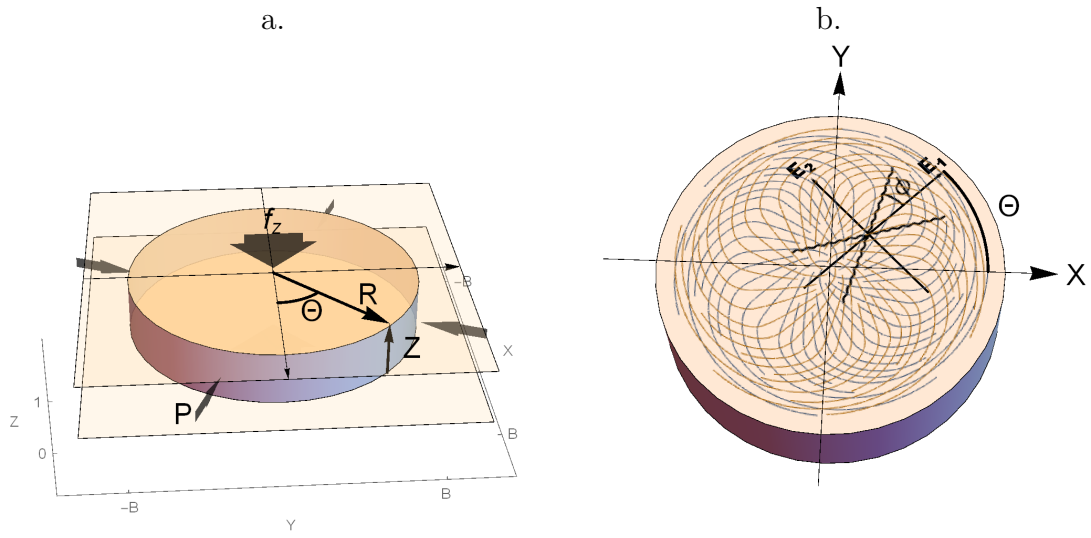

Figure 5.2: The material is a solid cylinder reinforced by two families of fibers arranged symmetrically in the $R\Theta$-plane. The orientation of fibers may vary with the radial position and is prescribed by angle $\phi(R)$.

5.2 The model

The material is defined in the reference configuration as a solid cylinder, or a thick disk, which occupies the region

$$\{(R, \Theta, Z) : 0 \leq R \leq B,\ \Theta \in [0, 2\pi),\ Z \in [0, 1]\} \subset \mathbb{R}^3, \tag{5.7}$$

where (R, Θ, Z) are conventional cylindrical coordinates in the reference configuration (Figure 5.2). We assume that the cylindrical shape of the material is preserved in the current configuration,

$$\{(r, \theta, z) : 0 \leq r \leq b,\ \theta \in [0, 2\pi),\ z \in [0, \zeta]\} \subset \mathbb{R}^3, \tag{5.8}$$

where (r, θ, z) are cylindrical coordinates in the current configuration. We impose translational and rotational symmetry with respect to the z-axis. This implies that all quantities may only depend on the radial position R, and ignore Θ and Z coordinates. This is consistent with the material being locally orthotropically symmetric,

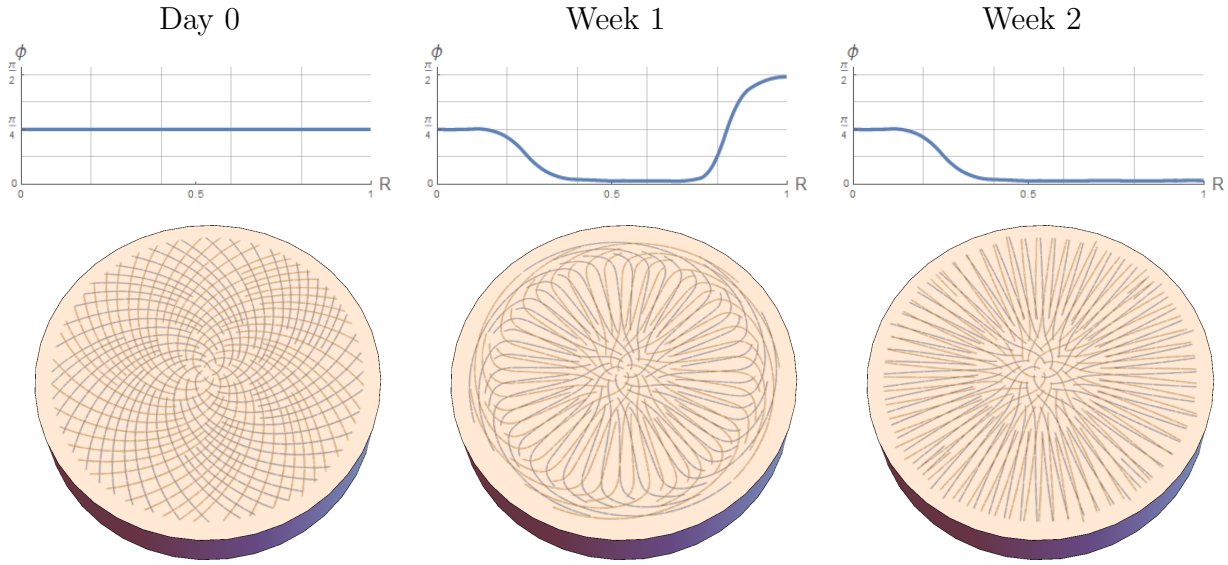

Figure 5.3: The orientation patterns of elongated structures and thick collagen fibers [10] represented by two symmetrically arranged families of fibers. Radial, isotropic and circumferential orientations are given by the values of the fiber angle $\phi = 0, \frac{\pi}{4}, \frac{\pi}{2}$ respectively. Note that the morphological anisotropy is not quantified in [10] and the distribution $\phi(R)$ provided here is our interpretation of the observations reported there. Compare to Table 5.1.

i.e. symmetric with respect to coordinate planes of the cylindrical coordinate system. Local and overall material symmetries imply that all tensor quantities are described by diagonal matrices in cylindrical coordinates. Hence the deformation is given by

$$r = r(R), \tag{5.9}$$

$$\theta = \Theta, \tag{5.10}$$

$$z = \zeta Z. \tag{5.11}$$

The corresponding deformation gradient in cylindrical coordinates reads

$$\mathbf{F} = \mathrm{diag}(\lambda_1(R), \lambda_2(R), \lambda_3(R)), \quad \lambda_1 = \frac{dr(R)}{dR}, \quad \lambda_2 = \frac{r(R)}{R}, \quad \lambda_3 = \zeta. \tag{5.12}$$

The growth, elastic deformation and Cauchy stress tensors are also diagonal when expressed in cylindrical coordinates,

$$\mathbf{G} = \mathrm{diag}(\gamma_1(R), \gamma_2(R), \gamma_3(R)), \tag{5.13}$$

$$\mathbf{A} = \mathrm{diag}(\alpha_1(R), \alpha_2(R), \alpha_3(R)) = \mathrm{diag}(\frac{\lambda_1(R)}{\gamma_1(R)}, \frac{\lambda_2(R)}{\gamma_2(R)}, \frac{\lambda_3(R)}{\gamma_3(R)}), \tag{5.14}$$

$$\boldsymbol{\sigma} = \mathrm{diag}(\sigma_1(R), \sigma_2(R), \sigma_3(R)). \tag{5.15}$$

The incompressibility condition (5.3) due to (5.1) and (5.12) reads

$$\alpha_1\alpha_2\alpha_3 = \frac{r'}{\gamma_1}\frac{r}{R\gamma_2}\frac{\zeta}{\gamma_3} = 1, \tag{5.16}$$

where $'$ denotes $\partial/\partial R$ and we may henceforth omit explicit indication of R as the argument.

It follows from (1.10) and (5.15) that the only non-vanishing component of the Cauchy equation (5.4) is

$$\frac{\partial}{\partial r}\sigma_1 + \frac{1}{r}(\sigma_1 - \sigma_2) = 0. \tag{5.17}$$

The boundary conditions are given by the uniform normal pressure P applied to the lateral surface of the cylinder and the overall tensile forces of magnitude f_z applied to the top and bottom faces,

$$\sigma \cdot \mathbf{e}_r = -P, \quad \text{at } r = b, \tag{5.18}$$

$$\int_0^{2\pi}\int_0^{b} \boldsymbol{\sigma} \cdot \mathbf{e}_z \, r \, dr \, d\theta = 2\pi f_z, \quad \text{at } z = 0, \zeta. \tag{5.19}$$

These conditions can be written in the reference configuration and simplified using

(5.15),

$$\sigma_1(B) = -P, \tag{5.20}$$

$$\int_0^B \sigma_3(R)\, r(R)\, r'(R)\, dR = f_z. \tag{5.21}$$

We consider an incompressible Neo-Hookean material reinforced by two symmetrically arranged fiber families with orientations given by the unit vectors

$$\mathbf{a}_0^{(1)} = (\cos\phi(R), \sin\phi(R), 0), \quad \mathbf{a}_0^{(2)} = (\cos\phi(R), -\sin\phi(R), 0),$$

where $\phi(R)$ is the fiber angle in the reference configuration. We use the standard reinforcing model (3.32) for the fibers, thus the strain energy function of this material is identical to those considered in Chapters 3 and 4. However, we allow here for inhomogeneous fiber orientations prescribed by $\phi(R)$. The diagonal components of the Cauchy stress tensor are given by

$$\sigma_1 = -p + \tilde{\sigma}_1 = -p + \mu\alpha_1^2 + 4\alpha_1^2 \cos^2\phi[\alpha_1^2\cos^2\phi + \alpha_2^2\sin^2\phi - 1]_+, \tag{5.22}$$

$$\sigma_2 = -p + \tilde{\sigma}_2 = -p + \mu\alpha_2^2 + 4\alpha_2^2 \sin^2\phi[\alpha_1^2\cos^2\phi + \alpha_2^2\sin^2\phi - 1]_+, \tag{5.23}$$

$$\sigma_3 = -p + \tilde{\sigma}_3 = -p + \mu\alpha_3^2, \tag{5.24}$$

where we introduced the notation $\tilde{\sigma}_i = \frac{\partial W}{\partial \alpha_i}\alpha_i$, $[I_\mathrm{f} - 1]_+ = \max(I_\mathrm{f} - 1, 0)$. Note that the shear modulus μ is the only constant in (5.22)-(5.24).

We postulate that the evolution laws for multiplicative growth and fiber angle are of the form

$$\frac{d}{dt}\phi = \eta_\phi(\phi_\mathrm{aim} - \phi), \tag{5.25}$$

$$\frac{d}{dt}\gamma_i = \eta_{\gamma i}(\gamma_{i\,\mathrm{aim}} - \gamma_i), \quad i = 1, 2, 3, \tag{5.26}$$

where ϕ_{aim}, $\gamma_{i\,\text{aim}}$ are respectively the preferred fiber orientation angle and growth tensor components, η_ϕ and $\eta_{\gamma i}$ are the respective remodeling rates. The values of ϕ_{aim}, $\gamma_{i\,\text{aim}}$, η_ϕ, $\eta_{\gamma i}$ may be constant or depend on the local principal stresses or principal elastic stretches. As long as the remodeling rates are greater than some positive constant, *i.e.*

$$\eta_\phi,\, \eta_{\gamma i} > \epsilon > 0, \tag{5.27}$$

the equilibrium values of growth tensor and fiber angle are defined by

$$\phi_{\text{aim}} = \phi, \qquad \gamma_{i\,\text{aim}} = \gamma_i, \quad i = 1, 2, 3. \tag{5.28}$$

In this case the exact choice of η_ϕ, $\eta_{\gamma i}$ only affects the transient dynamics and is irrelevant to the set of steady states.

We define the preferred fiber angle by

$$\phi_{\text{aim}} = \begin{cases} \arctan\left(\frac{\sigma_2}{\sigma_1}\right)^\beta, & \sigma_1, \sigma_2 > 0, \\ 0, & \sigma_1 > 0 \geq \sigma_2, \\ \frac{\pi}{2}, & \sigma_2 > 0 \geq \sigma_1, \\ \phi, & 0 \geq \sigma_1, \sigma_2. \end{cases} \tag{5.29}$$

which can be written in a brief form $\tan\phi \to \tan\phi_{\text{aim}} = \frac{[\sigma_2]_+^\beta}{[\sigma_1]_+^\beta}$, where $\beta > 0$ is a constant defining the degree of fiber alignment. For instance, $\beta = +\infty$ corresponds to fiber reorientation in the direction of maximum principal stress. A similar stress-induced reorientation law was suggested in [29]. We also postulate that the preferred state of growth is isotropic and uniform, defined by

$$\gamma_{i\,\text{aim}} = 0.5, \quad i = 1, 2, 3. \tag{5.30}$$

That is, the material is shrunk or rather resorbed by a factor of 2 in each dimension in the equilibrium state.

To summarize, the system is defined by Equations (5.17), (5.20)-(5.21), (5.25)-(5.30) with the deformation being restricted to (5.12), (5.16).

5.2.1 Solution to the static part

Here we describe a method for solving the static part of the model, which consists in finding deformation and stress ($r(R)$, ζ and $\sigma_i(R)$) from (5.17), (5.20)-(5.21) for given fiber orientation and growth ($\phi(R)$, $\gamma_i(R)$).

By integration (5.16) subject to $r(0) = 0$ we obtain

$$r(R) = \sqrt{\frac{2s(R)}{\zeta}}, \tag{5.31}$$

where

$$s(R) = \int_0^R \gamma_1(\tilde{R})\gamma_2(\tilde{R})\gamma_3(\tilde{R})\,\tilde{R}\,d\tilde{R}. \tag{5.32}$$

We note some useful identities,

$$\frac{r'}{r} = \frac{s'}{2s}, \qquad r'r = \frac{s'}{\zeta}, \tag{5.33}$$

$$s'(R) = R \det \mathbf{G}(R) = \gamma_1(R)\gamma_2(R)\gamma_3(R)\,R, \qquad s(0) = s'(0) = 0. \tag{5.34}$$

The Cauchy's equation of equilibrium (5.17) can be written in the reference configuration using (5.33),

$$\sigma_1'(R) = \frac{s'(R)}{2s(R)}(\tilde{\sigma}_2(R) - \tilde{\sigma}_1(R)), \tag{5.35}$$

where $\tilde{\sigma}_i$ are defined in (5.22)-(5.24). Boundary condition (5.21) can be replaced by

$$-\zeta f_z - Ps(B) + \int_0^B \left(-\frac{1}{2}(\tilde{\sigma}_1 + \tilde{\sigma}_2) + \tilde{\sigma}_3\right) s'\, dR = 0. \tag{5.36}$$

This follows from $\sigma_i = -p + \tilde{\sigma}_i$ and the identity

$$-\int_0^B ps'\, dR = -\int_0^B (\sigma_1 - \tilde{\sigma}_1)\, s' = [\sigma_1 s']_0^B - \int_0^B \tilde{\sigma}_1' s + \tilde{\sigma}_1 s'\, dR \tag{5.37}$$

$$= \sigma_1(B)s'(B) - \int_0^B \frac{1}{2}(\sigma_2 + \sigma_1)s', \tag{5.38}$$

where we used integration by parts, (5.20) and (5.34).

The only unknown in Equation (5.36) is ζ, which appears there explicitly and also implicitly via $\tilde{\sigma}_i$ and α_i. Hence ζ can be computed from equation (5.36) *e.g.* by solving it numerically using and iterative root finding algorithm. Once ζ is known, the deformation of the cylinder and principal elastic stretches can be found from (5.31), (5.12) and (5.14). Hence the stress field is determined up to a uniform isotropic summand, which can be computed from the boundary condition (5.20). Note that both boundary conditions determine the elastic deformation, as (5.36) is derived from (5.21) and (5.20). To find the radial stress $\sigma_1(R)$ we integrate Equation (5.35) starting from $R = B$ and using (5.20) as the initial data.

Equations (5.36) have a special form for our choice of constitutive relation. We define

$$\alpha_1^2 = \frac{1}{\zeta}\frac{s'^2}{2s\gamma_1^2} = \frac{g+h}{2}, \qquad g = \alpha_1^2 + \alpha_2^2, \tag{5.39}$$

$$\alpha_2^2 = \frac{1}{\zeta}\frac{2s}{R^2\gamma_2^2} = \frac{g-h}{2}, \qquad h = \alpha_1^2 - \alpha_2^2, \tag{5.40}$$

so that

$$\alpha_1^2 \cos^2\phi + \alpha_2^2 \sin^2\phi = \frac{1}{2}(g + h\cos 2\phi), \tag{5.41}$$

$$\alpha_1^2 \cos^2\phi - \alpha_2^2 \sin^2\phi = \frac{1}{2}(g\cos 2\phi + h), \tag{5.42}$$

and we have

$$\tilde{\sigma}_1 + \tilde{\sigma}_2 = \mu g + (g + h\cos 2\phi)[g + h\cos 2\phi - 2]_+, \tag{5.43}$$

$$\tilde{\sigma}_1 - \tilde{\sigma}_2 = \mu h + (g\cos\phi + h)[g + h\cos 2\phi - 2]_+. \tag{5.44}$$

Hence Equation (5.36) becomes

$$-\zeta f_z - Ps(B) + \int_0^B \left(\mu\frac{\zeta^2}{\gamma_3^2} - \frac{\mu g + (g + h\cos 2\phi)[g + h\cos 2\phi - 2]_+}{2}\right) s'\, dR = 0, \tag{5.45}$$

and the ODE (5.35) reads

$$\sigma_1'(R) = \frac{s'(R)}{2s(R)}\left(\mu h + 4(g\cos 2\phi + h)[g + h\cos 2\phi - 2]_+\right). \tag{5.46}$$

5.2.1.1 Special case of homogeneous growth

If the components of the growth tensor $\mathbf{G}$ in cylindrical coordinates do not depend on the radial position, *i.e.*

$$\gamma_i(R) = \text{const}, \quad i = 1, 2, 3, \tag{5.47}$$

then the expressions for the deformation, elastic stretch and stress can be greatly simplified. It follows that the integral in (5.32) can be evaluated immediately yielding

$$s(R) = \gamma_1\gamma_2\gamma_3\frac{R^2}{2}, \qquad \frac{s'(R)}{2s(R)} = \frac{1}{R}, \tag{5.48}$$

$$r(R) = \sqrt{\frac{\gamma_1\gamma_2\gamma_3}{\zeta}}R. \tag{5.49}$$

and therefore we have constant principal elastic stretches, given by

$$\alpha_1 = \sqrt{\frac{\gamma_2\gamma_3}{\zeta\gamma_1}}, \quad g = \frac{1}{\zeta}\left(\frac{\gamma_2\gamma_3}{\gamma_1} + \frac{\gamma_1\gamma_3}{\gamma_2}\right), \tag{5.50}$$

$$\alpha_2 = \sqrt{\frac{\gamma_1\gamma_3}{\zeta\gamma_2}}, \quad h = \frac{1}{\zeta}\left(\frac{\gamma_2\gamma_3}{\gamma_1} - \frac{\gamma_1\gamma_3}{\gamma_2}\right). \tag{5.51}$$

If in addition to being constant, the radial and circumferential growth components are equal,

$$\gamma_1 = \gamma_2 = \gamma = \text{const}, \quad \gamma_3 = \text{const}, \tag{5.52}$$

then the corresponding principal elastic stretches are also equal and constant,

$$\alpha_1^2 = \alpha_2^2 = \alpha^2 = \frac{g}{2} = \frac{\gamma_3}{\zeta}, \qquad h = 0. \tag{5.53}$$

In this case equations (5.45) and (5.46) become

$$-\zeta f_z + \left(-P + \mu\left(\alpha^{-4} - \alpha^2\right) - 2\alpha^2[\alpha^2 - 1]_+\right)\gamma^2\gamma_3\frac{B^2}{2} = 0, \tag{5.54}$$

$$\sigma_1'(R) = \frac{1}{R}4\cos 2\phi\alpha^2[\alpha^2 - 1]_+ \tag{5.55}$$

The left-hand side of (5.54) does not depend on ϕ, that is the boundary conditions define the same deformation for all fiber orientations. The role of ϕ is limited to defining the stress field.

In general, the right-hand side of (5.55) results in a logarithmic singularity and

infinite value of radial stress. Such singularities are of purely mathematical nature and do not point to any unphysical behaviour, as both the strains and the energy density everywhere are finite [74]. The value of stress is finite if there exist $\epsilon > 0$, such that

$$\cos 2\phi(R) = R^{\epsilon} + o(R), \qquad \text{as } R \to 0. \tag{5.56}$$

In this regard we note that the continuity of the structure tensor, defined by $\mathbf{H} = \frac{1}{2}\mathbf{a}_0^{(1)} \otimes \mathbf{a}_0^{(1)} + \frac{1}{2}\mathbf{a}_0^{(2)} \otimes \mathbf{a}_0^{(2)}$, implies $\phi(0) = \frac{\pi}{4}$ due to the symmetry assumptions, as provided by the Proposition 17 in the Appendix. Since the total structure tensor for $\phi = \frac{\pi}{4}$ is $\mathbf{H} = \mathbf{1}$, we refer to such fiber alignment as *isotropic*. Although in this case the material response is truly anisotropic, the anisotropy cannot be captured by deformations we are restricted to.

Remark. Proposition 17 demonstrates that the continuity of tensor quantities in some neighbourhood of the origin implies the transverse isotropy at the origin. However we do not assume the continuity of the structure and growth tensors, as it does not always hold in biological tissues. The only quantities we require to be continuous are the deformation $r(R)$ (due to the no cavitation assumption) and the radial component of the Cauchy stress tensor $\sigma_1(R)$ (due to Cauchy's equation of equilibrium).

5.2.2 Equilibrium solutions

It follows from (5.25)-(5.30) that a steady state is a solution of (5.17), (5.20)-(5.21) that satisfies

$$\tan^{\nu}\phi(R) = \begin{cases} \frac{\sigma_2(R)}{\sigma_1(R)}, & \text{if } \sigma_1(R) \text{ or } \sigma_2(R) > 0, \\ \text{any}, & \text{if } \sigma_1(R), \sigma_2(R) \leq 0. \end{cases} \tag{5.57}$$

$$\gamma_i(R) = \gamma = 0.5, \quad \forall R \in [0, B], \tag{5.58}$$

where $\nu = 1/\beta$ is a positive constant. The equilibrium state of growth is isotropic and homogeneous due to (5.58), therefore the deformation and the principal stretches are given by (5.49) and (5.53) with ζ computed from (5.54).

If $\sigma_1 > 0$ and $\phi \neq \frac{\pi}{4}$ then the first line of (5.57) is equivalent to

$$\sigma_1 = (\tilde{\sigma}_2 - \tilde{\sigma}_1)/(\tan^\nu \phi - 1). \tag{5.59}$$

Hence (5.57) may be written as

$$\begin{cases} \sigma_1 = 4\alpha^2[\alpha^2 - 1]_+ \cos^\nu \phi(\sin\phi + \cos\phi)\dfrac{\sin\phi - \cos\phi}{\sin^\nu \phi - \cos^\nu \phi}, & \sigma_1, \sigma_2 > 0, \\ \phi = 0, & \sigma_2 = 0,\ \sigma_1 > 0, \\ \phi = \frac{\pi}{2}, & \sigma_1 = 0,\ \sigma_2 > 0, \\ \phi = \frac{\pi}{4}, & \sigma_i - \text{any}, \\ \phi - \text{any}, & \sigma_1,\ \sigma_2 \leq 0. \end{cases} \tag{5.60}$$

Condition (5.60) states a relation between σ_1 and ϕ, which can be described as a subset of $\{(\phi, \sigma_1) : \phi \in [0, \frac{\pi}{2}]\} \subset \mathbb{R}^2$. Henceforth we will refer to this subset as the *equilibrium subset*. As shown in Figure 5.4a, the equilibrium subset consists of a continuous curve, a straight line $\phi = \frac{\pi}{4}$ and a solid region, which represent the respective lines in (5.60). Equation (5.55) implies that $\sigma_1(R)$ increases for $\phi > \frac{\pi}{4}$ and decreases for $\phi < \frac{\pi}{4}$, thereby defining the orientation of the curves and within the solid region.

An equilibrium solution corresponds to a path $(\phi(R), \sigma_1(R))$ within the equilibrium subset. This path is not necessarily continuous, but the continuity of $\sigma_1(R)$ must hold, meaning that "jumps" in ϕ are allowed, as shown in Figure 5.5c. Note that (5.60) does not define a bijection between the values of fiber angle ϕ and radial stress σ_1, suggesting that multiple equilibrium solutions may correspond to the same set of boundary conditions. In fact, the system can have more than a continuum of equi-

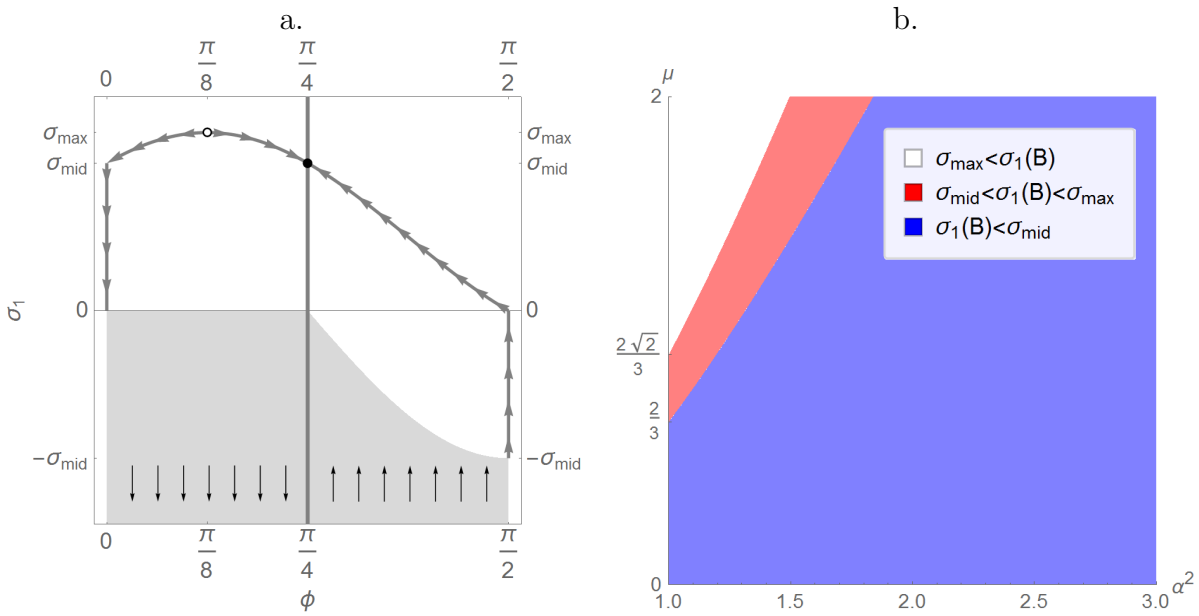

Figure 5.4: (**a**) The equilibrium subset for $\nu = 1$ consists of the curve representing the first 3 lines of (5.60), the straight line $\phi = \frac{\pi}{4}$ and the solid region $\sigma_1, \sigma_2 < 0$. The characteristic values of σ_1 are given by (5.61). (**b**) Arrangement of the radial stress at the boundary $\sigma_1(B)$ with respect to the characteristic values $\sigma_{\max}$, σ_{mid} as a function of α^2 and μ.

librium solutions. We provide a universal algorithm that to constructs any piecewise continuous equilibrium fiber orientation.

1. Find ζ from (5.54) by solving it for the given boundary conditions. Set $i = 0$, $R_i = B$, $\sigma_1(R_i) = -P$.

2. Choose any value of ϕ that satisfies condition (5.60) for $\sigma_1(R_i)$. It is always possible, as $\phi = \frac{\pi}{4}$ is a valid choice for any σ_1. Thus $\phi(R_i)$ is defined.

3. If the point $(\phi, \sigma_1)_{|R=R_i}$ belongs to the curve or the straight line of the equilibrium region, then ϕ can be locally defined as a function of σ_1. If the point $(\phi, \sigma_1)_{|R=R_i}$ belongs to the solid region of the equilibrium subset, then we define $\phi(R)$ arbitrarily for $R \in [0, R_i]$. In either case $\sigma_1(R)$, $\phi(R)$ can be computed by integrating (5.55) for $R \in (R_{i+1}, R_i]$, where R_{i+1} is one of the following:

   (a) a point at which we decide to jump to another point in the equilibrium

region that has the same value of σ_1. Set $i = i + 1$ and go to Step 2.

(b) a point at which we have to jump, as the integration of (5.55) cannot be continued. This happens when (ϕ, σ_1) leaves the equilibrium subset. Set $i = i + 1$ and go to Step 2.

(c) 0, meaning that the the equilibrium fiber orientation $\phi(R)$ and radial stress $\sigma_1(R)$ are computed for $R \in [0, B]$.

Note that the construction of the solution starts at $R = B$, the Cauchy equation (5.55) is integrated backwards, R_i is a decreasing sequence, and the corresponding path is laid onto the equilibrium region against the orientation depicted in Figure 5.4a. It is important to mention that the integration can always be continued at $\phi = \frac{\pi}{4}$, where $\sigma_1'(R) = 0$, and also that $\phi = \frac{\pi}{4}$ is an equilibrium fiber angle for all values of σ_1. This ensures that the algorithm can always be completed in a finite number of steps. An example of equilibrium solution is depicted in Figure 5.5.

The diversity of equilibrium solutions depends on the boundary conditions (5.20)-(5.21), as they specify the location of $\sigma_1(B) = -P$ with respect to the equilibrium region. We illustrate this for $\nu = 1$, $f_z = 0$ and $P < 0$. One can distinguish the following three cases:

(i) $\quad \sigma_{\max} < \sigma_1(B)$,

(ii) $\quad \sigma_{\text{mid}} < \sigma_1(B) \leq \sigma_{\max}$,

(iii) $\quad 0 < \sigma_1(B) \leq \sigma_{\text{mid}}$,

where the characteristic values of the radial stress are defined by

$$\sigma_{\text{mid}} = 4\alpha^2[\alpha^2 - 1]_+, \qquad \sigma_{\max} = \frac{1}{2}\left(1 + \sqrt{2}\right)\sigma_{\text{mid}}. \tag{5.61}$$

The case (i) is drastically different from the other cases, as it only allows for the trivial equilibrium fiber arrangement $\phi(R) = \frac{\pi}{4}$, $\forall R \in [0, B]$. This follows from the

fact that the only equilibrium fiber angle value available at $R = B$ is $\phi = \frac{\pi}{4}$ and that $\sigma_{1|\phi=\frac{\pi}{4}}' = 0$. Therefore, the point $(\phi(R), \sigma_1(R))$ cannot move in the equilibrium subset as R changes.

In order to tell which of the inequalities holds, we compute the signs of $\sigma_{\max} - \sigma_1(B)$ and $\sigma_{\text{mid}} - \sigma_1(B)$. Note that $\sigma_{\max}$, σ_{mid} depend on P through α, since α is determined by (5.54). In fact, Equation (5.54) defines a bijection between P and α, which allows $\sigma_{\max} - \sigma_1(B)$ and $\sigma_{\text{mid}} - \sigma_1(B)$ to be written as functions of α. Figure 5.4b. shows how the location of $\sigma_1(B)$ with respect to $\sigma_{\max}$, σ_{mid} depends on the values of μ and P. Interestingly, all three cases (i)-(iii) can take place if $\mu > \frac{2\sqrt{2}}{3}$. For $\frac{2}{3} < \mu < \frac{2\sqrt{2}}{3}$ only the cases (ii) and (iii) remain, while $0 < \mu < \frac{2}{3}$ guarantees that the case (iii) holds for all $P < 0$.

5.3 The dynamics of remodeling

We have demonstrated that the system defined by (5.17), (5.20)-(5.21), (5.25)-(5.30) has infinitely many equilibrium solutions, which were described in the previous section. Any solution of the system converges to one of these equilibria as $t \to \infty$, as long as condition (5.27) is satisfied. Therefore the outcome of the remodeling, *i.e.* the final fiber orientation, depends critically on the initial data. Since we are motivated to observe spontaneous self-organisation, the natural choice of the initial condition is the isotropic and homogeneous state of growth and fiber orientation, which is defined by

$$\mathbf{G}(R)_{|t=0} = \mathbf{1}, \qquad \phi(R)_{|t=0} = \frac{\pi}{4}, \quad \forall R \in [0, B]. \tag{5.62}$$

For such initial datum, no pattern formation can be observed, as the isotropy and homogeneity are preserved throughout the evolution and lead to the final state given by

$$\mathbf{G}(R)_{|t=+\infty} = \frac{1}{2}\mathbf{1}, \qquad \phi(R)_{|t=+\infty} = \frac{\pi}{4}, \quad \forall R \in [0, B]. \tag{5.63}$$

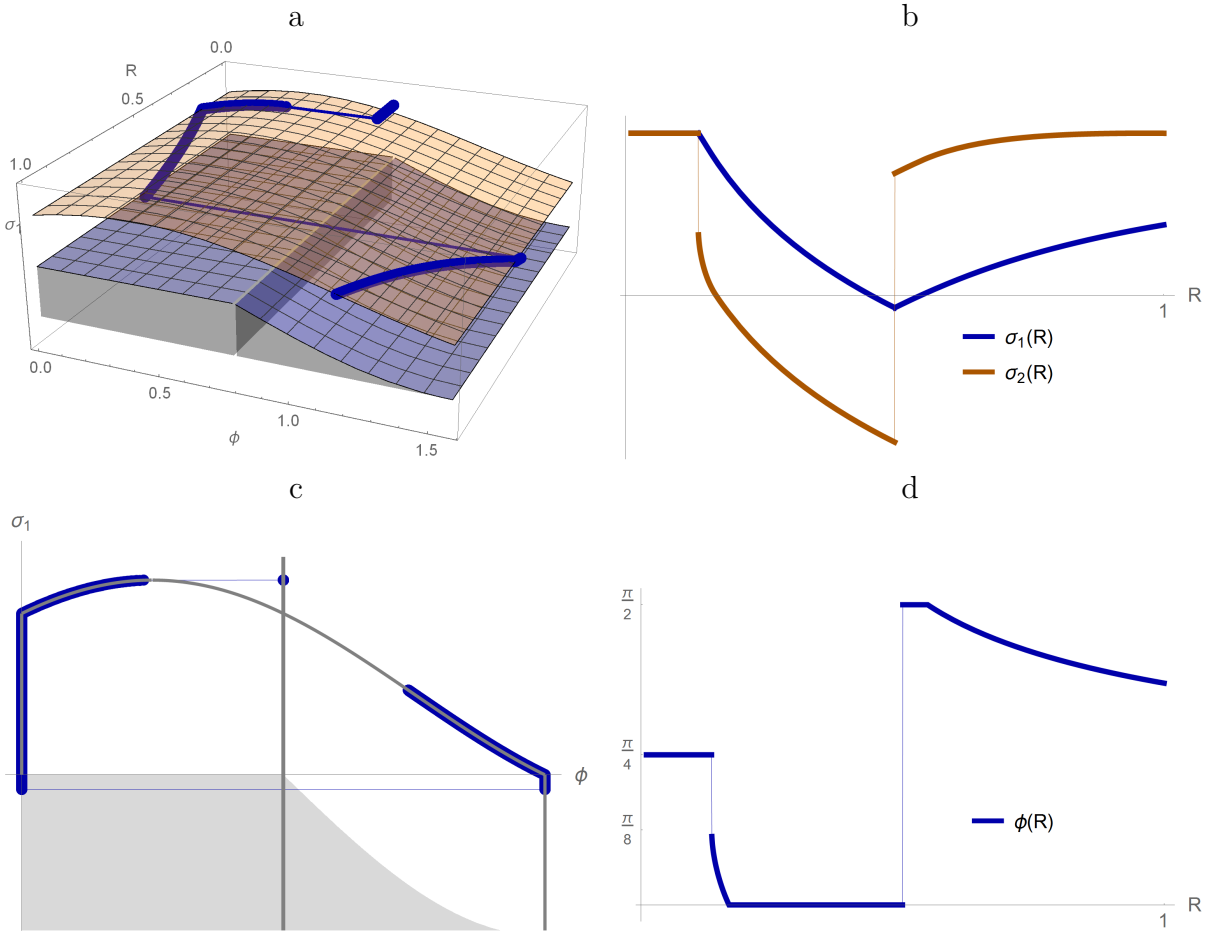

Figure 5.5: An example of equilibrium solution represented as a 3-dimensional curve $(R, \sigma_1(R), \phi(R)) \in \mathbb{R}^3$ (**a**) and its projections (**b**,**c**,**d**). This solution was constructed for $\nu = 1$, $B = 1$, $\mu = 1/30$, $P = -0.1\mu$. The radial component of the Cauchy stress $\sigma_1(R)$ must be continuous due to (5.55), whereas $\sigma_2(R)$ and $\phi(R)$ may be discontinuous as shown. The solution is not unique for the values of parameters used.

In order to induce the symmetry breaking, we consider perturbations of the isotropic homogeneous state, *i.e.*

$$\phi(R) = \frac{\pi}{4} + \varepsilon_\phi \tilde{\phi}(R), \tag{5.64}$$

$$\gamma_i(R) = 1 + \varepsilon_\gamma \tilde{\gamma}_i(R), \tag{5.65}$$

where ε_ϕ, ε_γ are small but finite positive scalars. We take (5.64)-(5.65) as the initial state and address the dynamics of the remodeling numerically.

The evolution of the system is extremely sensitive to the initial condition, as initially nearby solutions converge to distant equilibrium states (the distance is measured in the norm L^2). Since the relation between the random initial state and the final fiber arrangement is not known (besides the fact that the latter is the ω-limit of the former), the dynamics is regarded as a pseudo-random process. We investigate the effect of the remodeling rates η_ϕ, $\eta_{\gamma i}$ on the typical final fiber pattern. In order to identify the implications of simultaneous growth and fiber reorientation, we consider these processes separately, equating η_ϕ or $\eta_{\gamma i}$ to zero, and together, η_ϕ,$\eta_{\gamma i} \neq 0$.

We solve the system (5.17), (5.20)-(5.21), (5.25)-(5.30) by applying the forward Euler method both in space and time. That is, we define a fixed grid $\{R_j = j\Delta R\}$ to approximate functions $r(R)$, $\alpha_i(R)$, $\gamma_i(R)$, $\phi(R)$, $\sigma_i(R)$ at a given time step $t_k = k\Delta t$. The perturbations $\tilde{\phi}$, $\tilde{\gamma}_i$ in (5.64)-(5.65) are polynomial interpolants independently generated by choosing 15 grid points and allocating to them random values from $[-1, 1]$. The values of the respective factors are $\varepsilon_\phi = 0.05$, $\varepsilon_\gamma = 0.02$, unless stated otherwise. We repeat the following steps until the norm of the increments $\dot{\gamma}_i(R_j)$ and $\dot{\phi}(R_j)$ becomes less than a predefined threshold value.

- For the current values of growth and fiber angle, $\gamma_i(R)_{|t=t_k}$, $\phi(R)_{|t=t_k}$, we compute the deformation and the stress, as described in Section 5.2.1. We use the forward Euler method to integrate Equation (5.17) and the trapezoidal rule to evaluate $s(R)$, defined in (5.32).

- Knowing the principal elastic stretches and stresses, we can compute $\dot{\gamma}_i(R_j)_{|t=t_k}$ and $\dot{\phi}(R_j)_{|t=t_k}$ at each grid point R_j using (5.25)-(5.26). The values of $\gamma_i(R)$ and $\phi(R)$ at the next time step are given by

$$\gamma_i(R_j)_{|t=t_{k+1}} = \gamma_i(R_j)_{|t=t_k} + \dot{\gamma}_i(R_j)_{|t=t_k}\Delta t, \tag{5.66}$$

$$\phi(R)_{|t=t_{k+1}} = \phi(R)_{|t=t_k} + \dot{\phi}(R_j)_{|t=t_k}\Delta t. \tag{5.67}$$

The stability is verified heuristically by repeating the computations with smaller time steps Δt and spacings ΔR.

5.3.1 Dynamical growth in the absence of fiber reorientation

Dynamical growth in the absence of fiber orientation corresponds to the remodeling rates

$$\eta_{\gamma i} = 1, \qquad \eta_{\phi} = 0. \tag{5.68}$$

This case yields trivial equilibrium solution, as due to the growth law (5.26) the eventual material state is given by

$$\mathbf{G}(R)_{|t=+\infty} = \frac{1}{2}\mathbf{1}, \qquad \phi(R)_{|t=+\infty} = \phi(R)_{|t=0}, \quad \forall R \in [0, B]. \tag{5.69}$$

The transient dynamics consists in levelling out growth-related inhomogeneity and anisotropy if it is present. If the growth tensor is isotropic and homogeneous initially, *i.e.* $\mathbf{G}(R)_{|t=0} = \mathbf{1}$, then the elastic deformation and the stress field are constant.

5.3.2 Fiber reorientation in the absence of growth

In order to investigate the dynamics of fiber reorientation in the absence of growth, we set

$$\eta_{\gamma i} = 0, \qquad \eta_{\phi} = 1. \tag{5.70}$$

The remodeling process can then be summarized as follows. The initial fiber arrangement produces an inhomogeneous and anisotropic stress field, which leads to a non-uniform preferred fiber angle $\phi_{\text{aim}}(R)$ at $t = 0$. The R-axis is split into several intervals by the critical points R^*, which are defined by $\phi_{\text{aim}} = \phi = \frac{\pi}{4}$, $\sigma_1 = \sigma_2$,

$\dot{\phi} = 0$. Each interval between the critical points corresponds to a positive or negative feedback between ϕ_{aim} and ϕ. Thus, the values of ϕ and ϕ_{aim} in these intervals steadily increase or decrease, so that $\phi - \phi_{\text{aim}} \to 0$ as $t \to 0$. If $\varepsilon_\gamma = 0$, then the growth tensor is uniform and isotropic, $\mathbf{G}(R)_{|t=+\infty} = \mathbf{G}(R)_{|t=0} = \mathbf{1}$, and the final fiber arrangement matches an equilibrium solution described in Section 5.2.2. If $\varepsilon_\gamma \neq 0$ then the fiber orientation converges to a steady state with the inhomogeneous state of growth, $\mathbf{G}(R)_{|t=+\infty} = \mathbf{G}(R)_{|t=0}$. Representative final fiber orientations are shown in Figure 5.6a for $\varepsilon_\gamma = 0$ and in Figure 5.6b for $\varepsilon_\gamma \neq 0$.

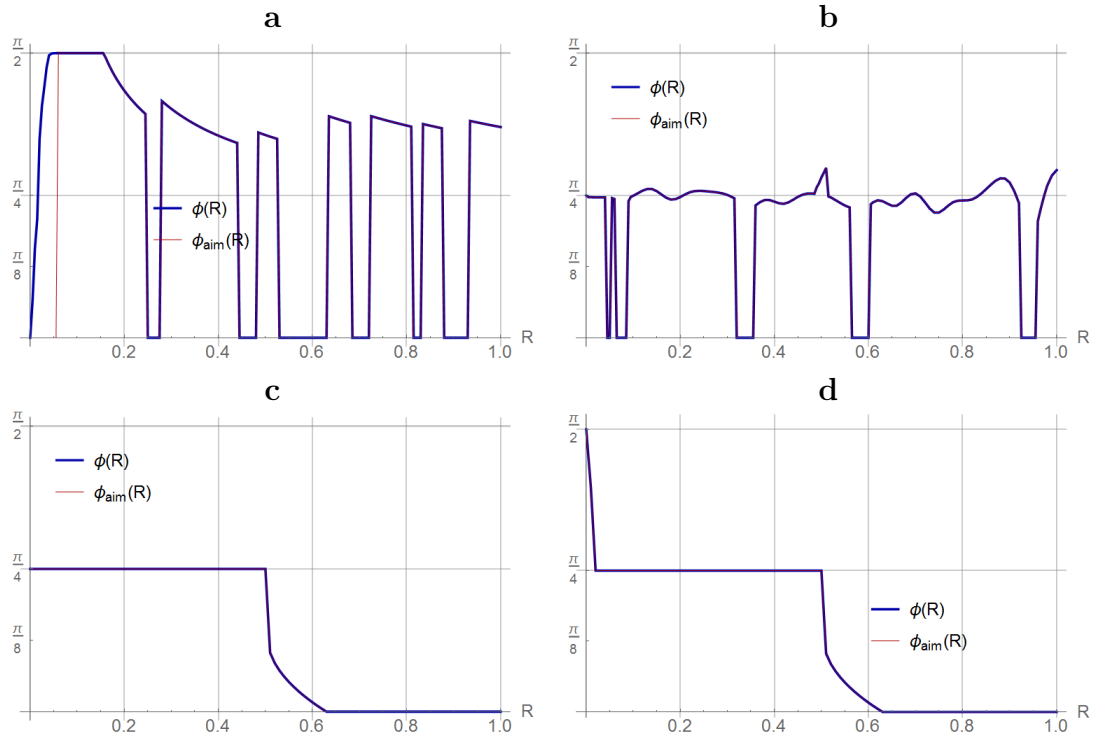

Figure 5.6: Representative final fiber orientations. $\nu = 1$, $B = 1$, $\mu = 1/30$, $P = -0.1\mu$. **a**. A pattern with multiple discontinuities is typical for $\eta_{\gamma i} = 0$, $\eta_\phi = 1$, $\varepsilon_\gamma = 0$. **b**. A typical pattern for $\eta_{\gamma i} = 0$, $\eta_\phi = 1$, $\varepsilon_\gamma \neq 0$. **c**,**d**. The "IR"-pattern (**c**, 6 of 20 cases) and the "IR"-pattern with a minor defect (**d**, 5 of 20 cases) are prevalent patterns if remodeling rates are given by $\eta_{\gamma i} = 0.1\tilde{\eta}_\gamma(\sigma_1, \sigma_2)$, $\eta_\phi = 1$.

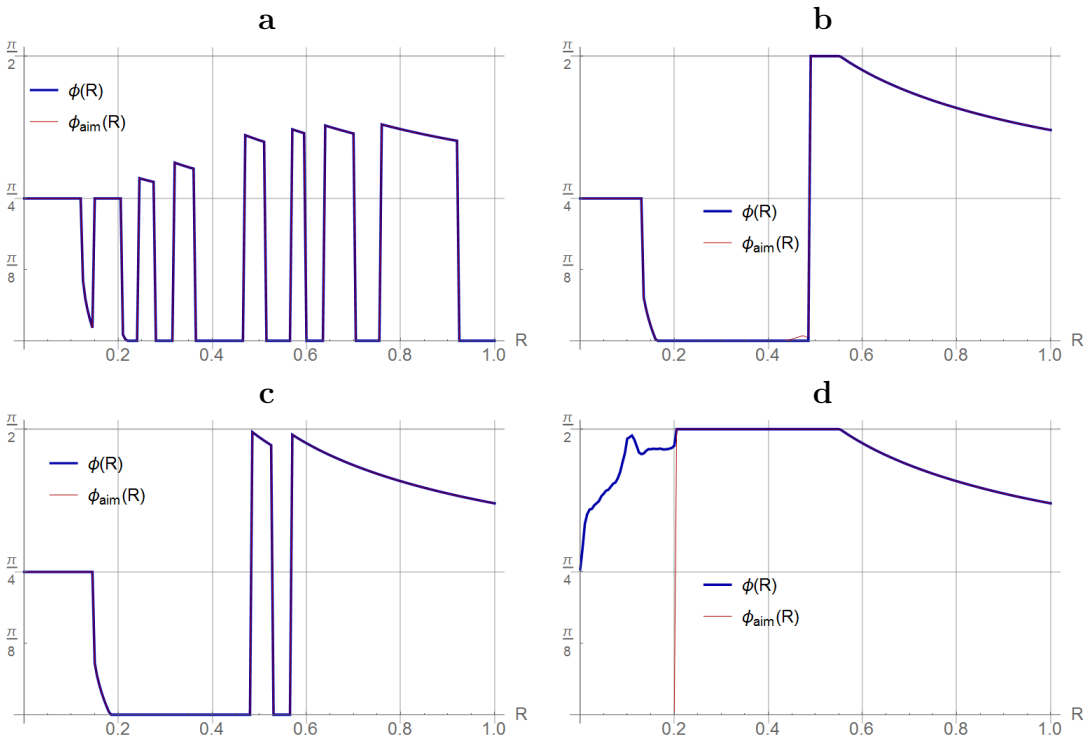

Figure 5.7: Representative final fiber orientations. $\nu = 1$, $B = 1$, $\mu = 1/30$, $P = -0.1\mu$. **a**. A pattern with multiple discontinuities is typical for $\eta_{\gamma i} = 1$, $\eta_\phi = 1$. **b**,**c**. The "IRC" pattern (**b**, 4 of 20 cases) and the "IRC"-pattern (**c**, 7 of 20 cases) with a single defect are prevalent patterns for the remodeling rates given by $\eta_{\gamma i} = \tilde{\eta}_\gamma(\sigma_1, \sigma_2)$, $\eta_\phi = 1$ **d**. The "CC"-pattern is another common pattern for $\eta_{\gamma i} = \tilde{\eta}_\gamma(\sigma_1, \sigma_2)$, $\eta_\phi = 1$ (4 of 20 cases). The central region is compressed, *i.e.* $\sigma_1, \sigma_2 < 0$, although the fibers are positively strained, $\alpha > 1$.

5.3.3 Combined dynamical growth and fiber reorientation

Dynamical growth and fiber reorientation are concurrent if both remodeling rates in (5.25)-(5.26) are positive. Consider constant rates, *e.g.*

$$\eta_{\gamma i} = 1, \qquad \eta_\phi = 1. \tag{5.71}$$

In this case the growth law (5.26) provides exponential decay of material anisotropy associated with inhomogeneous growth, while the fiber reorientation law (5.25) can reinforce the anisotropic fiber orientation through the positive feedback mechanism. After some time the smoothening effect of the dynamical growth cannot compensate

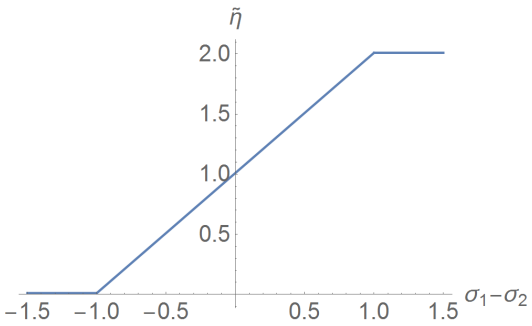

Figure 5.8: A stress-dependent remodeling rate (5.73).

for the sharpening action the fiber realignment, which results in multiple discontinuities of the final fiber angle (Figure 5.7a). In other words, the presence of growth or shrinkage has a little effect on the equilibrium fiber orientation pattern, as can be seen by comparing Figures 5.6a and 5.7a: in both cases we observe similar ragged fiber orientation patterns.

In order to understand how such patterns are formed and the effect of dynamical growth, we take homogeneous isotropic growth tensor and sinusoid fiber angle distribution as the initial data, Figure 5.9a. We keep track of critical points of fiber orientation, defined by $\{R^* \in [0,1] : \phi(R^*) = \phi_{\text{aim}}(R^*)\}$. We consider these points because discontinuities of final fiber orientation evolve from isolated critical points. Note that the value of $\phi(R^*)$ is constant, as we have $\dot{\phi}(R^*) = 0$ by (5.25). Since $\phi_{\text{aim}}(R^*)$ is a function of σ_1, σ_2, as defined by (5.29), we write

$$\frac{d}{dt}\phi_{\text{aim}} = \frac{\partial \phi_{\text{aim}}}{\partial \phi} \underbrace{\dot{\phi}}_{=0} + \frac{\partial \phi_{\text{aim}}}{\partial \sigma_1}\dot{\sigma}_1 + \frac{\partial \phi_{\text{aim}}}{\partial \sigma_2}\dot{\sigma}_2. \tag{5.72}$$

In general, $\dot{\sigma}_1, \dot{\sigma}_2 \neq 0$ and the critical points R^* move in the course of evolution. Note that σ_1, σ_2 depend non-locally on the growth components γ_i and fiber angle ϕ. However, the stress field ignores homogeneous and isotropic growth and is determined locally by the fiber angle ϕ, which is again constant at R^*. Thus, this particular choice of initial data results in $\frac{d}{dt}\phi_{\text{aim}} = 0$ and critical points R^* being stationary. As a

consequence, the isolated critical points persist and evolve into discontinuities of fiber orientation, as demonstrated in Figure 5.9. We conclude that constant remodeling rates tend to amplify initial inhomogeneities and cannot promotes a pattern formation that is not largely determined by small perturbations of the initial homogeneous isotropic state and the critical points they create.

These considerations motivate to consider a mechanically induced growth law. We propose a stress-dependent growth rate (Figure 5.8), defined by

$$\tilde{\eta}_\gamma = 1.01 + \begin{cases} -1 & \sigma_1 - \sigma_2 \leq -1, \\ \sigma_1 - \sigma_2, & -1 < \sigma_1 - \sigma_2 < 1, \\ 1 & 1 \leq \sigma_1 - \sigma_2. \end{cases} \tag{5.73}$$

The dynamics facilitated by this non-uniform growth rate function allows the critical points R^* to merge and disappear, thereby reducing the number of potential discontinuities, as demonstrated in Figure 5.10. One can see by comparing Figures 5.9a and 5.10a, b that the more rapid shrinkage found in the regions $\sigma_1 > \sigma_2$ reduces the difference between the principal stresses thereby flattening out the stress profile.

We observed that the material remodeling with the stress-dependent growth rate applied to a randomly perturbed initial data favours certain final fiber orientation patterns.

For instance, if

$$\eta_{\gamma i} = 0.1\tilde{\eta}_\gamma, \qquad \eta_\phi = 1, \tag{5.74}$$

then the predominant pattern consists in the isotropic fiber arrangement in the central part of the cylinder, followed by a short transition and radial fiber orientation in the peripheral region (*"IR"-pattern*). Approximately half of the randomly generated initial states resulted into this pattern, sometimes with minor defects, Figure 5.6c,d. Note that such fiber arrangement agrees with the orientation of elongated structures in [10]

during week 2, see Table 5.1, Figure 5.3.

A common orientation pattern is different if the growth rate is increased by a factor of 10, that is if we take

$$\eta_{\gamma i} = \tilde{\eta}_\gamma, \qquad \eta_\phi = 1. \tag{5.75}$$

Approximately half of the randomly perturbed initial states converged to equilibria with isotropically oriented fibers in the central region, radial orientation in the intermediate region and predominantly circumferential orientation in the peripheral region (*"IRC"-pattern*), see Figures 5.7b,c. Note the resemblance to the orientation of elongated structures during week 1, Table 5.1, Figure 5.3.

5.4 Conclusion and discussion

We proposed a model for simultaneous material growth and fiber reorientation in cylindrical geometry. The growth law (5.26) prescribed gradual material shrinkage, such that the growth tensor asymptotically approaches a multiple of the identity tensor. We used the growth rate (5.73) that depends on the value the Cauchy stress. The reorientation law for the reference fiber angle (5.25) defined fiber realignment with respect to the values of positive principal current stresses and allowed for intermediate equilibrium fiber angles.

We demonstrated that the material has infinitely many equilibrium states, which can be obtained through a discrete iteration process. The dynamical behaviour of the model was addressed numerically. We observe that small perturbations from the initial homogeneous isotropic state grow away from that state, indicating instability, and diverge, indicating extreme sensitivity of the system on the initial data. Nevertheless, about half of the randomly generated initial states converged to equilibria that followed certain patterns of fiber orientation, Figures 5.6c,d, 5.7b,c. These patterns are similar to the ones observed in cell aggregates in [10]. The dynamics of our model has certain

attributes of a self-organising system: it is driven by local remodeling laws and favours some global patterns over others. The coupling between the growth and the fiber reorientation is crucial for this behaviour.

Several critical remarks have to be made. First, the observed pattern formation is not robust and affects only half of the cases often resulting in minor defects. Second, the growth law is not objective, as it distinguishes the radial and circumferential components of the Cauchy stress due to Equation (5.73). Finally, the proposed model should be enhanced in several other aspects to qualify as a candidate model for the self-organisation observed in [10]. This includes incorporating a multiphase approach, micro-mechanically motivated remodeling laws and distributed fiber reinforcing.

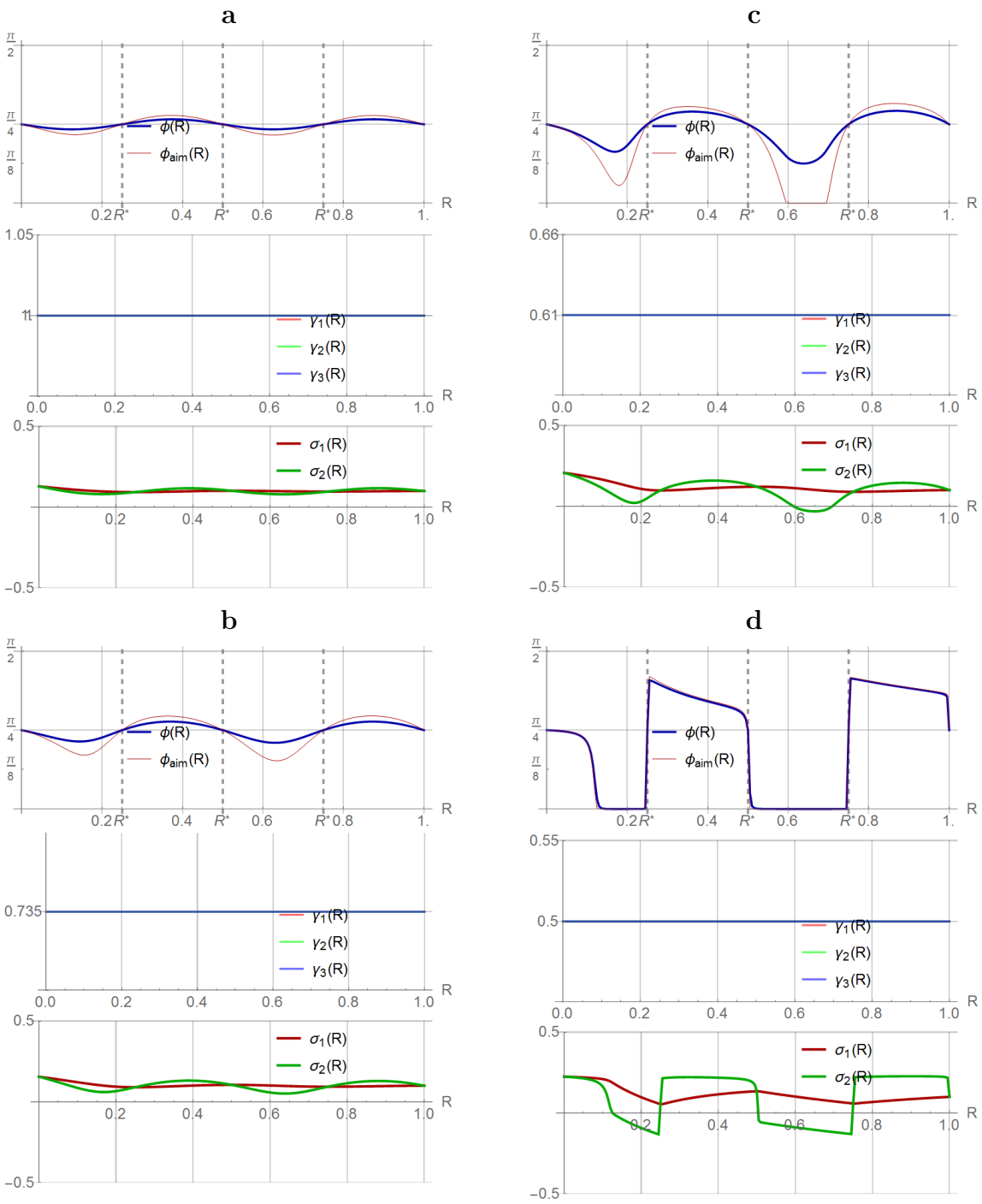

Figure 5.9: Fiber angle ϕ, preferred fiber angle ϕ_{aim}, growth tensor components γ_i and principal stresses σ_1, σ_2 plotted at different time points. The evolution of the system is given by Equations (5.25), (5.26), wherein $\eta_\phi = \eta_{\gamma i} = 1$. **a.** $t = 0$, the initial data is defined by $\phi(R) = \frac{\pi}{4} - 0.05\sin(4\pi R)$, $\gamma_i(R) = 1$. **b.** $t = 0.75$. **c.** $t = 1.5$. **d.** $t = 9$. These plots demonstrate that the critical points R^* are stationary and evolve into discontinuities of $\phi(R)$, as $t \to +\infty$.

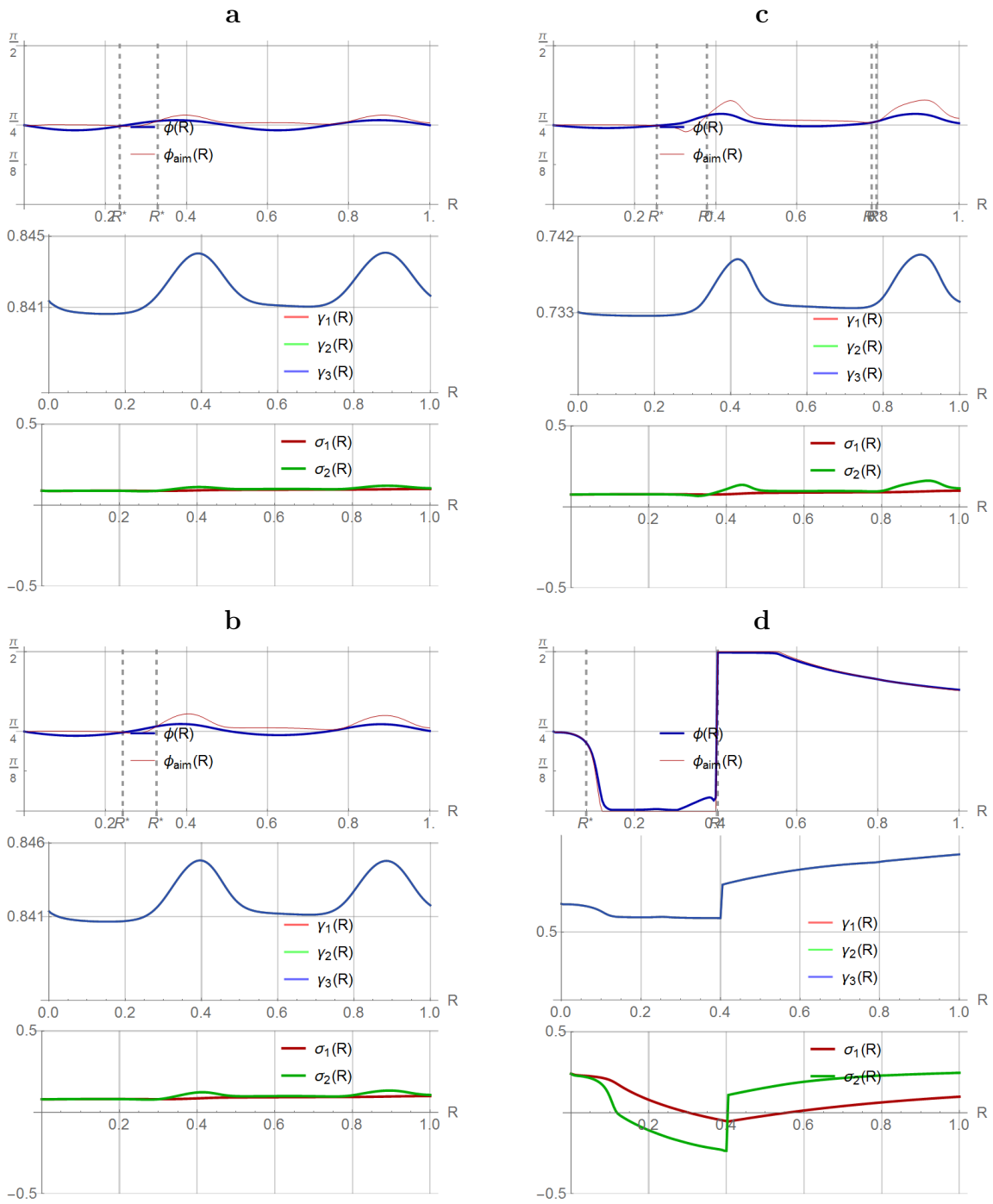

Figure 5.10: Fiber angle ϕ, preferred fiber angle ϕ_{aim}, growth tensor components γ_i and principal stresses σ_1, σ_2 plotted at different time points. The initial data is the same as in Figure 5.9a. The evolution of the system is given by Equations (5.25), (5.26), wherein $\eta_{\gamma i} = \tilde{\eta}_\gamma$, which is defined in Equation (5.73). **a.** $t = 0.375$, $\eta_\phi = 0$. **b.** $t = 0.75$, $\eta_\phi = 1$. **c.** $t = 1.5$, $\eta_\phi = 1$. **d.** $t = 9$, $\eta_\phi = 1$. The stress-dependent growth rate $\tilde{\eta}_\gamma$ results into a flatter stress profile, as compared to the constant growth rate (Figure 5.9). Consequently, the critical points R^* are not stationary, their number and position may change in the course of evolution. As $t \to +\infty$, only one critical point persists ($R^* \approx 0.4$) for this set of parameters and initial data.

Chapter 6

Conclusion

In this thesis, we studied mechanical properties of fiber-reinforced materials. In the first part of the thesis, we addressed the aspects of constitutive models for fibers that are associated with distributed fiber reinforcing and fiber dispersion (Chapters 2, 3). The second part was devoted to the dynamics of mechanically-induced fiber reorientation (Chapter 4) and the dynamics of fiber reorientation coupled with growth (Chapter 5).

In Chapter 2 we reviewed several models for distributed fiber reinforcing. These models are based on the integration of the orientation density function and allow to incorporate tissue's structural data directly into the constitutive equation. The original approach [43, 44] requires the integration of the stresses generated each fiber fraction and is therefore computationally costly. An alternative approach [22, 20] consists in calculating the deformation-independent generalized structure tensor. This approach is numerically efficient but results in large error for a high degree of fiber dispersion. Following this approach, two models incorporating higher-order structure tensors were suggested recently [58, 6]. We discussed the issues related to the compressed fibers and the correct derivation of the generalized structure tensor models. We introduced the iGST model, which excludes compressed fibers when computing the structure

tensor. This model can be used to identify the error in the generalized structure tensor approach associated with the compressed fibers, as opposed to the error introduced by the averaging of fiber stretch.

In Chapter 3 we studied the behaviour of a fiber reinforced material in uniaxial tension. We focused on the phenomenon of lateral extension of an incompressible material, which is associated with nonlinearity and anisotropy. We used this phenomenon as a qualitative measure of agreement between different models for fiber dispersion. We observed that the iGST model, unlike other generalized structure tensor models, predicts the behaviour similar to that of the original angularly integrated model, indicating that the error introduced by the compressed fibers is large enough to cause qualitative changes in the material response to uniaxial tension.

Chapter 4 was dedicated to the study of mechanically-induced fiber reorientation. We address analytically the models with various combinations of boundary conditions and stimuli for fiber reorientation. The role of constitutive equation in the dynamical behaviour is critical if the fiber reorientation law is given in terms of principal stretches in the case of constant loads and in terms of principal stresses in the case of fixed displacement. In the latter case, the system can have multiple equilibrium states. We also considered the effect of fiber dispersion and observed no difference in the global dynamics.

In Chapter 5 we proposed a model for coupled growth and fiber reorientation in an elastic incompressible disk. This model was motivated by an example of *in vitro* morphogenesis accompanied by collagen realignment and gel compaction. The dynamics of our model is extremely sensitive to the initial condition and characterized by an infinite number of equilibrium states. We observed that the stress-induced fiber reorientation and growth laws used in our model produce fiber orientation pattern similar to the ones observed in cell aggregates in [10]. We conclude that our model has attributes of a self-organising system and the coupling between the growth and

the fiber reorientation is crucial for this behaviour.

The results presented in this thesis suggest several ideas for the future research. As regards the distributed fiber reinforcing, we suggest considering a modification of generalized high-order structure tensor models, analogous to the iGST model. High-order tensors significantly decrease the error caused by the averaging of the stretch, leaving the compressed fiber as the main issue. The error introduced by the compressed fibers should be estimated by excluding them from the integrand.

We believe the most interesting and the promising direction of the future research suggested by this study is related to the coupling between the fiber reorientation and growth. First, some aspects of the existing model still have to be addressed, for instance, the effect of fiber dispersion. Second, the considered form of deformation and the imposed symmetries are too restrictive to take into account the variations in the disk thickness reported by [10]. The curvature of the top surface of the disk can possibly be the decisive factor in sef-organisation and morphogenesis. Finally, the interaction between the tensile fibers and the compressive ground substance in the collagen gel subject to traction-free boundary conditions can only be addressed using a multiphase approach.

Appendix A

Computation of GHOSTs (the transversely isotropic case)

We introduce spherical coordinates (r, θ, ϕ): $(x, y, z) = (r\cos\theta, r\sin\theta\cos\varphi, r\sin\theta\sin\varphi) \in \mathbb{R}^3$. That is, the components of a unit vector $\mathbf{m}_0 \in \mathbb{U}^2$ are given by

$$\mathrm{m}_{01} = \cos\theta, \quad \mathrm{m}_{02} = \sin\theta\cos\varphi, \quad \mathrm{m}_{03} = \sin\theta\sin\varphi. \tag{A.1}$$

A GHOST of order $2n$, $\mathbf{H}^n$, is defined by (2.42) and its Cartesian components are denoted $\mathrm{H}_{i_1 i_2 \ldots i_{2n}}$. The GHOST is symmetric in the sense that $\mathrm{H}_{i_1 i_2 \ldots i_{2n}} \equiv \mathrm{H}_{\tilde{i}_1 \tilde{i}_2 \ldots \tilde{i}_{2n}}$ if and only if $i_1 i_2 \ldots i_{2n}$ is a permutation of $\tilde{i}_1 \tilde{i}_2 \ldots \tilde{i}_{2n}$. Therefore, it is convenient to consider only non-decreasing sequences $i_1 \le i_2 \le \cdots \le i_{2n}$. As $i_1, \ldots, i_{2n} \in \{1, 2, 3\}$, we have

$$i_1 i_2 \ldots i_{2n} = \underbrace{1 \ldots 1}_{k_1} \underbrace{2 \ldots 2}_{k_2} \underbrace{3 \ldots 3}_{k_3}, \qquad \text{where } k_1 + k_2 + k_3 = 2n. \tag{A.2}$$

Due to transverse isotropy, the only non-zero components are those with even k_1, k_2,

k_3. For the non-zero terms we introduce the following notation

$$(j_1, j_2, j_3) := \mathrm{H}_{i_1 i_2 \ldots i_{2n}} = \langle \mathrm{m}_{01}^{2j_1} \mathrm{m}_{02}^{2j_2} \mathrm{m}_{03}^{2j_3} \rangle \tag{A.3}$$

$$= \int_0^{\pi} \rho(\theta) \cos^{2j_1} \theta \sin^{2j_2+2j_3+1} \theta d\theta \int_0^{2\pi} \cos^{2j_2} \varphi \sin^{2j_3} \varphi d\varphi. \tag{A.4}$$

We use $\mathrm{m}_{01}^2 = 1 - \mathrm{m}_{02}^2 - \mathrm{m}_{03}^2$ and the additivity of $\langle \bullet \rangle$ to derive recurrent relation

$$(j_1, j_2, j_3) = (j_1 - 1, j_2, j_3) - (j_1 - 1, j_2 + 1, j_3) - (j_1 - 1, j_2, j_3 + 1), \tag{A.5}$$

which allows to compute $\{(j_1, j_2, j_3) : j_1 + j_2 + j_3 = n\}$ once$\{(0, j_2, j_3) : j_2, j_3 \leq n\}$ are known. In order to compute components of type $(0, j_2, j_3)$ we define

$$(j_2, j_3) := \int_0^{2\pi} \cos^{2j_2} \varphi \sin^{2j_3} \varphi d\varphi, \tag{A.6}$$

and use recurrent relations

$$(j_2, j_3) = (j_2 - 1, j_3) - (j_2 - 1, j_3 + 1), \tag{A.7}$$

$$(j_2, j_3) = \frac{2j_3 - 1}{2j_2 + 1}(j_2 + 1, j_3 - 1), \qquad (0, 0) = 2\pi, \tag{A.8}$$

$$(j_2, j_3) = \frac{2j_2 - 1}{2j_3 + 1}(j_2 - 1, j_3 + 1), \qquad (0, 0) = 2\pi, \tag{A.9}$$

$$(j_2, j_3) = \frac{2j_3 - 1}{2j_2 + 2j_3}(j_2, j_3 - 1), \qquad (0, 0) = 2\pi. \tag{A.10}$$

The latter come from [26, 2.510]

$$\int \sin^p x \cos^q x dx = -\frac{\sin^{p-1} x \cos^{q+1} x}{q+1} + \frac{p-1}{q+1} \int \sin^{p-2} x \cos^{q+2} x dx \quad (A.11)$$

$$= \frac{\sin^{p+1} x \cos^{q-1} x}{p+1} + \frac{q-1}{p+1} \int \sin^{p+2} x \cos^{q-2} x dx \quad (A.12)$$

$$= -\frac{\sin^{p-1} x \cos^{q+1} x}{p+q} + \frac{p-1}{p+q} \int \sin^{p-2} x \cos^{q} x dx, \quad (A.13)$$

$$p = 2j_3,\ q = 2j_2. \quad (A.14)$$

Another useful identity is [26, 2.511.2]

$$\int \sin^{2l} x dx = \frac{(2l-1)!!}{2^l l!} x \quad (A.15)$$

$$-\frac{\cos x}{2l} \left\{ \sin^{2l-1} x + \sum_{k=1}^{l-1} \frac{(2l-1)(2l-3)\dots(2l-2k-1)}{2^k (l-1)(l-2)\dots(l-k)} \sin^{2l-2k-1} x \right\}, \quad (A.16)$$

which yields

$$(l,l) = \int_0^{2\pi} \cos^{2l} \varphi \sin^{2l} \varphi d\varphi = \frac{1}{2^{2l+1}} \int_0^{2\pi} \sin^{2l} 2\varphi 2 d\varphi \quad (A.17)$$

$$= \frac{1}{2^{2l+1}} \left[\frac{(2l-1)!!}{2^l l!} x \right]_{x=0}^{x=4\pi} = \frac{(2l-1)!!}{2^{3l} l!} 2\pi. \quad (A.18)$$

We define

$$\varkappa^n = \int_0^{\pi} \rho(\theta) \sin^{2n+1} \theta d\theta, \quad (A.19)$$

so that

$$(0, j_2, j_3) = \varkappa^{j2+j3}(j_2, j_3). \quad (A.20)$$

For an even $n = 2l$ we introduce

$$\kappa^n = (0, l, l) = \varkappa^n (l, l) = \frac{(2l-1)!!}{2^{3l} l!} 2\pi \varkappa^n, \quad (A.21)$$

and for an odd $n = 2l + 1$

$$\kappa^n = (0, l, l+1) = \varkappa^n(l, l+1) = \frac{2l+1}{4l+2}\varkappa^n(l, l) = \frac{(2l-1)!!}{2^{3l+1}l!}2\pi\varkappa^n. \tag{A.22}$$

The following algorithm is used to compute the entries of GHOSTs up to order $2n$.

- Evaluate $\varkappa^1, \ldots \varkappa^n$ by integrating $\rho(\theta)$ in (A.19).
- Let $(0, 0) = 2\pi$.
- Let $(0, 0, 0) = 1$.
- For $s = 1 \ldots n$ (consider $j_1 + j_2 + j_3 = s$)
  - Let $l = \lfloor s/2 \rfloor$.
  - If s is odd
    - $(l, l+1) = (l+1, l) = \frac{1}{2}(l, l)$.
    - For $k = 1 \ldots l$ compute $(l-k, l+1+k) = (l+1+k, l-k) = \frac{2l+2k+1}{2l-2k+1}(l+k, l-k+1)$.
    - For $k = 0, \ldots l$ compute $(0, l-k, l+1+k) = (0, l+1+k, l-k) = \varkappa^s(l-k, l+1+k)$.
  - If s is even and $l \neq 0$
    - Compute $(l, l) = \frac{(2l-1)!!}{2^{3l}l!}2\pi = \frac{(2l-1)}{8l}(l-1, l-1)$.
    - For $k = 1 \ldots l$ compute $(l-k, l+k) = (l+k, l-k) = \frac{2l+2k-1}{2l-2k+1}(l+k-1, l-k+1)$.
    - For $k = 0, \ldots l$ compute $(0, l-k, l+k) = (0, l+k, l-k) = \varkappa^s(l+k, l-k)$.
  - For $j_1 = 1, \ldots, s$
    - For $j_2 = 0, \ldots, s - j_1$
      - Let $j_3 = s - j_1 - j_2$.

· Compute $(j_1, j_2, j_3) = (j_1 - 1, j_2, j_3) - (j_1 - 1, j_2 + 1, j_3) - (j_1 - 1, j_2, j_3 + 1)$.

- For $s = 1 \dots n$
  - For each $2s$-tuple $i_1 i_2 \dots i_{2s}$, such that $i_m \in \{1, 2, 3\}$
    - Let $2j_1$, $2j_2$, $2j_3$ be the number of 1's, 2's and 3's in $i_1 i_2 \dots i_{2s}$.
    - If j_1, j_2, j_3 are integer then $A^n_{i_1 i_2 \dots i_{2n}} = (j_1, j_2, j_3)$ else $A^n_{i_1 i_2 \dots i_{2n}} = 0$.

Structure stretch tensors $\mathbf{I}^n_{\mathrm{f}}$ are defined in (2.43). If the material is transversely isotropic and the right Cauchy-Green deformation tensor $\mathbf{C}$ is diagonal, then $\mathbf{I}^n_{\mathrm{f}}$ is diagonal as well and its components are given by

$$\left(\mathbf{H}^{n+1} \overset{2n}{\odot} \mathbf{C}^{\otimes n}\right)_{11} = \sum_{j_1=0}^{n} \sum_{j_2=0}^{n-j_1} (j_1 + 1, j_2, j_3)\, \mathrm{per}(j_1, j_2, j_3)\, \mathrm{C}_{11}^{j_1} \mathrm{C}_{22}^{j_2} \mathrm{C}_{33}^{j_3}, \quad \text{(A.23)}$$

$$\left(\mathbf{H}^{n+1} \overset{2n}{\odot} \mathbf{C}^{\otimes n}\right)_{22} = \sum_{j_1=0}^{n} \sum_{j_2=0}^{n-j_1} (j_1, j_2 + 1, j_3)\, \mathrm{per}(j_1, j_2, j_3)\, \mathrm{C}_{11}^{j_1} \mathrm{C}_{22}^{j_2} \mathrm{C}_{33}^{j_3}, \quad \text{(A.24)}$$

$$\left(\mathbf{H}^{n+1} \overset{2n}{\odot} \mathbf{C}^{\otimes n}\right)_{33} = \sum_{j_1=0}^{n} \sum_{j_2=0}^{n-j_1} (j_1, j_2, j_3 + 1)\, \mathrm{per}(j_1, j_2, j_3)\, \mathrm{C}_{11}^{j_1} \mathrm{C}_{22}^{j_2} \mathrm{C}_{33}^{j_3}, \quad \text{(A.25)}$$

where $j_3 = n - j_1 - j_2$, $\mathrm{per}(j_1, j_2, j_3) = \frac{(j_1+j_2+j_3)!}{j_1! j_2! j_3!}$ is the number of permutations of a tuple $\underbrace{1 \dots 1}_{j_1} \underbrace{2 \dots 2}_{j_2} \underbrace{3 \dots 3}_{j_3}$, where $j_1 + j_2 + j_3 = n$. Note that expressions (A.23)-(A.25) are not valid for in a general case.

Appendix B

Methods for determining the number of perversion points

B.1 Perversion diagram for GST

The curves separating the regions of different number of perversion points in the parametric space (ϕ, μ) can be obtained analytically for the GST and GSTx models. With the notation $a = \mathrm{H}_{22}^2 > 0$, $b = \frac{\mu}{4} - \mathrm{H}_{11}\mathrm{H}_{22} - \mathrm{H}_{33}\mathrm{H}_{22}$, $c = \mathrm{H}_{11}\mathrm{H}_{33} > 0$ the left-hand side of (3.51) becomes

$$a\eta^2 + b\eta + c = 0, \tag{B.1}$$

where the roots η of this polynomial correspond to perversion points if and only if they satisfy $\eta \in (0, 1)$. The condition for existence of positive distinct roots $\eta_\pm = (-b \pm \sqrt{\Delta})/2a$ is

$$\begin{cases} \Delta = b^2 - 4ac > 0, \\ -b > 0, \end{cases} \tag{B.2}$$

which is equivalent to

$$\mu \leq 4\mathrm{H}_{22}(\sqrt{\mathrm{H}_{33}} - \sqrt{\mathrm{H}_{11}})^2, \tag{B.3}$$

where the equality corresponds to coinciding positive roots if $\mathrm{H}_{22}, \mathrm{H}_{33} \neq 0$. The requirement $\eta_+ < 1$ is equivalent to

$$\begin{cases} \mu > 4(\mathrm{H}_{22} - 2\mathrm{H}_{22}^2 - \mathrm{H}_{11}\mathrm{H}_{33}), \\ \mu > 4(\mathrm{H}_{22} - 3\mathrm{H}_{22}^2), \end{cases} \tag{B.4}$$

whereas the requirement $\eta_- < 1$ is equivalent to

$$\begin{cases} \mu < 4(\mathrm{H}_{22} - 2\mathrm{H}_{22}^2 - \mathrm{H}_{11}\mathrm{H}_{33}), \\ \mu > 4(\mathrm{H}_{22} - 3\mathrm{H}_{22}^2). \end{cases} \tag{B.5}$$

Here curly braces and square brackets denote logical "and" and "or" respectively. Combining the conditions, we discover that there exist two perversion points if

$$\begin{cases} \mu < 4\mathrm{H}_{22}(\sqrt{\mathrm{H}_{33}} - \sqrt{\mathrm{H}_{11}})^2, \\ \mu > 4(\mathrm{H}_{22} - 2\mathrm{H}_{22}^2 - \mathrm{H}_{11}\mathrm{H}_{33}), \\ \mu > 4(\mathrm{H}_{22} - 3\mathrm{H}_{22}^2), \end{cases} \tag{B.6}$$

and only one perversion if

$$\mu < 4(\mathrm{H}_{22} - 2\mathrm{H}_{22}^2 - \mathrm{H}_{11}\mathrm{H}_{33}). \tag{B.7}$$

Equation (B.1) in the case of perfect fiber alignment ($\kappa = 0$) clearly has a root $\eta = 0$, as $c = \mathrm{H}_{11}\mathrm{H}_{33} = \mathrm{H}_{11}\kappa = 0$. That is, one perversion point is achieved at the infinite axial stretch.

B.2 Perversion diagram for GSTx

The material in GSTx model "switches" to the isotropic behavior when $\lambda < \tan\phi$, where the notation $\lambda = \lambda_1$ is introduced. For $\lambda < \tan\phi$ we always have $\sigma_2(\lambda) < 0$,

and condition (3.50) can only be realized through its first part. The results obtained for the GST model remain unaffected if there are zero or one perversion points or if both perversion points occur in the anisotropic regime, *i.e.* they satisfy $\lambda > \tan\phi$. If there are two perversion points according to the GST model, and only one of them lies in the region $\lambda < \tan\phi$, then the total number of perversions does not change either due to the jump from $\sigma_2(\tan\phi - 0) < 0$ to $\sigma_2(\tan\phi + 0) > 0$. In order to identify the difference between the GST and GSTx models, it only remains to consider the case when both perversion points exist and are in the region $\lambda < \tan\phi$. The corresponding condition $\eta_+ > \eta_- > \tan^{-2}\phi$ is equivalent to

$$\begin{cases} \mu < 4\left(\mathrm{H}_{22} - \mathrm{H}_{22}^2(1 + 2\tan^{-2}\phi)\right), \\ \mu > 4\mathrm{H}_{33}(\mathrm{H}_{22}\tan^{-2}\phi - \mathrm{H}_{33})(\tan^2\phi - 1). \end{cases} \tag{B.8}$$

This defines the region in the parameter space where the GST model predicts two perversion points, whilst the GSTx model predicts none.

B.3 Perversion diagram for AI, iGST

For the AI and iGST approaches one has to solve equations (3.47), (3.48) numerically. Knowing that the ground substance response is neo-Hookean, we can write (3.47), (3.48) as

$$\mu = \lambda^4\sigma_{21\mathrm{f}}, \tag{B.9}$$

$$0 = \lambda^4(\lambda^{-2} - 1)\sigma_{21\mathrm{f}} + \sigma_{2\mathrm{f}}, \tag{B.10}$$

which are decoupled and can be solved one-by-one for λ and μ, if ϕ is known. At the intersection of the curves given by (B.9), (B.10) the perversions have algebraic

multiplicity of at least three and are given by

$$\sigma_2 = 0, \quad \sigma_{21} = 0, \quad \sigma_{22} = 0, \tag{B.11}$$

which can also be written as

$$\begin{aligned} \mu &= \lambda^4 \sigma_{21\mathrm{f}}, & \text{(B.12)} \\ 0 &= \sigma_{21\mathrm{f}} \lambda^4 (\lambda^{-2} - 1) + \sigma_{2\mathrm{f}}, & \text{(B.13)} \\ 0 &= \sigma_{21\mathrm{f}} \lambda^{-2} + \sigma_{22\mathrm{f}}, & \text{(B.14)} \end{aligned}$$

where the first equation is decoupled from the remaining, and the remaining two can be solved by a root finding algorithm for λ, ϕ.

One can also be interested in finding local extrema of the curves $\mu = \mu(\phi)$, which are given by $d\mu/d\phi = 0$. In order to find a convenient way to describe these extrema, we differentiate (3.47) and (3.48) to obtain

$$\begin{aligned} \frac{d}{d\phi}\sigma_2 &= \frac{\partial}{\partial\phi}\sigma_2 + \frac{\partial\sigma_2}{\partial(\lambda^2)} \cdot \frac{d\lambda^2}{d\phi} + \frac{\partial\sigma_2}{\partial\mu} \cdot \frac{d\mu}{d\phi} = \sigma_{20\phi} + \sigma_{21} \cdot \frac{d\lambda^2}{d\phi}, & \text{(B.15)} \\ \frac{d}{d\phi}\sigma_{21} &= \frac{\partial}{\partial\phi}\sigma_{21} + \frac{\partial\sigma_{21}}{\partial(\lambda^2)} \cdot \frac{d\lambda^2}{d\phi} + \frac{\partial\sigma_{21}}{\partial\mu} \cdot \frac{d\mu}{d\phi} = \sigma_{21\phi} + 2\sigma_{22} \cdot \frac{d\lambda^2}{d\phi}, & \text{(B.16)} \end{aligned}$$

where $\sigma_{2\phi} = \partial\sigma_2/\partial\phi$, $\sigma_{21\phi} = \partial\sigma_{21}/\partial\phi$. After eliminating $d\lambda^2/d\phi$ we have $2\sigma_{22}\sigma_{20\phi} = \sigma_{21}\sigma_{21\phi}$, so that the extrema of $\mu(\phi)$ are determined by

$$\begin{aligned} \mu &= \lambda^4 \sigma_{21\mathrm{f}}, & \text{(B.17)} \\ 0 &= \sigma_{21\mathrm{f}} \lambda^4 (\lambda^{-2} - 1) + \sigma_{2\mathrm{f}}, & \text{(B.18)} \\ 0 &= 2\sigma_{22}\sigma_{20\phi} - \sigma_{21}\sigma_{21\phi}. & \text{(B.19)} \end{aligned}$$

As before, the second and the third equations are to be solved by a root finding

algorithm for λ, ϕ, after which μ is found from the first equation.

B.4 Expressions for the AI model

In order to express an integral over the unit sphere as an iterated integral, we introduce spherical coordinates $(\tilde{\theta}, \tilde{\varphi})$ and let

$$\mathbf{m}_0 = (m_{01}, m_{02}, m_{03}) = (\sin\tilde{\theta}\cos\tilde{\varphi}, \sin\tilde{\theta}\sin\tilde{\varphi}, \cos\tilde{\theta}). \tag{B.20}$$

By (3.37), (3.28) we have

$$\sigma_{2\mathrm{f}} = 8\int_0^{\pi}\int_{-\tilde{\varphi}^*}^{\tilde{\varphi}^*} \rho\cdot\psi_{\mathrm{f}}'\cdot(m_{02}^2\lambda^{-2} - m_{03}^2)\sin\tilde{\theta}d\tilde{\theta}\,d\tilde{\varphi}, \tag{B.21}$$

where $\tan\tilde{\varphi}^* = \lambda$, $\rho = \rho(\mathbf{R}_1^T\mathbf{m}_0) = \tilde{\rho}(\theta)$, $\theta(\tilde{\theta},\tilde{\varphi},\phi) = \arccos(\sin\tilde{\theta}\cos(\phi+\tilde{\varphi}))$, $\psi_{\mathrm{f}}' = \psi_{\mathrm{f}}'(\mathbf{m}_0\otimes\mathbf{m}_0 : \mathbf{C})$. We also have

$$\begin{aligned}\sigma_{21\mathrm{f}} &= 8\int_0^{\pi}\int_{-\tilde{\varphi}^*}^{\tilde{\varphi}^*} \rho\cdot\left[\psi_{\mathrm{f}}''\cdot(m_{01}^2 - m_{02}^2\lambda^{-4})(m_{02}^2\lambda^{-2} - m_{03}^2) + \psi_{\mathrm{f}}'\cdot(-m_{02}^2\lambda^{-4})\right]\\ &\quad \sin\tilde{\theta}d\tilde{\theta}\,d\tilde{\varphi},\end{aligned} \tag{B.22}$$

$$\begin{aligned}\sigma_{22\mathrm{f}} &= 4\int_0^{\pi}\int_{-\tilde{\varphi}^*}^{\tilde{\varphi}^*} \rho\cdot\left[\psi_{\mathrm{f}}'''\cdot(m_{01}^2 - m_{02}\lambda^{-4})^2(m_{02}^2\lambda^{-2} - m_{03}^2)\right.\\ &\quad \left.+\psi_{\mathrm{f}}''\cdot 2m_{02}^2\lambda^{-4}(2m_{02}^2\lambda^{-4} - m_{01}^2 - m_{03}^2\lambda^{-2}) + \psi_{\mathrm{f}}'\cdot 2m_{02}^2\lambda^{-6}\right]\sin\tilde{\theta}d\tilde{\theta}\,d\tilde{\varphi}\\ &\quad +4\int_0^{\pi}\left[\rho_{|\tilde{\varphi}=\tilde{\varphi}^*} + \rho_{|\tilde{\varphi}=-\tilde{\varphi}^*}\right]\cdot\\ &\quad \left[\psi_{\mathrm{f}}''\cdot(m_{01}^2 - m_{02}^2\lambda^{-4})(m_{02}^2\lambda^{-2} - m_{03}^2)\right]_{|\tilde{\varphi}=\tilde{\varphi}^*}\frac{\sin\tilde{\theta}}{2\lambda(1+\lambda^2)}d\tilde{\theta},\end{aligned} \tag{B.23}$$

$$\sigma_{2\phi} = 8\int_0^{\pi}\int_{-\tilde{\varphi}^*}^{\tilde{\varphi}^*} \rho\cdot\psi_{\mathrm{f}}'\cdot(m_{02}^2\lambda^{-2} - m_{03}^2)(-2b\sin 2(\phi+\tilde{\varphi}))\sin^3\tilde{\theta}d\tilde{\theta}\,d\tilde{\varphi}, \tag{B.24}$$

$$\sigma_{21\phi} = \frac{d}{d\phi}\sigma_{21} = 8\int_0^{\pi}\int_{-\tilde{\varphi}^*}^{\tilde{\varphi}^*} \rho\cdot\left[\psi_{\rm f}''\cdot(m_{01}^2-m_{02}^2\lambda^{-4})(m_{02}^2\lambda^{-2}-m_{03}^2)+\psi_{\rm f}'\cdot(-m_{02}^2\lambda^{-4})\right] (-2b\sin 2(\phi+\tilde{\varphi}))\sin^3\tilde{\theta}d\tilde{\theta}\,d\tilde{\varphi}, \tag{B.25}$$

$$\begin{aligned}\sigma_{22\phi} &= 4\int_0^{\pi}\int_{-\tilde{\varphi}^*}^{\tilde{\varphi}^*} \rho\cdot\left[\psi_{\rm f}'''\cdot(m_{01}^2-m_{02}\lambda^{-4})^2(m_{02}^2\lambda^{-2}-m_{03}^2)\right.\\ &\left.+\psi_{\rm f}''\cdot 2m_{02}^2\lambda^{-4}(2m_{02}^2\lambda^{-4}-m_{01}^2-m_{03}^2\lambda^{-2})+\psi_{\rm f}'\cdot 2m_{02}^2\lambda^{-6}\right]\\ &(-2b\sin 2(\phi+\tilde{\varphi}))\sin^3\tilde{\theta}d\tilde{\theta}\,d\tilde{\varphi}\\ &+4\int_0^{\pi}[\rho_{|\tilde{\varphi}=\tilde{\varphi}^*}\sin 2(\phi+\tilde{\varphi}^*)+\rho_{|\tilde{\varphi}=-\tilde{\varphi}^*}\sin 2(\phi-\tilde{\varphi}^*)]\cdot\\ &\left[\psi_{\rm f}''\cdot(m_{01}^2-m_{02}^2\lambda^{-4})(m_{02}^2\lambda^{-2}-m_{03}^2)\right]_{|\tilde{\varphi}=\tilde{\varphi}^*}\frac{-2b\sin^3\tilde{\theta}}{2\lambda(1+\lambda^2)}d\tilde{\theta},\end{aligned} \tag{B.26}$$

where we used

$$\frac{d\rho}{d\phi}=\frac{d\rho}{d\tilde{\varphi}}=-2b\sin^2\tilde{\theta}\sin 2(\phi+\tilde{\varphi})\cdot\rho. \tag{B.27}$$

B.5 Expressions for the iGST model

Let us denote $g = \mathrm{H}_{22}\lambda^{-2}-\mathrm{H}_{33}$, $I_{\rm f} = (\mathrm{H}_{11}\lambda^2+\mathrm{H}_{22}\lambda^{-2}+\mathrm{H}_{33})\,/\,(\mathrm{H}_{11}+\mathrm{H}_{22}+\mathrm{H}_{33})$. From (3.38) we have

$$\sigma_{2\rm f} = 4g\cdot\psi_{\rm f}', \tag{B.28}$$

$$\sigma_{21\rm f} = 4g'\cdot\psi_{\rm f}'+4g\cdot\psi_{\rm f}''\cdot I_{\rm f}', \tag{B.29}$$

$$\sigma_{22\rm f} = 2g''\cdot\psi_{\rm f}'+2\psi_{\rm f}''\,(2g'\cdot I_{\rm f}'+g\cdot I_{\rm f}'')+2g\cdot\psi_{\rm f}'''\cdot I_{\rm f}'^2, \tag{B.30}$$

$$\sigma_{2\phi} = 4g_\phi\cdot\psi_{\rm f}'+4g\cdot\psi_{\rm f}''\cdot I_{{\rm f}\phi}, \tag{B.31}$$

$$\sigma_{21\phi} = 4g_\phi'\cdot\psi_{\rm f}'+4\psi_{\rm f}''\,(g'\cdot I_{{\rm f}\phi}+g_\phi\cdot I_{\rm f}')+4g\cdot\psi_{\rm f}'''\cdot I_{\rm f}\cdot I_{{\rm f}\phi}, \tag{B.32}$$

$$\begin{aligned}\sigma_{22\phi} &= 2g''_{\phi}\cdot\psi'_{\mathrm{f}}+2\psi''_{\mathrm{f}}\left(2g'_{\phi}\cdot I'_{f}+2g'\cdot I'_{\mathrm{f}\phi}+g''I_{\mathrm{f}\phi}+g_{\phi}\cdot I''_{\mathrm{f}}+g\cdot I''_{\mathrm{f}\phi}\right)\\ &\quad +2\psi'''_{f}\cdot\left(g_{\phi}I'^{2}_{\mathrm{f}}+2gI'_{\mathrm{f}}I'_{\mathrm{f}\phi}\right)+2g\psi''''_{\mathrm{f}}\cdot I'^{2}_{\mathrm{f}}I_{\mathrm{f}\phi},\end{aligned}\tag{B.33}$$

where the expressions for the derivatives of g and I_f can be computed by the chain rule. From (3.41) we have

$$\begin{pmatrix}\mathrm{H}_{11}\\ \mathrm{H}_{22}\\ \mathrm{H}_{33}\end{pmatrix} = \int_0^{\pi}\int_0^{2\pi}\rho(\mathbf{m}_0)\begin{pmatrix}m_{01}^2\\ m_{02}^2\\ m_{03}^2\end{pmatrix}\sin\tilde{\theta}d\tilde{\varphi}d\tilde{\theta}\tag{B.34}$$

$$= 2\int_0^{\pi}\int_{-\tilde{\varphi}^*}^{\tilde{\varphi}^*}\rho\cdot\begin{pmatrix}\sin^3\tilde{\theta}\cos^2\tilde{\varphi}\\ \sin^3\tilde{\theta}\sin^2\tilde{\varphi}\\ \sin\tilde{\theta}\cos^2\tilde{\theta}\end{pmatrix}d\tilde{\varphi}d\tilde{\theta}.\tag{B.35}$$

We denote $\rho_+=\tilde{\rho}(\theta_+)$, $\theta_+=\arccos(\sin\tilde{\theta}\cos(\phi+\tilde{\varphi}^*))$,$\rho_-=\tilde{\rho}(\theta_-)$, $\theta_-=\arccos(\sin\tilde{\theta}\cos(\phi-\tilde{\varphi}^*))$, and the derivatives of H_i are given by

$$\mathrm{H}'_{11}=\frac{1}{\lambda(1+\lambda^2)}\int_0^{\pi}(\rho_++\rho_-)\sin^3\tilde{\theta}\cos^2\tilde{\varphi}^*d\tilde{\theta}=\frac{1}{\lambda(1+\lambda^2)^2}\int_0^{\pi}(\rho_++\rho_-)\sin^3\tilde{\theta}d\tilde{\theta},\tag{B.36}$$

$$\mathrm{H}'_{22}=\frac{1}{\lambda(1+\lambda^2)}\int_0^{\pi}(\rho_++\rho_-)\sin^3\tilde{\theta}\sin^2\tilde{\varphi}^*d\tilde{\theta}=\frac{\lambda}{(1+\lambda^2)^2}\int_0^{\pi}(\rho_++\rho_-)\sin^3\tilde{\theta}d\tilde{\theta},\tag{B.37}$$

$$\mathrm{H}'_{33}=\frac{1}{\lambda(1+\lambda^2)}\int_0^{\pi}(\rho_++\rho_-)\sin\tilde{\theta}\cos^2\tilde{\theta}d\tilde{\theta}=\frac{\lambda}{(1+\lambda^2)}\int_0^{\pi}(\rho_++\rho_-)\sin\tilde{\theta}\cos^2\tilde{\theta}d\tilde{\theta},\tag{B.38}$$

$$\mathrm{H}''_{11} = \int_0^{\pi} \frac{\sin^3\tilde{\theta}}{2\lambda^3(1+\lambda^2)^3} \Big(\rho_+ \cdot \Big[-1-5\lambda^2-2\lambda b\sin^2\tilde{\theta}\sin 2(\tilde{\varphi}^*+\phi)\Big] \tag{B.39}$$

$$+\rho_- \Big[-1-5\lambda^2+2\lambda b\sin^2\tilde{\theta}\sin 2(-\tilde{\varphi}^*+\phi)\Big]\Big)\, d\tilde{\theta}, \tag{B.40}$$

$$\mathrm{H}''_{22} = \int_0^{\pi} \frac{\sin^3\tilde{\theta}}{2\lambda(1+\lambda^2)^3} \Big(\rho_+ \cdot \Big[-3\lambda^2-2\lambda b\sin^2\tilde{\theta}\sin 2(\tilde{\varphi}^*+\phi)\Big] \tag{B.41}$$

$$+\rho_- \Big[-3\lambda^2+2\lambda b\sin^2\tilde{\theta}\sin 2(-\tilde{\varphi}^*+\phi)\Big]\Big)\, d\tilde{\theta}, \tag{B.42}$$

$$\mathrm{H}''_{33} = \int_0^{\pi} \frac{\sin\tilde{\theta}\cos^2\tilde{\theta}}{2\lambda^3(1+\lambda^2)^3} \Big(\rho_+ \cdot \Big[-1-3\lambda^2-2\lambda b\sin^2\tilde{\theta}\sin 2(\tilde{\varphi}^*+\phi)\Big] \tag{B.43}$$

$$+\rho_- \Big[-1-3\lambda^2+2\lambda b\sin^2\tilde{\theta}\sin 2(-\tilde{\varphi}^*+\phi)\Big]\Big)\, d\tilde{\theta}, \tag{B.44}$$

$$\begin{pmatrix} \mathrm{H}_{11\phi} \\ \mathrm{H}_{22\phi} \\ \mathrm{H}_{33\phi} \end{pmatrix} = 2\int_0^{\pi}\int_{-\tilde{\varphi}^*}^{\tilde{\varphi}^*} -2b\sin 2(\tilde{\varphi}+\phi)\rho \cdot \begin{pmatrix} \sin^5\tilde{\theta}\cos^2\tilde{\varphi} \\ \sin^5\tilde{\theta}\sin^2\tilde{\varphi} \\ \sin^3\tilde{\theta}\cos^2\tilde{\theta} \end{pmatrix} d\tilde{\varphi}d\tilde{\theta} \tag{B.45}$$

$$\mathrm{H}'_{11\phi} = \frac{-2b\sin^5\tilde{\theta}}{\lambda(1+\lambda^2)^2} \int_0^{\pi} \left(\rho_+ \cdot \sin 2(\tilde{\varphi}^*+\phi) + \rho_- \cdot \sin 2(-\tilde{\varphi}^*+\phi)\right) d\tilde{\theta}, \tag{B.46}$$

$$\mathrm{H}'_{22\phi} = \frac{-2\lambda b \sin^5\tilde{\theta}}{(1+\lambda^2)^2} \int_0^{\pi} \left(\rho_+ \cdot \sin 2(\tilde{\varphi}^* + \phi) + \rho_- \cdot \sin 2(-\tilde{\varphi}^* + \phi)\right) d\tilde{\theta}, \tag{B.47}$$

$$\mathrm{H}'_{33\phi} = \frac{-2b\lambda \sin^3\tilde{\theta}\cos^2\tilde{\theta}}{(1+\lambda^2)} \int_0^{\pi} \left(\rho_+ \cdot \sin 2(\tilde{\varphi}^* + \phi) + \rho_- \cdot \sin 2(-\tilde{\varphi}^* + \phi)\right) d\tilde{\theta}, \tag{B.48}$$

$$\begin{aligned}
\mathrm{H}''_{11\phi} \;=\; & \int_0^{\pi} \frac{\sin^5\tilde{\theta}}{2\lambda^3(1+\lambda^2)^3} \Big(\rho_+ \cdot (-2b \sin 2(\tilde{\varphi}^* + \phi)) \Big(-1 - 5\lambda^2 - 2\lambda b \sin^2\tilde{\theta} \sin 2(\tilde{\varphi}^* + \phi)\Big) \\
& -\rho_+ 4\lambda b \cos 2(\tilde{\varphi}^* + \phi) + \\
& +\rho_- \cdot (-2b \sin 2(-\tilde{\varphi}^* + \phi)) \Big(-1 - 5\lambda^2 + 2\lambda b \sin^2\tilde{\theta} \sin 2(-\tilde{\varphi}^* + \phi)\Big) \\
& +\rho_- 4\lambda b \cos 2(-\tilde{\varphi}^* + \phi)) \, d\tilde{\theta},
\end{aligned} \tag{B.49}$$

$$\begin{aligned}
\mathrm{H}''_{22\phi} \;=\; & \int_0^{\pi} \frac{\sin^5\tilde{\theta}}{2\lambda(1+\lambda^2)^3} \Big(\rho_+ \cdot (-2b \sin 2(\tilde{\varphi}^* + \phi)) \Big(-3\lambda^2 - 2\lambda b \sin^2\tilde{\theta} \sin 2(\tilde{\varphi}^* + \phi)\Big) + \\
& -\rho_+ \cdot 4\lambda b \cos 2(\tilde{\varphi}^* + \phi) \\
& +\rho_- \, (-2b \sin 2(-\tilde{\varphi}^* + \phi)) \Big(-3\lambda^2 + 2\lambda b \sin^2\tilde{\theta} \sin 2(-\tilde{\varphi}^* + \phi)\Big) \\
& +\rho_- 4\lambda b \cos 2(-\tilde{\varphi}^* + \phi)) \, d\tilde{\theta},
\end{aligned} \tag{B.50}$$

$$
\begin{aligned}
\mathrm{H}''_{33\phi} \;=\; & \int_0^{\pi} \frac{\sin^3\tilde{\theta}\cos^2\tilde{\theta}}{2\lambda^3(1+\lambda^2)^3}\Big(\rho_+\cdot(-2b\sin 2(\tilde{\varphi}^*+\phi))\Big(-1-3\lambda^2-2\lambda b\sin^2\tilde{\theta}\sin 2(\tilde{\varphi}^*+\phi)\Big) \\
& -\rho_+ 4\lambda b\cos 2(\tilde{\varphi}^*+\phi) \\
& +\rho_-\,(-2b\sin 2(-\tilde{\varphi}^*+\phi)) \\
& \Big(-1-3\lambda^2+2\lambda b\sin^2\tilde{\theta}\sin 2(-\tilde{\varphi}^*+\phi)\Big)+\rho_- 4\lambda b\cos 2(-\tilde{\varphi}^*+\phi)\Big)\,d\tilde{\theta}. \qquad \text{(B.51)}
\end{aligned}
$$

Appendix C

An implication of rotational symmetry for diagonal tensors

Proposition 17. *Suppose a tensor* $\mathbf{A}$ *is defined and continuous in a circle* $\{(r,\phi) \in \mathbb{R}^2 : 0 \leq r \leq B,\, \theta \in [0, 2\pi)\}$*, where* (r,θ) *are planar polar coordinates. Assume that* $\mathbf{A}$ *for* $r \neq 0$ *can be written in the form*

$$\mathbf{A}(r,\phi) = a_r(r)\mathbf{e}_r \otimes \mathbf{e}_r + a_\theta(r)\mathbf{e}_\theta \otimes \mathbf{e}_\theta, \tag{C.1}$$

where $\mathbf{e}_r$, $\mathbf{e}_\theta$ *are the local unit basis vectors. Then there exist limits* $\lim_{r\to 0} a_r(r) = a_r(0)$, $\lim_{r\to 0} a_\theta(r) = a_\theta(0)$ *and* $a_r(0) = a_\theta(0)$ *holds.*

Proof. Let $\mathbf{e}_x$, $\mathbf{e}_y$ be the basis vectors in a Cartesian frame. The continuity of $\mathbf{A}$ reads $\lim_{(x,y)\to(0,0)} \mathbf{A} = \mathbf{A}$, and for constant $\mathbf{e}_x$ we have

$$\lim_{\substack{x \to +0 \\ y = 0}} \mathbf{A}\mathbf{e}_x = \mathbf{A}\mathbf{e}_x = \lim_{\substack{y \to -0 \\ x = 0}} \mathbf{A}\mathbf{e}_x. \tag{C.2}$$

Note that

$$\lim_{\substack{x \to +0 \\ y = 0}} \mathbf{A}\mathbf{e}_x = \lim_{\substack{x \to +0 \\ y = 0}} \mathbf{A}\mathbf{e}_r \overset{\text{by (C.1)}}{=} \lim_{\substack{x \to +0 \\ y = 0}} a_r(r)\mathbf{e}_r = \lim_{\substack{x \to +0 \\ y = 0}} a_r(r)\mathbf{e}_x$$

$$= \Big(\lim_{\substack{x \to +0 \\ y = 0}} a_r(r)\Big)\mathbf{e}_x = \Big(\lim_{r \to 0} a_r(r)\Big)\,\mathbf{e}_x, \tag{C.3}$$

where the existence of $\lim a_r(r)$ follows from the existence of $\lim a_r(r)\mathbf{e}_x$ and that $\mathbf{e}_x$ is constant. Similarly, we have

$$\lim_{\substack{y \to -0 \\ x = 0}} \mathbf{A}\mathbf{e}_x = \lim_{\substack{y \to -0 \\ x = 0}} \mathbf{A}\mathbf{e}_\theta \overset{\text{by (C.1)}}{\to} \lim_{\substack{y \to -0 \\ x = 0}} a_\theta(r)\mathbf{e}_\theta = \lim_{\substack{y \to -0 \\ x = 0}} a_\theta(r)\mathbf{e}_x$$

$$= \Big(\lim_{\substack{y \to -0 \\ x = 0}} a_\theta(r)\Big)\mathbf{e}_x = \Big(\lim_{r \to 0} a_\theta(r)\Big)\,\mathbf{e}_x, \tag{C.4}$$

and due to (C.2) obtain

$$\lim_{r \to 0} a_r(r) = a_r(0) = a_\theta(0) = \lim_{r \to 0} a_\theta(r). \tag{C.5}$$

□

Remark. This proposition also applies to the case of cylindrical coordinates and tensors of the form $\mathbf{A} = a_r(r)\mathbf{e}_r \otimes \mathbf{e}_r + a_\theta(r)\mathbf{e}_\theta \otimes \mathbf{e}_\theta + a_z(r)\mathbf{e}_z \otimes \mathbf{e}_z$.

Bibliography

[1] V. Alastrué, B. Calvo, E. Pena, and M. Doblaré. Biomechanical modeling of refractive corneal surgery. *J. Biomech. Eng.*, 128(1):150–160, 2006.

[2] D. Ambrosi, G.A. Ateshian, E.M. Arruda, S.C. Cowin, J. Dumais, A. Goriely, G. A. Holzapfel, J.D. Humphrey, R. Kemkemer, E. Kuhl, et al. Perspectives on biological growth and remodeling. *J. Mech. Phys. Solids*, 59(4):863–883, 2011.

[3] S. Antman. *Nonlinear Problems of Elasticity*. Applied Mathematical Sciences. Springer, 2006.

[4] M. Ben Amar and A. Goriely. Growth and instability in elastic tissues. *J. Mech. Phys. Solids*, 53(10):2284–2319, 2005.

[5] D. L. Butler, S. A. Goldstein, R. E. Guldberg, X. E. Guo, R. Kamm, C. T. Laurencin, L. V. McIntire, V. C. Mow, R. M. Nerem, R. L. Sah, et al. The impact of biomechanics in tissue engineering and regenerative medicine. *Tissue Eng. Pt. B-Rev.*, 15(4):477–484, 2009.

[6] D. H. Cortes and D. M. Elliott. Accurate prediction of stress in fibers with distributed orientations using generalized high-order structure tensors. *Mech. Mater.*, 75:73–83, 2014.

[7] D. H. Cortes, S. P. Lake, J. A. Kadlowec, L. J. Soslowsky, and D. M. Elliott. Characterizing the mechanical contribution of fiber angular distribution in connective

tissue: comparison of two modeling approaches. *Biomech. Model. Mechanobiol.*, 9(5):651–658, 2010.

[8] J. Dervaux and M. Ben Amar. Morphogenesis of growing soft tissues. *Phys. Rev. Lett.*, 101:068101, Aug 2008.

[9] M. Destrade, B. Mac Donald, J. G. Murphy, and G. Saccomandi. At least three invariants are necessary to model the mechanical response of incompressible, transversely isotropic materials. *Comput. Mech.*, 52(4):959–969, 2013.

[10] E. Dhimolea, M. V. Maffini, A. M. Soto, and C. Sonnenschein. The role of collagen reorganization on mammary epithelial morphogenesis in a 3d culture model. *Biomaterials*, 31(13):3622–3630, 2010.

[11] N. J. B. Driessen, R. A. Boerboom, J. M. Huyghe, C. V. C. Bouten, and F. P. T. Baaijens. Computational analyses of mechanically induced collagen fiber remodeling in the aortic heart valve. *J. Biomech. Eng.*, 125:549, 2003.

[12] N. J. B. Driessen, M. A. J. Cox, C. V. C. Bouten, and F. P. T. Baaijens. Remodelling of the angular collagen fiber distribution in cardiovascular tissues. *Biomech. Model. Mechanobiol.*, 7(2):93–103, 2008.

[13] N. J. B. Driessen, G. W. M. Peters, J. M. Huyghe, C. V. C. Bouten, and F. P. T. Baaijens. Remodelling of continuously distributed collagen fibres in soft connective tissues. *J. Biomech.*, 36(8):1151–1158, 2003.

[14] N. J. B. Driessen, W. Wilson, C. V. C. Bouten, and F. P. T. Baaijens. A computational model for collagen fibre remodelling in the arterial wall. *J. Theor. Biol.*, 226(1):53–64, 2004.

[15] M. Eastwood, V.C. Mudera, D.A. McGrouther, and R.A. Brown. Effect of precise mechanical loading on fibroblast populated collagen lattices: morphological changes. *Cell Motil. Cytoskeleton*, 40(1):13–21, 1998.

[16] M. Epstein. *The Elements of Continuum Biomechanics*. Wiley, 2012.

[17] S. Federico and T. C. Gasser. Nonlinear elasticity of biological tissues with statistical fibre orientation. *J. R. Soc. Interface*, 7(47):955–966, 2010.

[18] S. Federico and W. Herzog. Towards an analytical model of soft biological tissues. *J. Biomech.*, 41(16):3309–3313, 2008.

[19] P. Fratzl. *Collagen: structure and mechanics*. Springer Verlag, 2008.

[20] A. D. Freed, D. R. Einstein, and I. Vesely. Invariant formulation for dispersed transverse isotropy in aortic heart valves. *Biomech. Model. Mechanobiol.*, 4(2-3):100–117, 2005.

[21] Y. C. Fung. *Biomechanics: Mechanical Properties of Living Tissues*. Springer New York, 2010.

[22] T. C. Gasser, R. W. Ogden, and G. A. Holzapfel. Hyperelastic modelling of arterial layers with distributed collagen fibre orientations. *J. R. Soc. Interface*, 3(6):15–35, 2006.

[23] A. Goriely and M. Tabor. Spontaneous rotational inversion in phycomyces. *Phys. Rev. Lett.*, 106(13):138103, 2011.

[24] A. Goriely and M. Tabor. Rotation, inversion and perversion in anisotropic elastic cylindrical tubes and membranes. *Proc. R. Soc. A*, 469(2153):20130011, 2013.

[25] A. Goriely and R. Vandiver. On the mechanical stability of growing arteries. *IMA J. Appl. Math.*, page hxq021, 2010.

[26] I. S. Gradshteyn and I.M. Ryzhik. Table of integrals. *Series, and Products (Academic, New York, 1980)*, 1, 1980.

[27] R. Grytz and G. Meschke. A computational remodeling approach to predict the physiological architecture of the collagen fibril network in corneo-scleral shells. *Biomech. Model Mechanobiol.*, 9(2):225–235, 2010.

[28] Z. Y. Guo, X. Q. Peng, and B. Moran. A composites-based hyperelastic constitutive model for soft tissue with application to the human annulus fibrosus. *J. Mech. Phys. Solids*, 54(9):1952–1971, 2006.

[29] I. Hariton, G. deBotton, T. C. Gasser, and G. A. Holzapfel. Stress-modulated collagen fiber remodeling in a human carotid bifurcation. *J. Theor. Biol.*, 248(3):460–470, 2007.

[30] I. Hariton, G. DeBotton, T.C. Gasser, and G.A. Holzapfel. Stress-driven collagen fiber remodeling in arterial walls. *Biomech. Model. Mechanobiol.*, 6(3):163–175, 2007.

[31] J. W. Hennel and J. Klinowski. Magic-angle spinning: a historical perspective. In *New techniques in solid-state nmr*, pages 1–14. Springer, 2005.

[32] G. Himpel, A. Menzel, E. Kuhl, and P. Steinmann. Time-dependent fibre reorientation of transversely isotropic continua - finite element formulation and consistent linearization. *Internat. J. Numer. Methods Engrg.*, 73(10):1413–1433, 2008.

[33] G. A. Holzapfel. *Nonlinear solid mechanics: a continuum approach for engineering*. John Wiley & Sons Ltd., 2000.

[34] G. A. Holzapfel, T. C. Gasser, and R. W. Ogden. A new constitutive framework for arterial wall mechanics and a comparative study of material models. *J. Elasticity*, 61(1-3):1–48, 2000.

[35] G. A. Holzapfel and R. W. Ogden. Constitutive modelling of arteries. *Philos. Trans. R. Soc. Lond. Ser. A Math. Phys. Eng. Sci*, 466(2118):1551–1597, 2010.

[36] G.A. Holzapfel. *Nonlinear solid mechanics: a continuum approach for engineering.* John Wiley & Sons Ltd., 2000.

[37] C. O. Horgan and G. Saccomandi. A new constitutive theory for fiber-reinforced incompressible nonlinearly elastic solids. *J. Mech. Phys. Solids*, 53(9):1985–2015, 2005.

[38] J. D. Humphrey. *Cardiovascular Solid Mechanics: Cells, Tissues, and Organs.* Springer, 2002.

[39] D. Ingber et al. Mechanobiology and diseases of mechanotransduction. *Ann. Med.*, 35(8):564–577, 2003.

[40] E. Kuhl, K. Garikipati, E. M. Arruda, and K. Grosh. Remodeling of biological tissue: mechanically induced reorientation of a transversely isotropic chain network. *J.Mech. Phys. Solids*, 53(7):1552–1573, 2005.

[41] E. Kuhl, K. Garikipati, E.M. Arruda, and K. Grosh. Remodeling of biological tissue: mechanically induced reorientation of a transversely isotropic chain network. *J. Mech. Phys. Solids*, 53(7):1552–1573, 2005.

[42] E. Kuhl and G.A. Holzapfel. A continuum model for remodeling in living structures. *J. Mater. Sci.*, 42(21):8811–8823, 2007.

[43] Y. Lanir. A structural theory for the homogeneous biaxial stress-strain relationships in flat collagenous tissues. *J. Biomech.*, 12(6):423–436, 1979.

[44] Y. Lanir. Constitutive equations for fibrous connective tissues. *J. Biomech.*, 16:1–12, 1983.

[45] V. I. Lebedev and D. N. Laikov. A quadrature formula for the sphere of the 131st algebraic order of accuracy. In *Dokl. Math.*, volume 59, pages 477–481. MAIK Nauka/Interperiodica, 1999.

[46] A. V. Melnik and A. Goriely. Dynamic fiber reorientation in a fiber-reinforced hyperelastic material. *Math. Mech. Solids*, 18(6):634–648, 2013.

[47] A. Menzel. Modelling of anisotropic growth in biological tissues. *Biomech. Model. Mechanobiol.*, 3(3):147–171, 2005.

[48] A. Menzel. Modelling of anisotropic growth in biological tissues. A new approach and computational aspects. *Biomech. Model. Mechanobiol.*, 3(3):147–71, March 2005.

[49] A. Menzel and E. Kuhl. Frontiers in growth and remodeling. *Mechanics research communications*, 2012.

[50] J. Merodio and R. W. Ogden. Mechanical response of fiber-reinforced incompressible non-linearly elastic solids. *Int. J. Nonlin. Mech.*, 40(2):213–227, 2005.

[51] D. E. Moulton, A. Goriely, and R. Chirat. Mechanical growth and morphogenesis of seashells. *J. Theor. Biol.*, 311:69–79, 2012.

[52] J. G. Murphy and G. Saccomandi. Exploitation of the linear theory in the nonlinear modelling of soft tissue. *Math. Mech. Solids*, page 1081286514544261, 2014.

[53] J. D. Murray, P. K. Maini, and R. T. Tranquillo. Mechanochemical models for generating biological pattern and form in development. *Phys. Rep.*, 171(2):59–84, 1988.

[54] L. E. Niklason, J. Gao, W. M. Abbott, K. K. Hirschi, S. Houser, R. Marini, and R. Langer. Functional arteries grown in vitro. *Science*, 284(5413):489–493, 1999.

[55] R.W. Ogden. *Non-linear Elastic Deformations*. Dover Civil and Mechanical Engineering Series. Dover Publications, 1997.

[56] T. K. Ohsumi, J. E. Flaherty, M. C. Evans, and V. H. Barocas. Three-dimensional simulation of anisotropic cell-driven collagen gel compaction. *Biomech. Model. Mechanobiol.*, 7(1):53–62, 2008.

[57] A. Pandolfi and G. A. Holzapfel. Three-dimensional modeling and computational analysis of the human cornea considering distributed collagen fibril orientations. *J. Biomech. Engineering*, 130(6):061006, 2008.

[58] A. Pandolfi and M. Vasta. Fiber distributed hyperelastic modeling of biological tissues. *Mech. Mater.*, 44:151–162, 2012.

[59] R. Parrish. Lebedev quadratures on the surface of the unit sphere at double precision. `http://www.mathworks.co.uk/matlabcentral/fileexchange/27097-getlebedevsphere`, March 2010.

[60] E. Pucci and G. Saccomandi. On the use of universal relations in the modeling of transversely isotropic materials. *Int. J. Solids Struct.*, 51(2):377–380, 2014.

[61] P. S. Robinson, S. L. Johnson, M. C. Evans, V. H. Barocas, and R. T. Tranquillo. Functional tissue-engineered valves from cell-remodeled fibrin with commissural alignment of cell-produced collagen. *Tissue Eng. Pt. B-Rev.*, 14(1):83–95, 2008.

[62] E. K. Rodriguez, A. Hoger, and A. D. McCulloch. Stress-dependent finite growth in soft elastic tissues. *J. Biomech.*, 27(4):455–467, 1994.

[63] R. K. Sawhney and J. Howard. Slow local movements of collagen fibers by fibroblasts drive the rapid global self-organization of collagen gels. *J. Cell Biol.*, 157(6):1083–1092, 2002.

[64] P. Skacel and J. Bursa. Numerical implementation of constitutive model for arterial layers with distributed collagen fibre orientations. *Comput. Methods Biomech. Biomed. Engin.*, (ahead-of-print):1–13, 2013.

[65] A. J. M. Spencer. *Deformations of fibre-reinforced materials*. Oxford Univ. Press. New York, 1972.

[66] A. J. M. Spencer, editor. *Continuum theory of the mechanics of fibre-reinforced composites*, volume 282. Springer New York:, 1984.

[67] A. J. M. Spencer. *Continuum mechanics*. Courier Dover Publications, 2004.

[68] L. A. Taber. Biomechanics of growth, remodeling, and morphogenesis. *Appl. Mech. Rev.*, 48(8):487–545, 1995.

[69] N. Triantafyllidis and R. Abeyaratne. Instabilities of a finitely deformed fiber-reinforced elastic material. *J. Appl. Mech.*, 50(1):149–156, 1983.

[70] C. Truesdell, W. Noll, and S. Antman. *The Non-Linear Field Theories of Mechanics*. Number v. 3 in The non-linear field theories of mechanics. Springer, 2004.

[71] J. H. C. Wang, F. Jia, T. W. Gilbert, and S. L. Y. Woo. Cell orientation determines the alignment of cell-produced collagenous matrix. *J. Biomech.*, 36(1):97–102, 2003.

[72] Y. Wang, S. Son, S. M. Swartz, and N. C. Goulbourne. A mixed von mises distribution for modeling soft biological tissues with two distributed fiber properties. *Int. J. Solids Struct.*, 49(21):2914–2923, 2012.

[73] H.-C. Wu and R.-F. Yao. Mechanical behavior of the human annulus fibrosus. *J. Biomech.*, 9(1):1–7, 1976.

[74] A. Yavari and A. Goriely. On the stress singularities generated by anisotropic eigenstrains and the hydrostatic stress due to annular inhomogeneities. *J. Mech. Phys. Solids*, 2014.

[75] Y. Zou and Y. Zhang. An experimental and theoretical study on the anisotropy of elastin network. *Ann. Biomed. Eng.*, 37(8):1572–1583, 2009.